PiT Proteins, from Molecular Mechanism to Physiological Regulation.

Dissertation

zur

Erlangung der naturwissenschaftlichen Doktorwürde

(Dr. sc. nat.)

vorgelegt der

Mathematisch-naturwissenschaftlichen Fakultät

der

Universität Zürich

von

Silvia Ravera

aus

Italien

Promotionskomitee

Dr. Ian Forster

Prof. Dr. Heini Murer

Prof. Dr. François Verrey

Prof. Dr. Laurent Schild

Zürich 2009

Summary

Members of the SLC20 solute carrier family, PiT1 and PiT2, originally identified as retroviral receptors, transport inorganic phosphate (P_i) in a Na^+-dependent manner. In addition to a proposed housekeeping role for phosphate homeostasis, recent studies also implicate them in bone mineralization and vascular calcification, thereby suggesting patho-physiological relevance. This underscores the need for detailed characterization of their transport mechanism, physiological role in P_i homeostasis and structure-function relations. To characterize their transport mechanism three SLC20 clones (*Xenopus* PiT1, human PiT1, and human PiT2) were expressed in *Xenopus* oocytes. Each clone gave robust Na-dependent ^{32}P uptake, but only *Xenopus* PiT1 showed sufficient activity for complete kinetic characterization by using two-electrode voltage clamp and radionuclide uptake. Compared with the well-characterized electrogenic SLC34 proteins (NaPi-IIa/b) that preferentially cotransport divalent P_i with a 3:1 Na^+:P_i stoichiometry, PiT1 was found to have a stoichiometry of 2:1 Na^+:P_i and prefers monovalent P_i, 1 charge was translocated per P_i. Unlike SLC34 proteins, PiT1 transport activity was less sensitive to acid pH. Significantly, in contrast to type II Na^+/P_i cotransporters, the transport inhibitor phosphonoformic acid (PFA) did not inhibit PiT1 or PiT2 activity. This latter finding was used as a tool to identify PiT2 as a potential contributor to renal P_i uptake in the rat kidney. Here, it was shown that ^{32}P uptake in rat renal brush border membrane vesicles was incompletely suppressed in the presence of high concentrations of PFA that would normally fully inactivate the contribution due to the main mediators of Na^+-coupled P_i cotransport (NaPi-IIa, NaPi-IIc). Moreover, PiT2 was localized to the brush border membrane (BBM) of the proximal tubule epithelia and its abundance, confirmed by western blot and immunohistochemistry of rat kidney slices, was regulated by dietary P_i. Taken together these findings define a new role for PiT2 in renal phosphate homeostasis. Because of its relative insensitivity to changes in tubular pH and its adaptive time course of down regulation that is intermediate between that of NaPi-IIa and NaPi-IIc, PiT2 may play a significant role in the physiological response to changes in P_i diet. Finally, structure-function studies were performed on the *Xenopus* PiT1 isoform with the aim of identifying functionally important sites in the protein and establishing the topology in regions exposed to the extracellular medium. Previous topology studies have identified residues associated with the retrovirus receptor binding site but the remaining secondary topology is less well-defined. For the PiT2 isoform the predicted first extracellular loop has been reported to contain residues critical for substrate interaction and transport function. This region is identical in the *Xenopus* PiT1 isoform. Therefore the substituted cysteine accessibility method (SCAM) was applied to investigate structure-function relationships. Residues important for the transport function were identified and the accessibility of this region from the extra-

cellular medium was confirmed and quantitated in terms of the rate of modification of the substituted cysteines.

Zusammenfassung

PiT1 und PiT2, zwei Vertreter der SLC20 (solute carrier) Familie, welche ursprünglich als retrovirale Rezeptoren identifiziert wurden, transportieren anorganische Phosphat-jonen (P_i) zusammen mit Na^+-jonen durch zelluläre Plasmamembranen. Zusätzlich zu der vorgeschlagenen "housekeeping" Funktion in der Phosphathomeostase bringen kürzlich veröffentlichte Studien PiT1 und PiT2 in einen Zusammenhang mit der Knochenmineralisation und der vaskulären Kalzifizierung und zeigen dadurch ihre physiologische und pathophysiologische Relevanz. In dieser Arbeit wurden die Transportmechanismen, die Rolle in der renalen Ausscheidung von P_i sowie Struktur-Funktions-Beziehungen der PiT1 /PiT2 Na/P_i-Kotransporter untersucht.

Um den Transportmechanismus zu charakterisieren wurden drei veschiedene SLC20 Na/P_i-Kotransporter (*Xenopus* PiT1, human PiT1 und human PiT2) in Oozyten von *Xenopus laevis* exprimiert. Expression jeder der verwendeten Isoformen zeigte Na^+-abhängige Aufnahme von (^{32}P) P_i, jedoch zeigte nur die Expression von *Xenopus* PiT1 ausreichende Aktivität, welche für eine umfassende Charakterisierung unter Verwendung von elektrophysiologischen Techniken erforderlich ist. Die Ergebnisse dieser Untersuchungen zeigten, dass der PiT1 vermittelte Na/P_i-cotransport elektrogen ist, dass aber im Gegesatz zu den elektrogenen SLC34 Na/P_i-Kotransportern (NaPi-IIa/b), welche bevorzugt divalentes P_i mit einer 3 Na^+:1:HPO_4^{2-} Stöchiometrie kotransportieren, PiT1 monovalentes P_i bevorzugt und der Transportvorgang eine Stöchiometrie von 2 Na^+:1H_2PO^- aufweist. Im Vergleich zu den SLC34 Proteinen zeigte die Transportaktivität von PiT1 eine geringere pH-Sensitivität, und im Gegensatz zu Typ II Na^+/P_i-Kotransportern, wurden die Transportaktivitäten von PiT1 oder PiT2 durch Phosphonoameisensäure (PFA) nicht gehemmt.

Die letztere Erkenntnis wurde als Werkzeug zur Identifizierung von PiT2 als einem potentiellen Mitspieler der renalen Rückresorption von P_i in der Niere benutzt. Es konnte gezeigt werden, dass die Aufnhame von ^{32}P in isolierte Membranvesikel der Bürstensaummembran des proximalen Tubulus der Rattenniere in Gegenwart hoher Konzentrationen von PFA nicht vollständig unterdrückt wurde. Dabei handelte es sich um PFA-Konzentrationen, welche die beiden Hauptmediatoren der renalen Rückresorption von P_i (NaPi-IIa bzw. NaPi-IIc) vollständig inaktivieren. Darüber hinaus wurde gezeigt, dass PiT2 an der Bürstensaummembran des proximalenTubulus lokalisiert ist und dass die Anzahl PiT2 Kotransporter durch in der Nahrung aufgenommenes P_i reguliert wird. Interessanterweise unterscheidet sich der zeitliche Verlauf der Regulation von PiT2 von demjenigen der NaPi-IIa und NaPi-IIc Na/P_i-Kotransporter. Zusammengenommen definieren diese Ergebnisse eine neue Funktion für PiT2 für die renale Rückresorption von P_i und somit auch für die gesamte Phosphathomeostase

Struktur-Funktions Studien unter Verwendung der *Xenopus*-PiT1 Isoform wurden mit dem

Ziel durchgeführt, funktionelle Stellen im Protein zu identifizieren, welche für den Transportvorgang wichtig sind. Dabei wurde ein Modell der Sekundärstruktur verwendet, welches bei der Aufklärung der Bindungsstelle für Retroviren verwendet wurde. Um Struktur-Funktions-Beziehungen zu erarbeiten, wurde die sogenannte "substituted cysteine accessibility" Methode (SCAM) angewandt. Es wurde hauptsächlich die erste extrazelluläre Domäne untersucht, welche bei PiT1 und PiT2 Kotransportern identisch ist. Dabei wurden für die Transportfunktion wichtige Aminosäuren identifiziert und deren Anordnung wurde aufgrund der Kinetik der Modifikationsreaktion der substituierten Cysteine beschrieben.

Contents

Part I

Introduction

Chapter 1

Transport across the plasma membrane.

The plasma membrane defines the physical boundary of the cell and acts as permeation barrier so that essential differences in the fluid composition between the intracellular and the extracellular compartments can be established, maintained and regulated throughout the life of the cell. In all cells the plasma membrane is made up of a 5 nm double layer of phospholipids, orientated with the hydrophobic chains facing together and the hydrophilic heads facing the aqueous compartments [1]. Movement of solutes as well as water across the plasma membrane is mediated by membrane transport proteins. These can be conveniently classified according to their structure-function properties as pores, channels and carriers (see fig. 1.1). This classification is largely based on how the solutes access the transmembrane pathway [1].

1.1 Pores.

Pores provide an aqueous transmembrane passageway that is always open. A pore allows the passage of approximately 10^9 particles per second (water, glycerol, small lipids etc.). Among the large-size pores are the *porins* found in the outer membranes of gram-negative bacteria and mitochondria that allow solutes as large as 5 kDa to diffuse passively from the cytosol into the mitochondria's intermembrane space. The plasma membranes of many types of cells have proteins that form channels large enough to allow only water molecules to pass through, like the aquaporin 1 (AQP1) (see example b in fig. 1.2: the pathway between the two sides of the membrane is always open). AQP1 belongs to a larger family of aquaporins that has representatives in organisms as diverse as bacteria, plants, and animals. In mammals, the various aquaporin isoforms have different tissue distributions, different mechanisms of

regulation, and varying abilities to transport small neutral molecules other than water. In the lipid bilayer, AQP1 exists as tetramers [2].

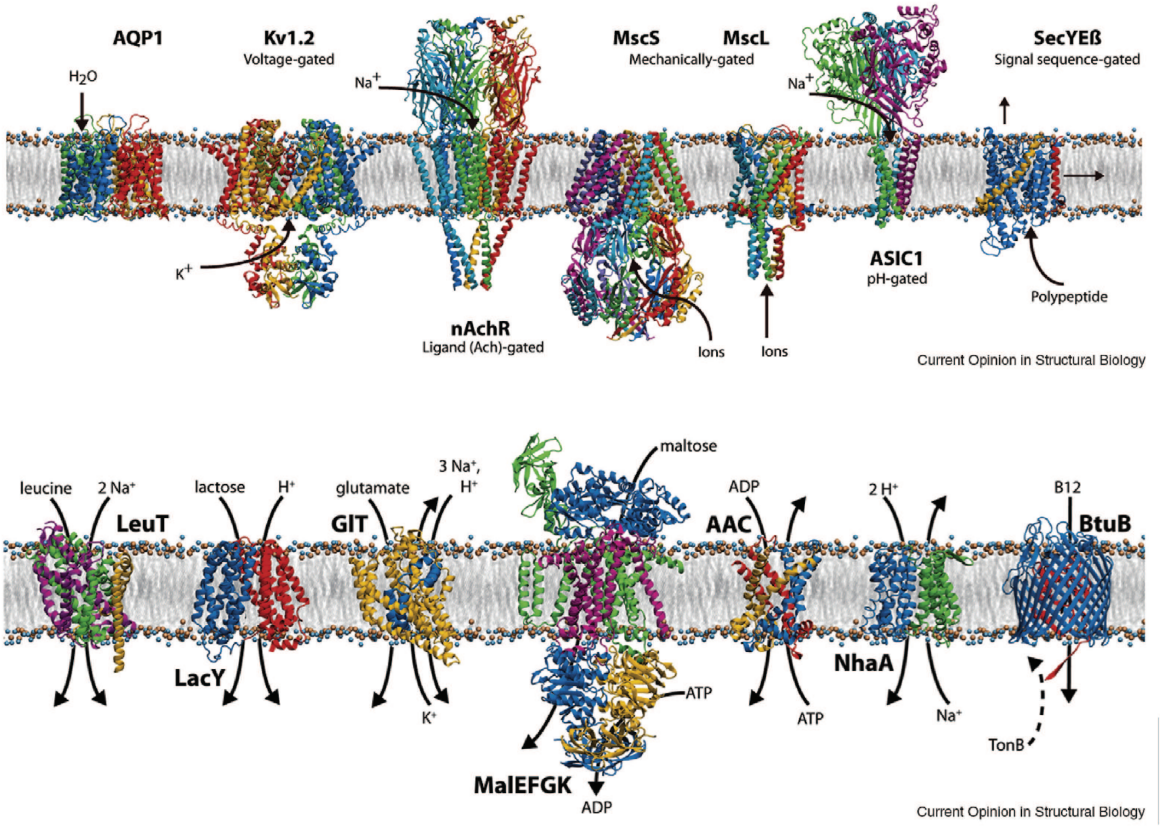

Figure 1.1: Representative structures of channels above and transporters below obtained from crystallographic data [3].

1.2 Ion channels.

Channels specifically allow the selective passage of ions across the membrane. Ion channels are composed of one or more polypeptide subunits with α helical membrane transmembrane domains (see example a in fig. 1.2). Channels have several functional components that can now be related to their structure:

1. gate - determines whether the channel is open or closed
2. sensor - responds to one of several different types of signals: changes in membrane potential, second messenger systems that act at the cytoplasmic face of the membrane protein, or ligands like neurohumoral agonists that bind to the extracellular face of the membrane protein
3. selectivity filter - determines the kind of ions that have access to the channel pore

4. pore - provides the continuous pathway between the two sides of the membrane so that ions can flow passively by diffusion until the channel closes.

When the gate is open the two sides of the membrane are in direct communication as shown in fig. 1.2. Channels can be ligand gated like the nicotinic acetylcholine receptor (nAchR in fig. 1.1), voltage gated (like Kv1.2 in fig. 1.1), mechanosensitive like the K^+ channels TRAAK (example MscS and MscL in fig. 1.1), etc. Channels are extremely selective for specific ions (cations or anions) and allow the passage of up to 10^8 ions per second according to the prevailing electrochemical gradient; this means that in terms of solute energetics they are dissipative.

1.3 Carriers.

Carriers show a complex secondary structure involving multiple transmembrane domains (see example c in fig.1.2). They have been classically viewed as "vectorial" enzymes whose catalytic cycle involves:

1. relatively selective recognition/binding of the substrates
2. conformational changes in the transporter itself due to binding of the substrates
3. coupling of these conformational changes to physical movement of the ions across the membrane

Each carrier protein has a specific affinity for binding one or a small number of solutes, and transporting them across the bilayer. Carriers have a limited speed with which they can cycle through the various steps. A progressive increase of the solute concentration leads the carrier to transport solute at maximum rate. In contrast to channels and pores a ideal carrier never allows direct communication between the two sides of the membrane as shown in fig. 1.2. Carriers exhibit a wide range of flux rates from 10-50000 substrate molecules $\cdot$ s^{-1}. GAT1 (γ-aminobutyric acid (GABA) transporter 1) for example show a unitary turnover rate of 15 $\pm$ 2 s^{-1} (21°C, -50 mV) [4], the Na^+-K^+-ATPase show a turnover rate of 500 at 37°C [5] and the Cl/Cl exchanger 50000 s^{-1} at 37°C [6]. They can be subdivided into three categories:

- *uniporters*, which move a solute in one direction only
- *symporters* (or *cotransporters*), which translocate two or more solutes in the same direction like cation- or proton-coupled cotransporters
- *antiporters* (or *exchangers*), which translocate two or more solutes in opposite directions

In terms of energetics, membrane transport proteins can function PASSIVELY or ACTIVELY. Like pores and channels, uniporter carriers transport solutes "downhill" according to the chemical potential difference for the specific substrate across the membrane, like the glucose transporter GLUT. Due to the fact that they follow the electrochemical gradient they cannot concentrate a solute in a particular side of the membrane. Symporters and antiporters can move the substrate "uphill" against its electrochemical gradient using various energy sources [1, 7, 8]. They can generate a solute gradient, exploiting the electrochemical gradient of another solute. They can be:

- primary active carriers, that use the energy available from the direct hydrolysis of the high energetic pyrophosphate bonds like ATP and GTP. These are exemplified by the exchanger Na^+-K^+-ATPase or the uniporter H^+-ATPase.
- secondary-active carriers, that utilize the energy stored in the electrochemical gradient of ions like Na^+ to move other substrates across the membrane. A typical example is the Na^+ coupled glucose transporter (SGLT1).

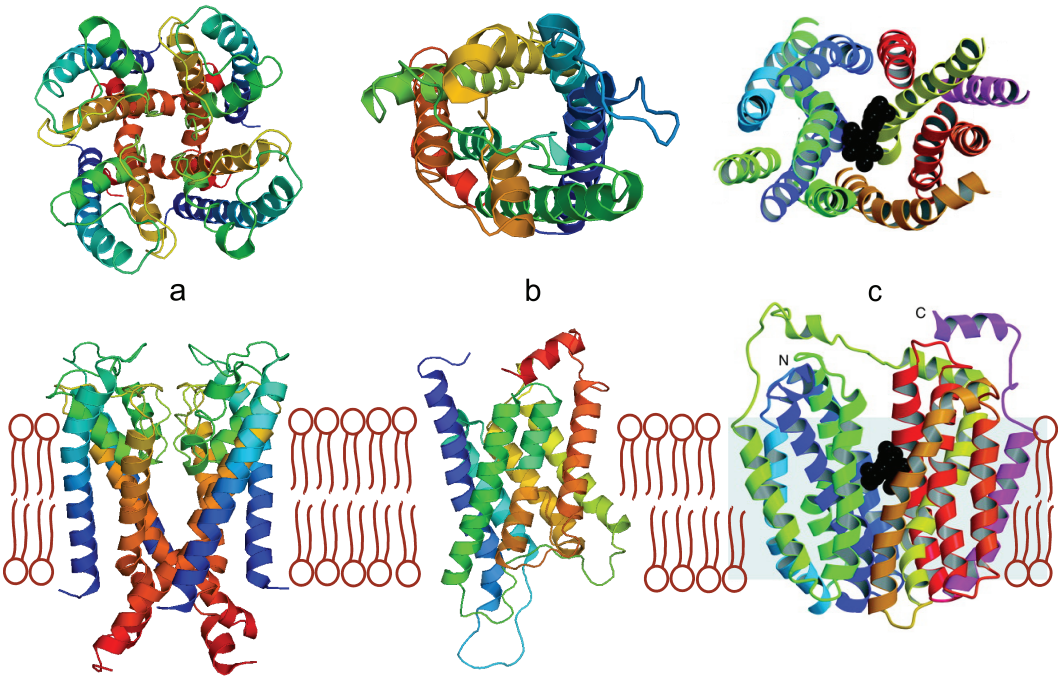

Figure 1.2: 3-D structures of (a) potassium channel KcsA [9], (b) water channel Aquaporin-1 (represented the functional unit) [2] and (c) lactose permease LacY [10]. In the upper part: view from the top of the membrane, in the lower part: the side view. Note that clear transmembrane pore region is only seen for the pore and the channel.

1.4 Channels *vs* Carriers.

The existence of proteins in the membrane that facilitate the passage of solutes was postulated in the fifties by Hodgkin and Huxley to explain the Na^+ and K^+ permeability in neurons [11]. In 1952 the concept of a cotransporter was introduced: a protein that exploit the driving force of a substrate to drive another one [12]. The transport of molecules against their electrochemical gradient was mechanistically explained using an enzyme theory associated with carrier kinetics developed in the late sixties [13]. With the development of new investigation techniques, using electrical recordings and radiolabeled flux measurements, channels and carriers could be distinguished one from the other. The transport rate is usually many times faster for a channel than for a transporter because it does not require a defined sequence of energetic interactions between the channel and the transported ions, like occur for a transporter. This constitutes one of the major functional criteria classically used to distinguish channels *vs.* transporters. With the introduction of high-resolution electrophysiology techniques, like the patch clamp, this clear division began to blur because the recognition of channel-like currents in cotransporters.

One example is the glutamate transporter that belongs to the excitatory amino acid transporter (EAATs) family (SLC1) expressed in neurons and glial cells, where they limit the extracellular glutamate concentration. EAATs exhibit an anion channel activity which, although uncoupled from the glutamate transport mechanisms, is nevertheless gated by glutamate. The EAAT channel is Cl^- selective, and its activation alters synaptic currents more rapidly than Na^+-coupled glutamate transport turnover (10 s^{-1}). In voltage-clamped *Xenopus laevis* oocytes, in which it is possible to measure ion current and substrate flux simultaneously, charge-flux ratios may vary from 12 to more than 100 [14].

In contrast, Accardi, Miller, and colleagues showed that ClC-ec1, a membrane protein predicted by homology to be a Cl^- channel, is actually a Cl^-/H^+ exchanger [15], Cl^- flux in one direction is positively coupled with H^+ flux in the opposite direction with a stoichiometry of 1H:2Cl. ClC-ec1 does not have an obvious channel motif, but then neither do homologous members of the CLC family, which are all thought to be authentic Cl^- channels. Channel-like activity and transporter-type activity can be encounted within the basic structures of most ion transport proteins.

There are examples of transporters that have been modified either chemically (e.g. toxin binding) or by point mutation that exhibit channel-like properties. One of them is the Na^+-K^+-ATPase pump that can be mutated into a cation channel by palytoxin (PTX), a marine coral toxin that selectively binds to the Na^+-K^+-ATPase. It is converted into a non-selective cation channel that acts to dissipate the transmembrane Na^+ and K^+ gradients which are generated by the Na^+-K^+-ATPase acting in its normal transporter mode [16]. Another exam-

ple was demonstrated by Dutzler and co-workers who showed that a single mutation returned ClC-ec1 to a pure chloride selectivity with channel-like properties [17, 18].

Chapter 2

Characterization of secondary active transport proteins.

Characterization of secondary active transport proteins can be undertaken at different levels that varies from the whole organ and specific cells, down to the protein itself together with its interacting on associated protein. By integrating information from different levels a complete characterization can be obtained. In this chapter the characterization will be treated at the levels that correspond to the three main themes covered in this dissertation: mechanism, regulation, structure-function. The most convenient approach to study a secondary-active transport proteins is clone it and over-express it in a simplified system where its characteristics can be studied without significant contamination from endogenous membrane proteins. A common expression system for membrane proteins is the oocyte extracted from the *Xenopus laevis* frog. RNA coding for the protein of interest is injected in each egg and after a given time (few hours-few days) it will be translated into the protein by the oocyte ribosomes and moved to the membrane. One of the main goals of the characterization of a secondary active transporter is to build a model based on biophysical principles that describes its transport mechanism.

2.1 Transport mechanism of secondary active carriers.

Important properties that characterize a secondary-active transporter are:

- specificity of substrates and co-substrates,
- K_m -apparent affinity - for substrates and co-substrates
- stoichiometry: number of substrate and co-substrates involved in each transport cycle

- binding mechanism: order of substrates and co-substrates interactions with the transporter
- turnover rate: number of transport cycles that a carrier performs per second
- transport cycle: constituted by the partial reactions that correspond to binding / debinding of each substrate or co-substrate and the associated conformational changes that allow the carrier to translocate them across the membrane.
- dependence on pH, membrane voltage, presence of the co-substrates
- inhibitors and their mechanism of interaction: competitive, non-competitive or mixed.
- electrogenicity

A transporter can be electrogenic, it can translocate electrical charges per cycle of transport, or electroneutral. If the transporter is electrogenic it is possible to investigate the currents induced by the substrates by electrophysiology using two-electrode voltage clamp or patch clamp, there one must first establish if the currents directly reflect the transport process. For electroneutral transporters it is possible to perform assays with radiolabeled substrates or label the transporter with fluorescent dyes. To show that an interacting molecule is really transported across the membrane it is necessary to use isotopes such as ^{32}P for the phosphate transporters or aminoacids containing ^{14}C for the amino acid transporters or tritium for proton-coupled transporters. Applying different concentrations of substrates allows the determination of the apparent affinity by recording the response to the substrate and fitting the data with model equations to obtain so-called phenomenological parameters. For example it is possible to fit the data with a Hill equation:

$$V_0 = \frac{V_{max} \cdot [S]^{n_H}}{[S]^{n_H} + [K^S_{0.5}]^{n_H}} \tag{2.1}$$

where V_0 is the response (initial reaction rate for the enzymatic reactions), V_{max} is the maximum predicted response and [S] is the substrate concentration. $K^S_{0.5}$ represents the substrate concentration at which the response is half maximal. The Hill coefficient, n_H, indicates cooperativity of the substrates: if $n_H = 1$ the dependence on [S] is hyperbolic and corresponds to the Michaelis-Menten equation; if $n_H > 1$ the dependence on [S] is sigmoidal and indicates cooperativity of the substrate interaction.

It is important to evaluate the carrier behavior at different pHs modifying the pH of the media and comparing the values obtained for the K_m and the V_{max} to understand the interaction of protons with the transporter. They can in fact stimulate or inhibit the interaction

between carrier and substrates or compete with the substrates. In case of multiple substrates that bind, it is important to define if the binding is an ordered or random process. This is done by varying the concentration of one substrate *vs.* the other and see how that influence the transport. To establish the stoichiometry, it is useful to perform assays with both substrates and co-substrates radioactive, or, in case of an electrogenic carrier, to perform two electrode voltage clamp with radioactive tracers, to evaluate the ratio charge/molecule translocated.

To describe the transport mechanism of a secondary active transporter two models have been proposed:

- Alternating access model (fig. 2.1)
- Multi-substrate single-file model (fig. 2.2)

The alternating access model considers a carrier like a gated channel, with a pore containing the binding site for the substrates, and two gates that are alternatively closed or open, preventing the communication pathway between the two sides of the membrane (see fig. 2.1). When the first gate is open, the first substrates can access to the binding site. This induces a conformational change that allows the second substrate to bind and so on, until all the binding sites are fully loaded. The external gate would close, occluding substrates and binding sites. This closed complex is instable and a second gate would open to release the substrates and return to the empty state [19, 20]. This model can explain only some of the carrier-mediated transport properties like coupling stoichiometry or transient currents, in case of an electrogenic transporter. Newer measurements have also revealed additional classes of complexities that cannot be explained by straightforward alternating-access models. There are leakage currents - Na^+ fluxes in the absence of substrates [21]. There are major departures from accepted stoichiometry, so that transport associated currents are several times larger than the flux of organic substrate [22]. There are quantized current events that exceed by several orders of magnitude the single-charge events expected from the model [23].

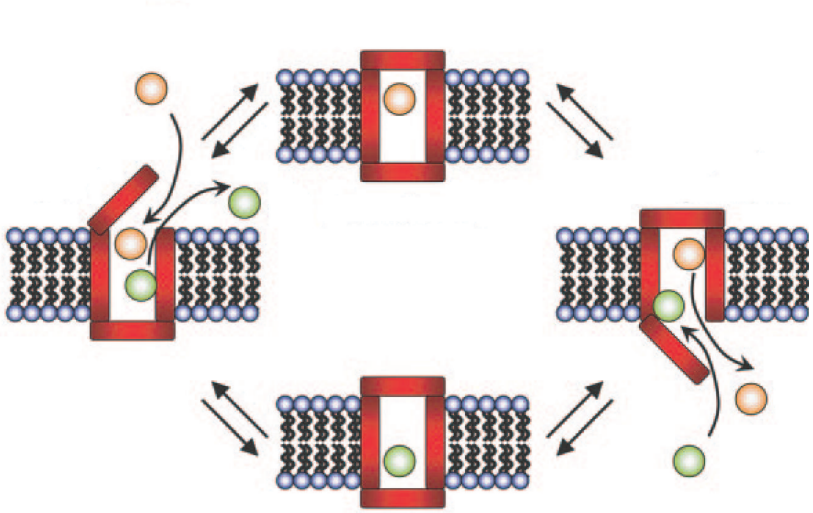

Figure 2.1: Schematic representation of the alternating access model, adapted from [24]

The multi-substrate single-file model has been proposed as an alternative to address these issues. Here, the transporter is considered as a channel with all the binding sites "linearly" distributed along a pore structure similar to the earlier Hodgkin and Keynes model for single-file ion movement in a K^+ channel [25]. After the substrate enters the transporter it can move from one site to the other as soon it will be free. This "single-file" substrate movement proceeds until the exit from the transporter. Each binding site is separated by an energy barrier that needs to be passed to precede to the next binding site. In this model the transporter forms a pore that is always open and ready to translocate the substrates in a defined direction depending on substrate availability (see fig. 2.2). This model has been tested on GAT1, 5-HTT and SGLT1 and it was qualitatively in agreement with the steady state data but does not furnished any information about the transport function. The major limitation of this method is the impossibility, so far, to deal with antiporter or exchanger [20].

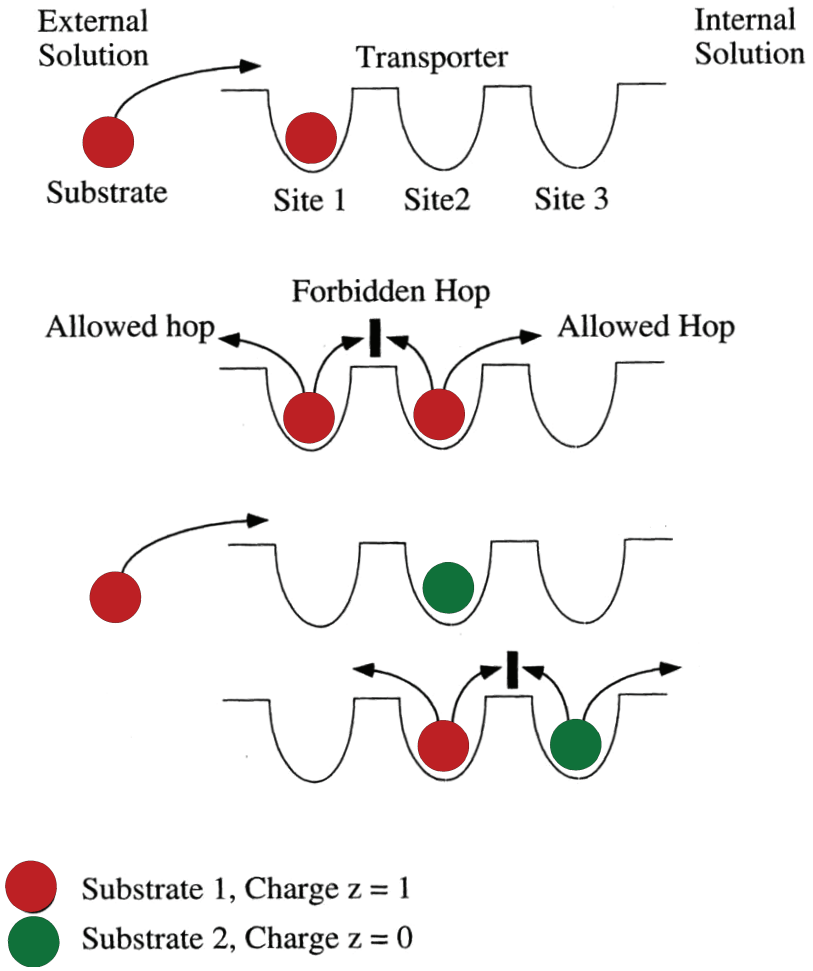

Figure 2.2: Schematic representation of the multi-substrate single-file model. Top: the structure of a transporter with three binding sites, center: the events that are allowed, bottom: the transporter in presence of two substrates (figure adapted from [20]).

Both models take into account the influence of the membrane potential on the transport rate. To understand which model better describes the transporter behavior intensives studies have been done on the GABA transporter GAT1, the result was in favour of the alternating access model [26]. These models are useful tools to understand the transport mechanism but they cannot provide a link between the mechanism with the structure-function aspect of a transporter.

2.2 Structure and structure-function studies.

The essential structural and functional elements of proteins, rather than their amino acid residues, are conserved during evolution. The tertiary structure of a protein describes the folding of its secondary structural elements and specifies the position of each atoms, including its side chains, in the protein. To describe structure-function relationships of a protein is done by identifying functionally important elements in the protein that confer the transport properties and thus contribute to the ultimate goal of having a 3-D model of the protein that conveys both structural and functional information [27].

2.2.1 Crystallographic approach to investigate protein structure-function.

The knowledge of the 3D structure of a protein is extremely useful to identify functionally important sites, like substrate binding sites, voltage or pH sensitive sites, and to acquire information about the possible conformational changes involved in the mechanism of the protein. Obtaining a protein 3D structure is a multi-step process involving extraction, purification, crystallization of the protein and X-ray diffraction of the crystal. The resolution of the crystals can vary from 2Å to 10Å. Membrane proteins show a typical structure composed of alternated hydrophobic and hydrophilic domains stabilized by a phospholipid bilayer, they are insoluble in aqueous buffers and they can denaturate in organic solvents. Direct consequences of these properties are the difficulty to extract and purify enough protein to proceed with the crystallization and to stabilize of the protein during the crystallization phase. Another significant problem in protein structure determination comes from the extreme non-physiological conditions of the crystallization process: high pH, low temperature, complexes with the antibodies needed to stabilize the protein. All these conditions can lead to structural artefacts. The knowledge of the crystal structure of a membrane protein can still leave open questions such as whether the folding revealed in the crystal is the same architecture as in the phospholipid bilayer and under physiological conditions. Information on the molecular dynamics is missing and the structure corresponds to only one possible conformation of the protein.
Structure of channels and pores have been the first to be resolved by X-ray diffraction of the crystals [28–30]. Fortunately also some carrier type membrane proteins have been crystallized and their structure resolved like the Na^+/H^+ antiporter from *E.coli* [31] or lactose permease LacY from *E.coli* [10] or the glutamate transporter homologous of *P.horikshii* [32] or the bacterial homolog Na^+/Cl^- neurotransmitter transporter [33]. Many of the resolved crystal structures are from bacteria, expression and purification of mammalian proteins still present many difficulties and this leads to a lack of knowledge in the structure of mammalian isoforms. Many protein structures show a two-fold symmetry: the division of the protein

structure in two structurally similar half that may have evolved from a gene duplication [30]. The 3D structure so far obtained from the X-ray diffraction of the crystal immortalize the protein in an unique conformation. Ideally to have crystal for every conformational change of the protein would help to better understand the transport cycle. Crystal studies need to be integrated with structure-function studies conducted under physiological conditions.

2.2.2 Non-crystallographic approaches to investigate protein structure-function.

The possibility to study under physiological conditions the functioning of a protein allows the identification of important sites and link them with the structure where possible. Some methods have been proposed to investigate structure-function properties of proteins and they have became extremely useful when applied to membrane proteins that have resisted to the crystallization or where the crystals have yielded poor resolution.

Biochemical methods

SCAM. The substituted-cysteine accessibility method (SCAM) was first introduced by the Karlin group to study ion channel lining residues of the acetylcholine receptor channel [34], and then was extended to other multiple transmembrane segment proteins such as LacY [35], or AE1 the erythrocyte anion exchanger [36] and the type IIa Na^+-P_i cotransporter [27, 37]. It is a powerful technique that uses the specificity of sulfhydryl chemistry [38]. Cysteine residues contain sulfhydryl groups that react with a variety of sulfhydryl-specific reagents. To evaluate the importance of a specific residue within a protein it is possible to mutate it to a cysteine. The cys-modification may result in a clear alteration of the transport properties that can be detected by electrophysiology or tracer-flux techniques. One class of compounds that can react with the cysteine are the methane-thiosulfonate reagents (MTS) by creating disulfide bridges (fig. 2.3). There are different MTS reagents with different charges and volumes. SCAM is based on certain observations. In aqueous media sulfhydryl reagents react with ionized sulfhydryls about $5{\cdot}10^9$ times faster than with unionized SH. Thus, if a sulfhydryl group is in the lipid-accessible surface or in the protein interior, it will not be reactive, because ionization of SH is suppressed due to the low dielectric constant of the environment. The sulfhydryl group of a cysteine residue in a membrane embedded channel or transport protein could be in one of three environments: the water accessible surface, the lipid-accessible surface, or the protein interior. In the presence of sulfhydryl-specific reagents, sulfhydryls in the water accessible surface will be covalently modified by the reagents [39]. The presence of this added molecule reveal information about accessibility and is importance in the functioning of the protein of that residue and the region around it. This new structure

can further modify the properties of the mutant compared to the wild type.

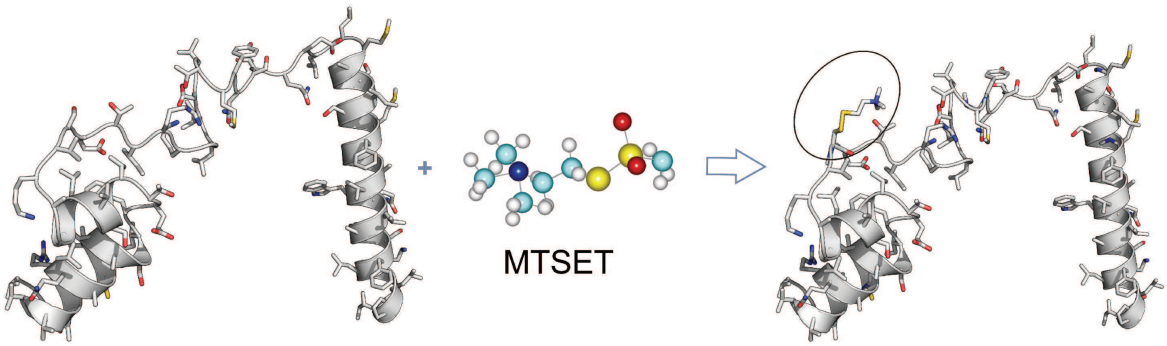

Figure 2.3: Example of a MTS reagent (MTSET) reacting with a cysteine.

Using the information obtained with cysteine scanning it is possible to study the protein topology, the presence of a secondary structure element like α helix or β sheet or investigate a pore or a cavity in the structure. If native cysteines react with the thiol reagent they can give artefacts or allosteric effects, thus ideally all native cysteine should be removed, with the risk that the cys-free mutant construct no longer behaves as the wild type. If any non native Cys reacts with the MTS reagent, it is usually assumed that only the novel one is reacting and all the information are from that particular site of the protein [34, 40].

Thiol cross-linking. This method allows the evaluation of the helix packing of a protein. It is possible to introduce two novel cysteines in two potential sites of the protein and expose them to a cross linking reagent that contains two thiol groups that react with the two Cys to form a disulfide bridge. The crosslinker may alter the properties of the transporter allowing one to infer the distance between two residues and their mobility. In a reducing environment the disulfide bridge can break and the function can be restored. Reducing agents can interact also with native disulfide bridges and break them altering the tertiary structure of the protein. This method has been used with success to elucidate the helix distances in the structure of LacY [41].

FRET. Fluorescence Resonance Energy Transfer is a mechanism describing energy transfer between two chromophores. FRET is a useful tool to quantify molecular dynamics such as protein-protein interactions and protein conformational changes. To investigate, for example, the complex formation between two molecules, one of them is labelled with a donor and the other with an acceptor, and these fluorophore-labelled molecules are mixed. When they are

dissociated, the donor emission is detected upon the donor excitation. On the other hand, when the donor and acceptor are in proximity (1-10 nm) due to the interaction of the two molecules, the acceptor emission is predominantly observed because of the intermolecular FRET from the donor to the acceptor. For monitoring protein conformational changes, the target protein is labelled with a donor and an acceptor at two positions. When a twist or bend of the protein alters the distance or relative orientation of the donor and acceptor, FRET change is observed. The common FRET pair for biological use is a cyan fluorescent protein (CFP)-yellow fluorescent protein (YFP) pair, colour variants of green fluorescent protein (GFP). To study intramolecular interactions like such as protonation and the sugar binding on Lac Y, it is preferable to use smaller chromophores like DACM (N-(7-dimethylamino-4-methylcoumarin-3-yl)maleimide) or MIANS (2-(4'-maleimidylanilino)naphthalene-6-sulfonic acid) organic compound characterized by a multiple-ring system [42]. They in fact interfere less with the movement of the protein thank to the reduced dimensions and emits fluorescence thanks to the highly mobile electrons of the ring system.

SDSL. Site-directed spin labelling (SDSL) is a useful technique employed for mapping elements of secondary structure. The common approach in SDSL is to introduce a novel cysteine into a protein with all non disulfide bonded cysteines removed by site-directed mutagenesis and then to modify this unique cysteine with a nitroxide spin label. This introduces at a specific site within a protein a molecular probe that provides unique spectral signatures in conventional electron paramagnetic resonance (EPR) experiments. The SDSL method was extended to site-specific spin labelling of two sites in a protein or peptide (double site-directed spin labelling, D-SDSL). The distance, and in some cases the relative orientation, between the two spin labels were determined from analysis of spin-spin. If is already available an high resolution structure for a given protein it is interesting to determine how this structure changes under conditions relevant to the function, or to understand the kinetics of structural changes related to the function [43–45].

2.2.3 In silico approaches.

Although large amounts of protein sequence data are produced by modern large-scale DNA sequencing efforts, the output of experimentally determined protein structures is not even comparable due to the high time-consuming and costs of the two main techniques X-ray crystallography and NMR spectroscopy. The possibility to predict the structure of a protein starting from the primary sequence becomes an important goal. Protein structure prediction is made difficult by many factors, the main ones being that the number of possible protein structures is extremely large, and that the physical basis of protein structural stability is not

fully understood. Direct simulation of protein folding in atomic detail, via methods such as molecular dynamics with a suitable energy function, is limited by the number of residues, due to the high computational cost. In addition: -1- some proteins require stabilization by additional domains or binding partners to adopt their native structure -2- the tertiary structure of a native protein may not be readily formed without the aid of additional agents, for example, chaperone proteins. Other proteins cannot fold properly without modifications such as glycosylation -3- a particular protein may be able to assume multiple conformations depending on its chemical environment -4- the biologically active conformation may not be the most thermodynamically favorable. Due to the increase in computer power, and new algorithms, much progress is being made however, routine *de novo* prediction of protein structures, even for small proteins, is still not achieved.

Comparative protein modelling. This uses previously solved structures as starting points or templates. This is effective because it appears that although the number of actual proteins is vast, there is a limited set of tertiary structural motifs to which most proteins belong. It has been suggested that there are only around 2000 distinct protein folds in nature, though there are many millions of different proteins. The homology modelling is based on the reasonable assumption that two homologous proteins will share very similar structures. Because a protein's fold is more evolutionarily conserved than its amino acid sequence, a target sequence can be modelled with reasonable accuracy on a very distantly related template, provided that the relationship between target and template can be discerned through sequence alignment. Homology modelling can produce high-quality structural models when the target and template are closely related, in fact given an amino acid sequence of an unknown structure and the solved structure of a homologous protein, each residue in the solved structure is computationally mutated into the corresponding one of the unknown one. The distance and the dihedral angle restraints for the model are calculated from the alignment with the template 3D structure. This method has been applied with success for example to predict the structure of the human facilitative glucose transporter GLUT1 [46], modelled on the basis of the glycerol-3-phosphate transporter and for the serotonin transporter SERT on the basis of the LeuT structure [47]. For both transporters the experimental data were in agreement with the model proposed.

2.3 Physiological regulation.

Many transporters physically associate with adapter proteins that regulate their subcellular localization. Additionally, the associated protein may control the direct interaction of the transport protein with signal transduction complexes that include receptors, second messenger-producing effector enzymes, and protein kinases. A typical example is the involvement of NHERF-family proteins in the localization and acute regulation of the type II Na^+-P_i cotransporter within apical signaling complexes of renal epithelial cells. Via immunoprecipitation and immunohistological methods has been demonstrated that many transport proteins interact, via direct protein-protein association, with a variety of regulatory proteins that have been generically termed "adapter proteins". They contain several different types of highly conserved modular protein-protein interaction domains (for example the src homology 2 domains that recognize phosphotyrosine motifs) that allow the associated proteins to act as molecular bridges between two or more different proteins (see fig. 2.4). These associated proteins include signaling proteins, membrane transport proteins, and cytoskeletal elements. They can affect the function of transporters mainly in two ways: - 1 - modulate the steady-state population at the plasma membrane by affecting trafficking - 2 - concentrate the transport protein within subdomains of the plasma membrane that are also enriched in the receptors or other signaling proteins known to acutely regulate the trafficking or activity of the transport protein [24]. Adapter proteins often contain so-called PDZ interaction domains [48] (the name derives from three proteins in which the motif was first recognized). NHERFs comprise a family of PDZ-containing adapter proteins that play important roles in the regulation of several ion transport proteins [49]. The type II Na^+/P_i cotransporter in the proximal tubule is responsible for most of the reabsorption of phosphate from the glomerular filtrate. Increases in serum phosphate (due to diet and other factors) elevate PTH levels, which, in turn, act to decrease the NaPi-II-mediated recovery of filtered phosphate. This PTH-induced decrease in NaPi-II transport activity involves a rapid decrease in the abundance of NaPi cotransporters in the apical membrane due to acute changes in the steady-state trafficking of NaPi-II between cell surface and intracellular membrane pools [50]. Is has been shown that the mechanisms by which PTH triggers the changes in NaPi-II involves NHERFs as the directly coordinator of the regulation of both Na^+/P_i type II cotransporters and PTH receptors [24].

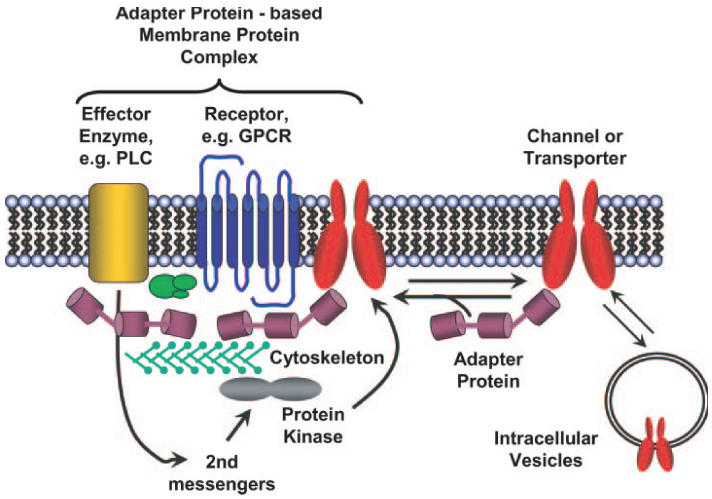

Figure 2.4: Scheme of how adapter proteins can regulate the trafficking of ion transport proteins and the assembly of the signaling complexes that include ion transport proteins, receptors, effector enzymes, and cytoskeletal proteins. PLC, phospolipase C; GPCR, G protein-coupled receptor (from Dubyak et al. 2004 [24]).

Also phospholipids can interact and influence the membrane protein behavior, the function of many transporters is directly modulated by the specific binding of phosphatidyl-inositol-4,5-bisphosphate (PIP_2). This binding permits rapid modulation of substrate transport activity by highly localized changes in PIP_2 synthesis or degradation. The activity of some transporters increases as the local PIP_2 is elevated, whereas others exhibit reduced activity in the presence of PIP_2. Membrane transport proteins positively regulated by PIP_2 include plasma membrane Ca^{2+}-ATPase pumps (PMCA), Na^+/Ca^{2+} exchangers (NCX), Na^+/H^+ exchangers (NHE) [51]. The ability of PIP_2 to act as a positive or negative modulator of membrane transport proteins underscores its important role in signal transduction at the cellular level.

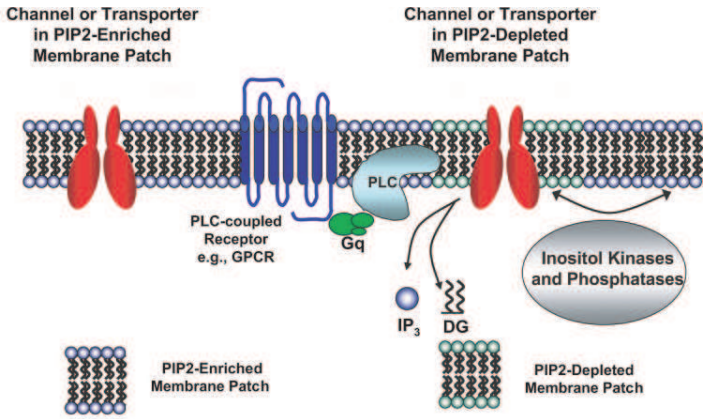

Figure 2.5: Scheme of how local changes in phosphatidylinositol-4,5-bisphosphate (PIP_2) levels can regulate the functional characteristics of a nearby ion transport protein (from Dubyak et al. 2004 [24]).

Chapter 3

Transport of inorganic phosphate.

3.1 Phosphate as a physiological solute.

The phosphate ion is a polyatomic ion with empirical formula and PO_4^{3-} and mass of 94.973 g/mol; the central phosphorus atom is surrounded by four identical oxygens in a tetrahedral arrangement. The phosphate ion carries a negative three formal charge and is the conjugate base of the hydrogen phosphate ion, HPO_4^{2-}, which is the conjugate base of $H_2PO_4^-$, the dihydrogen phosphate ion, which in turn is the conjugate base of H_3PO_4, phosphoric acid. In dilute aqueous solution, phosphate exists in four forms. In strongly-basic conditions, the phosphate ion (PO_4^{3-}) predominates, whereas in weakly-basic conditions, the hydrogen phosphate ion HPO_4^{2-} is prevalent. In weakly-acid conditions, the dihydrogen phosphate ion ($H_2PO_4^-$) is most common. In strongly-acid conditions, aqueous phosphoric acid (H_3PO_4) is the main form. The equilibrium between the species in aqueous solution is regulated by the following reactions:

1. $H_3PO_4 \rightleftharpoons H^+ + H_2PO_4^-$
2. $H^+ + H_2PO_4^- \rightleftharpoons H^+ + HPO_4^{2-}$
3. $HPO_4^{2-} \rightleftharpoons H^+ + PO_4^{3-}$

The second reaction predominates under physiological conditions with a pKa = 6.8. In the extracellular fluid (pH = 7.4) only $H_2PO_4^-$ and HPO_4^{2-} ions are in significant amounts. Their proportion is 1:4.

Phosphorus plays an important role in many aspects of cellular metabolism like in the synthesis of ATP, source of energy for many cellular reactions, in the synthesis of DNA, RNA and of 2,3-diphosphoglycerate, which regulates the dissociation of oxygen from haemoglobin. It is also crucial for intracellular signaling and it is one of the components of the membrane phospholipids. Inorganic phosphate (P_i) is essential for the formation and mineralization

of bone. P_i is not only an integral component of the hydroxyapatite crystal, but is also necessary for the development and the activity of osteogenic cells, which are involved in the synthesis and calcification of bone extracellular matrix [52]. Changes in phosphorus content, concentration, or both, modulate the activity of a number of metabolic pathways.

Distribution In the body 80% to 85% of the phosphorus is found in the skeleton (approximately 0.6 kg of elemental phosphorus). A smaller amount of phosphorus (0.1 kg) exists in the soft tissues, mainly as organic phosphates such as phospholipids, phosphoproteins, nucleic acids, and nucleotides. An even smaller amount (∼500 mg) is present in the extracellular fluid as inorganic phosphate. The daily dietary intake of phosphorus is typically 1200 mg, mostly as inorganic phosphate. Dairy products are the major source. The net absorption of phosphate by the intestines is approximately 950 mg/day. In the steady state, bone has relatively small phosphate turnover, about 300 mg/day. The kidneys filter approximately 14 times the total extracellular pool of phosphate per day (∼7000 mg/day) and reabsorb about 6100 mg/day. The net renal excretion of phosphorus is around 800 mg/day, the same as the net absorption by the GI tract, as shown in fig. 3.1

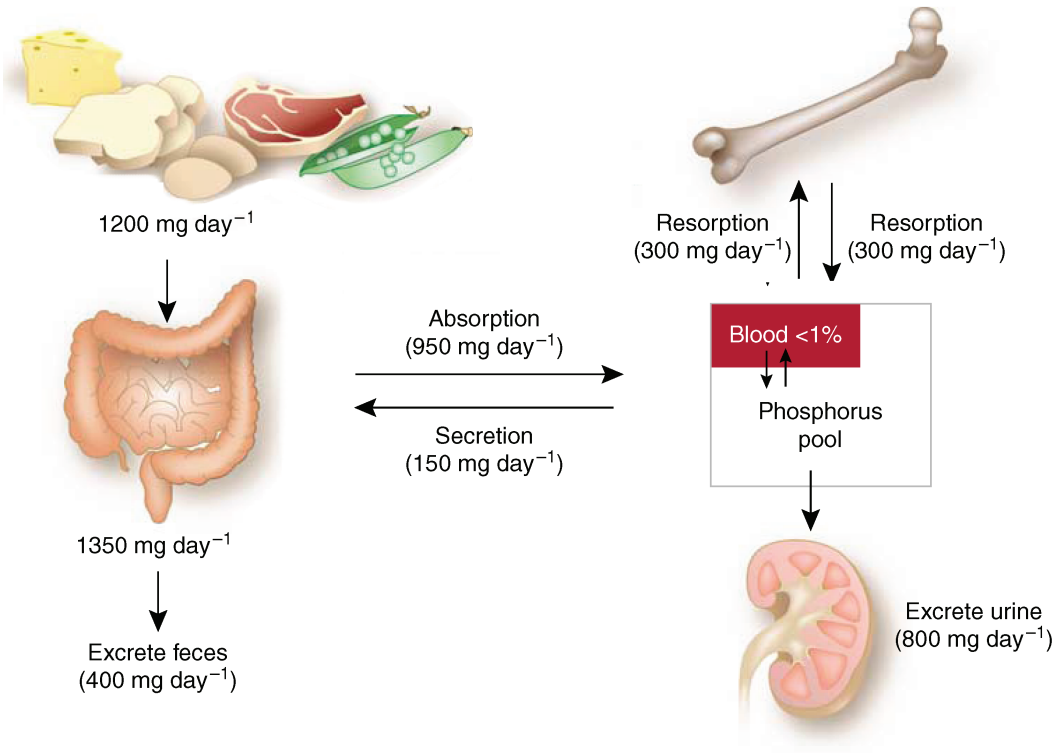

Figure 3.1: Daily phosphate equilibrium between the major body compartments (from Hruska et al. 2008 [53]).

Regulation The plasma concentration of total inorganic phosphate depends mainly on of the equilibrium between bone metabolism, gastrointestinal absorption, and kidney excretion-reabsorption. About half of total plasma phosphate is in an ionized form, and the rest either complexed to small solutes (∼40%) or bound to protein (∼15%). Both hypo- and hyperphosphatemia have severe clinical consequences [53, 54]. The plasma concentration varies rather widely, between 0.8 and 1.5 mM (2.5-4.5 mg/dl of elemental phosphorus) a variation of 80% and the filterable phosphate (both the ionized and complexed) varies between about 0.7 and 1.3 mM. Between 85% and 90% of the circulating phosphate is filterable by the kidneys. Each day the kidneys filter approximately 7 g of phosphate. As this is more than an order of magnitude greater than the total extracellular pool of phosphate, this fact suggests that the kidney must reabsorb most of the phosphate filtered in the glomerulus (fig.3.2).

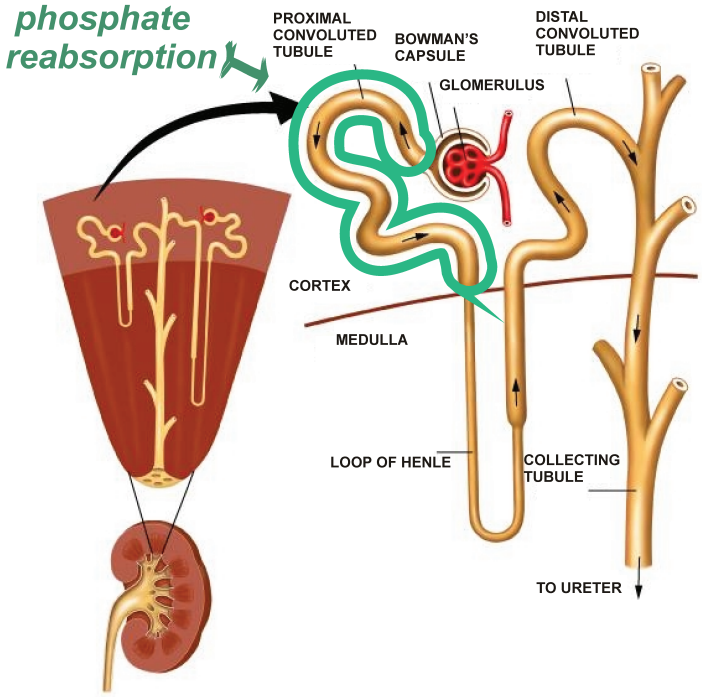

Figure 3.2: Schematic representation of a kidney vertical section and in detail the scheme of a nephron (adapted from www.uptodate.com).

Thus kidneys (fig.3.2) are the major players in keeping constant the concentration of the phosphate in the extracellular fluids and they work under strict physiological regulation. The net excretion of phosphate is the result of the equilibrium between glomerular filtration and tubular reabsorption. Under normal physiological conditions ∼80-90% of the phosphate filtrate is reabsorbed, mainly in the proximal tubule of juxtamedullary nephrons with a higher rate in the S1 segments [55]. The reabsorption of phosphate in the proximal tubule is in-

fluenced by various factors, the three most important are: dietary phosphate, parathyroid hormone (PTH), vitamin D and fibroblast growth factor-23 (FGF23). A low dietary phosphate intake can induce almost a 100% of P_i reuptake from the primary urine, whereas a high content of P_i in the diet leads to a reduction of proximal tubular reabsorption. PTH administration induces phosphaturia whereas removal of PTH cause reduction of phosphate in the urine. The vitamin D effect is opposite to the PTH one, stimulating reabsorption of P_i [56]. FGF23, in mice leads to hyperphosphaturia owing to a reduction of NaPi-IIa in the proximal BBM whereas FGF23 deficient mice show hyperphosphatemia [57]. Other factors that regulate the P_i reabsorption in the proximal tubule are: insulin that enhance the P_i reuptake and prevent the action of PTH, growth hormone also enhance the reuptake, glucocorticoids, atrial natriuretic peptide, prostaglandin and also non-hormonal factors like fasting, plasma calcium acid-base and volume expansion.

Patho-physiology In addition to the physiological regulatory factors there are some patho-physiological conditions that can alter phosphate homeostasis. Several genetic defects can cause renal phosphate wasting like X-linked hypophosphatemic rickets, autosomal dominant hypophosphatemic rickets not associated with hypercalcinuria and hereditary hypophosphatemic rickets with hypercalciuria [54, 58]. A form of genetically determined reduction in renal phosphate handling is detected in Dent's disease, where mutations in a chloride channel (CLC5) lead to an apparent P_i transport defect [59]. Disturbance in tubular phosphate transport seems to be an early indicator of non specific proximal tubular alteration like in the diabetes mellitus where the augmented glucose load leads to a phosphaturia induced by the reduced driving force for the P_i reuptake. The reabsorption of P_i can be reduced also by a damage of the brush border membrane of the proximal tubule or by the administration of diuretics like acetazolamide [55, 59, 60]

3.2 Protein family identified as phosphate transporters.

In principle, two kinds of membrane transport proteins could mediate transport of phosphate across plasma membrane:

- *phosphate selective anion channels*
- *phosphate transporters*

Phosphate channels have been identified in organelles like vacuoles. Movement of phosphate through slow vacuolar (SV) ion channels and the effects of phosphate on SV currents were investigated using vacuoles from beetroots of *Beta vulgaris* [61]. In mammalian skeletal

muscle sarcoplasmic reticulum, two anion channels , the small conductance (SCl) and big conductance (BCl) chloride channels, were both found to have a $P_i$conductance. The SCl channel is a divalent anion channel which can pass HPO_4^{-2}. The BCl channel is primarily a monovalent anion channel [62]. Channels would not be good in creating a P_i gradient across the membrane compared to the P_i tranporters.

Phosphate cotransporters have been found in all phyla: they translocate P_i using the electrochemical gradient of either Na^+ ions or protons. Phosphate reabsorption at the brush border membrane of proximal tubule is strictly dependent on the presence of sodium ions, which indicates that there is no paracellular phosphate pathway [63]. Thus the reuptake of P_i is mediated by phosphate transporters that use the Na^+ electrochemical gradient, maintained by the Na^+/K^+-ATPase at the basolateral membrane, as driving force. Two unrelated families [1] of Na^+/P_i cotransporters have been identified as being mainly responsible for this function: the type II and the type III sodium coupled phosphate cotransporters. They have been named as SLC34 (NaPi-II) and SLC20 (NaPi-III) according to the Human Gene Nomenclature Committee Database. So far no detailed information is available about the identity of proteins that mediate P_i efflux at the basolateral membrane.

3.2.1 Type II Na^+/P_i cotransporter.

The SLC34 family comprises three members: NaPi-IIa, mainly localized in kidney proximal tubules and also in osteoclasts and neurons, NaPi-IIb, in small intestine, lung testis, liver, secreting mammary gland and prostate gland, NaPi-IIc in kidney proximal tubules [66]. Non mammalian homologs of the SLC34 proteins have been identified in bacteria (*Vibrio cholera*), amphibians (*Xenopus laevis*), invertebrates (*Caenorhabditis elegans*), and fish (zebrafish or flounder). That indicates an early evolutionary appearance of the type II Na^+/P_i cotransporters [66].

NaPi-IIa.

This was identified by functional expression cloning using *Xenopus laevis* oocytes from a rat and human kidney cDNA library. The major site of expression is the renal proximal tubule and here, this protein (80-90 kDa) is localized in microvilli that constitute the brush border membrane. Under normal physiological conditions, the abundance of NaPi-IIa is

[1] **Type I Na^+/P_i cotransporter.** A gene product from the SLC17 family was identified as Na^+/P_i cotransporter, NaPi type I, in a study where it has been expressed in *Xenopus* oocytes and was founded in brush border membrane of proximal tubules [64]. It has been shown that it is not involved in phosphate reuptake but in organic anion transport [65].

highest in S1 proximal tubular segments of juxtamedullary nephrons [67]. When the NaPi-IIa gene is knocked out the mice show a reduction of 70% in the P_i reuptake [59,68]. Na^+/P_i cotransport by NaPi-IIa is electrogenic, involving the inward transfer of one net positive charge per transport cycle. Divalent phosphate is the preferred species and is transported together with three Na^+ ions [69]. The substrates (three Na^+ ions and one HPO_4^{2-} ion) bind in an ordered manner: $2Na^+/P_i/Na^+$ (see fig. 3.3) [70]. Typical apparent substrate affinities are: Km^{P_i} ∼0.1 mM; Km ^{Na} ∼50 mM. In the absence of P_i, the transporter operates in a uniport mode, whereby Na^+ ions leak according to the electrochemical gradient with a probable stoichiometry of 1 Na^+ ion [71]. Protons interact with the empty carrier and the final Na^+ binding steps. Higher transport rates are observed at more basic external pH [27]. The trasnporter show high sensitivity to phosphonoformic acid (PFA) [72].

NaPi-IIb.

NaPi II-b was identified based on EST clones derived from lung tissue [73]. Expression of NaPi-IIb mRNA has been detected in a number of tissues such as small intestine, lung, mammary glands, testis, and liver [74]. By immunofluorescence, NaPi-IIb was localized in brush border membranes of enterocytes, in the apical pole of alveolar type II cells as well as in apical membranes of mammary secretory cells [66, 73]. On Western blots, fully glycosylated NaPi-IIb is observed as a band of approximately 108 kDa [66] whereas in weaning animals NaPi-IIb was reported to be only partially glycosylated [75]. At the primary sequence level NaPi-IIb differs from NaPi-IIa mainly in the C-terminus, which is rich in cys residues and longer by approximately 50 amino acids for the NaPi-IIb. Na^+/P_i-cotransport is also electrogenic with a stoichiometry of 3Na:1Pi and with Km^{P_i} ∼50 μM and Km ^{Na} ∼40 mM. Dependence on pH is moderate, slightly higher cotransport is observed at more acidic pH [73]. NaPi-IIb is involved in transcellular flux of phosphate in the small intestine [73,76]. The most prominent regulators of NaPi-llb in small intestine are 1,25-$(OH)_2$-vitaminD_3 and low-phosphate diet. Up-regulation of NaPi-IIb induced by these factors is manifested by an increase of the protein abundance and appears, in adults, to be non-transcriptional [76, 77].

NaPi-IIc.

The NaPi-IIc cotransporter was identified based on its homology with the NaPi-IIa cotransporter [78]. The NaPi-IIc transporter has a high affinity for P_i (Km^{P_i} ∼70 μM; Km ^{Na} ∼50 mM). It is highly pH dependent and exhibits higher transport at more alkaline pH [78, 79], is electroneutral and exhibits a 2:1 stoichiometry. In rodents NaPi-IIc is localized only in the apical membranes of the renal proximal tubule - S1 segment- [80, 81]. The relative abundance of NaPi-IIc protein is significantly greater in the kidney of weaning rodents than

adult animals, which suggests that the NaPi-IIc transporter is a growth-related renal NaPi transporter [78]. The key regulators of NaPi-IIc expression are dietary P_i intake, PTH and FGF23 [78, 81]

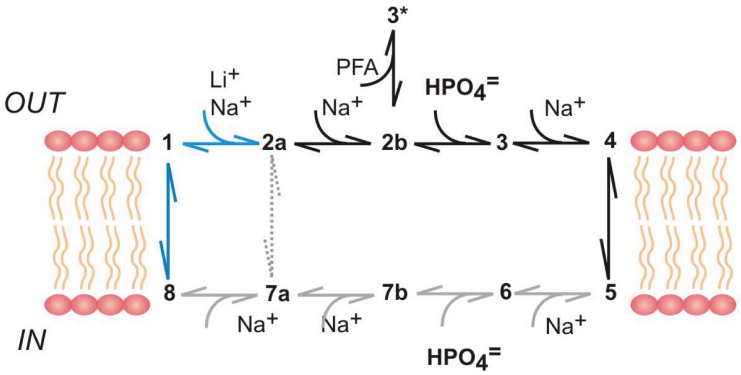

Figure 3.3: Proposed transport mechanism scheme for SLC34 proteins, numbers indicate conformational states of the protein. Light grey indicates transitions for intracellularly facing conformational changes that are uncharacterized (from Virkki et al. 2007 [82]).

Structural aspects of type II Na^+/P_i-cotransporters show similarity between the isoforms. As predicted from structure-function studies [27], each type II Na^+/P_i-cotransporter protein most likely has eight transmembrane domains (see fig. 3.4). Both N- and C-termini are located in the cytoplasm and all the isoform present multiple N-glycosylation sites in a large extracellular loop. Furthermore, two short loops (one extracellular and one intracellular) have been postulated to be important functional regions for the transport pathway (see blue circles on fig. 3.4)[10, 24]. This model is based on data obtained studying NaPi-IIa and appears to be valid for the other family members as well, since in all members, the transmembranous regions are over 80% identical and exhibit the same hydropathy profile [10]. The largest dissimilarities are found in the N- and C-termini and in the large extracellular loop. Based on results obtained with tandem constructs of NaPi-IIa, it is assumed that the monomeric form is sufficient for full type II-mediated Na^+/P_i cotransport [66]. There is only one known inhibitor of the type II of Na^+/P_i cotransporter: phosphonoformic acid (PFA) [71, 72].

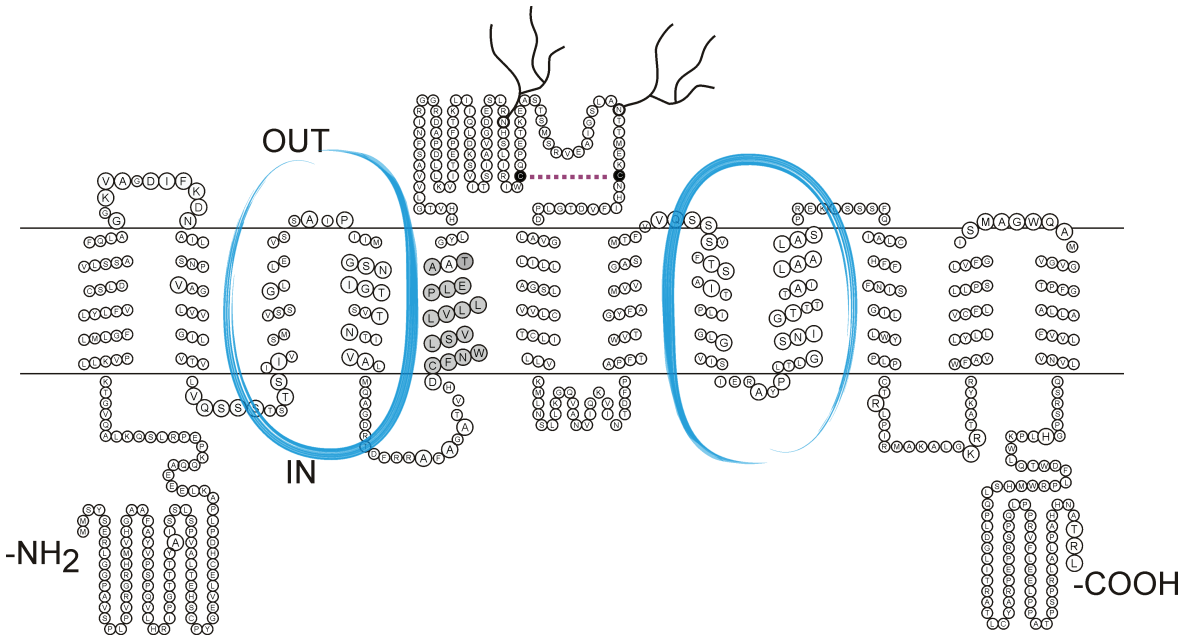

Figure 3.4: NaPiIIa proposed topology [82]. In blue the re-entrant loops.

3.2.2 Type III Na^+/P_i cotransporter: PiT1&2.

The SLC20 family is composed of two members: PiT1 and PiT2. These two proteins were identified as Na^+/P_i cotransporters about 15 years ago; before then they were studied in the context of their function as surface receptor for Gibbon Ape Leukemia Virus (Galvr-1: PiT1) and Amphothophic Leukemia Virus (Ram-1: PiT2). One of the most important issues in virology is the identification of cell surface receptors that act as portals of virus entry into animal cells. These receptors were first characterized not as molecules, but as genetic determinants of pseudotype or vector entry [83]. The determination of receptor expression patterns, and elucidation of the effects of infection on the normal functions of these molecules are critical investigation points, especially in the case of retroviruses because cells can become chronically infected, leading to receptor down-modulation and subsequent derangements in cellular functions.

Several retroviral receptor cDNAs have been isolated like those that mediate infections of gibbon ape leukemia virus (GALV) and of mouse amphotropic retrovirus, Glvr-1 and Ram-1, respectively [84–86]. They are distinct proteins with putative multiple hydrophobic transmembrane domains. They share about 60% overall sequence identity and they show about 25% identity with a putative phosphate permease of *Neurospora crassa* [85–88]. These data have suggested that Glvr-1 and Ram-1 might be transporters. The transporter activities of Glvr-1 and Ram-1 have been investigated by a systematic approach that involved expression of these proteins in *Xenopus laevis* oocytes and measurement of transmembrane currents

during exposure of the oocytes to different salts and nutrients and by ^{32}P uptake [89, 90]. Results have been confirmed by expression in mammalian cells and measurement of ^{32}P uptake. These studies concluded that Glvr-1 and Ram-1 are Na^+/P_i symporters characterized by phosphate transport rates affected both by retroviral infection and by changes in extracellular phosphate concentrations. These transporters are electrogenic and mediate net cation influx [89]. PiT-1- and PiT-2-related proteins are present in all phyla (fig.3.5)

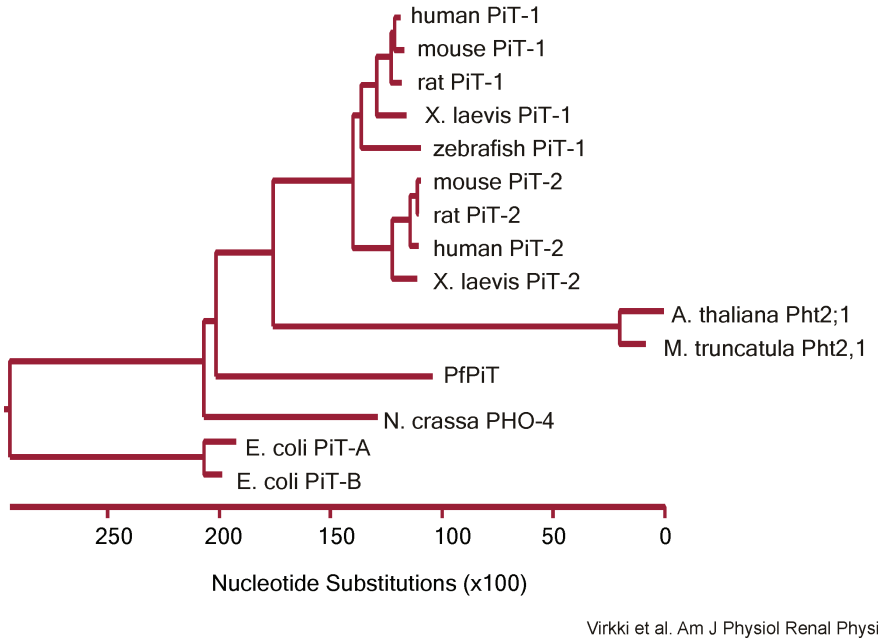

Figure 3.5: Phylogenetic tree of SLC20 cotransporter families. Amino acid sequences were aligned using ClustalW. GenBank accession numbers are listed in parenthesis. The following sequences were used: human PiT-1 (NM_005415), mouse PiT1 (AAB31458), rat PiT1 (NM_031148), X. laevis PiT-1 (AAH59957), Danio rerio PiT-1 (NM_213179), mouse PiT-2 (NM_011394), rat PiT-2 (NM_017223), human PiT-2 (NM_006749), X. laevis PiT-2 (BC084098), Arabidopsis thaliana Pht2;1 (NM_113565), Medicago truncatula Pht2;1 (AAN46087), Plasmodium falciparum PfPiT (AJ580003), Neurospora crassa Pho-4 (XM_954396), Escherichia coli PitA (NC_002655), and E. coli PitB (NC_000913) from Virkki et al. 2007 [82].

In prokaryotes and in plants, P_i transport is coupled to the H^+ gradient [91–93], whereas in animals and fungi, the driving cation is Na^+ [94–96]. In the bacterium *Bacillus subtilis*, the related protein CysP mediates H^+/SO_4^{2-} cotransport [97], but so far no other PiT family member has been shown to transport SO_4^{2-}.

3.2.3.1 Tissue distribution and proposed physiological roles.

Levels of virus receptor expression in different tissues influence the course of retroviral infection and thus the gravity of the consequent disease. The expression pattern is an important parameter for gene transduction studies, especially in the case of gene therapy. RNAs of both PiT1 and PiT2 were detected in mouse, rat and human tissues: kidney, heart, brain,

placenta, lung, liver, skeletal muscle, pancreas, spleen, thymus, prostate, testis, ovary, small intestine, colon, and peripheral blood leukocytes (see fig. **??**) [84, 88, 89, 98–100]. The expression patterns vary for each protein: for example in the bone marrow, which contains little PiT2 RNA but abundant PiT1 RNA, or in the heart, where the proportionS are opposite [89, 101]. The relevance of inorganic phosphate for the formation and mineralization of bone prompted a detailed investigation of the P_i transporters involved in the development and activity of osteogenic cells that are involved in the synthesis and calcification of the bone extracellular matrix. The presence of PiT1 mRNA has been show in osteoblast-like cells like in human osteosarcoma-derived SaOS-2 [52] or MC3T3 [102] PyMS and *calvaria* primary cultured cells from new born and adults rats [101]. However it has been shown that the amount of RNA did not correlate with either the retrovirus infectibility [98] or probably with the amount of protein expressed at the plasmamembrane. At the protein level the expression has been documented in liver (PiT1 and 2) [103] and in the kidney (PiT2) [104], mouse tissues kidney, heart, thymus, muscle and brain (PiT1) [105], in crude membrane preparations from OK cells and umbilical cord endothelial cells from human, rat, rabbit, hamster and mouse (PiT1) [105].

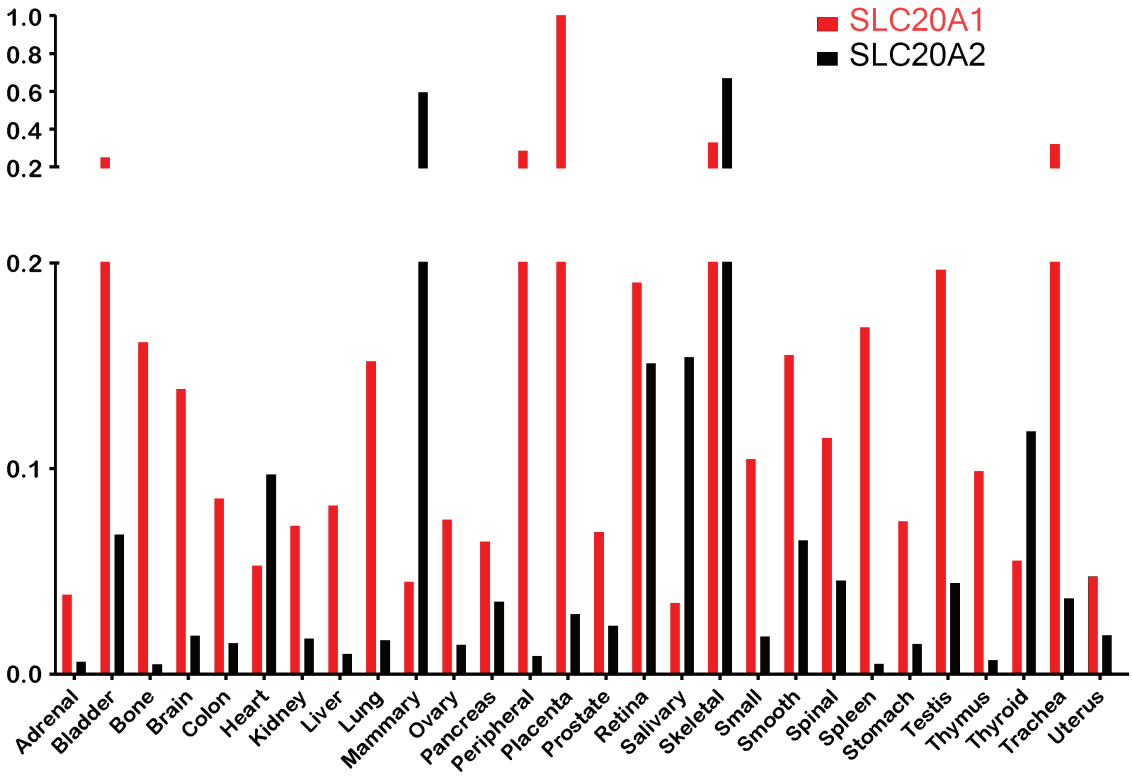

Figure 3.6: Expression of human SLC20A1 and SLC20A2 transporter mRNAs in various tissues. Values are from Nishimura and Naito 2008, normalized to the highest expression level (placenta-SLC20A2: 0.96) [106].

This broad tissue distribution suggested a possible role as phosphate housekeeping but

recent studies see PiT proteins involved in various physiological and pathophysiological processes. For example, PiT-mediated P_i transport appears important in bone mineralization [101, 107–111]. It has been shown that in cultured bone-derived cells P_i transport and PiT mRNA levels are regulated by many factors like P_i, epinephrine, platelet-derived growth factor (PDGF), insulin-like growth factor (IGF-1), and basic fibroblast growth factor (bFGF) in osteoblast-like cells [101,112–114]. In addition to playing a role in normal calcification, PiT proteins were recently implicated in pathological processes, such as calcification of vascular tissue induced by hyperphosphatemia [115, 116].

Regulation of PiT function has also been shown for extra-skeletal cells and tissues like in human embryonic kidney cells (HEK-293) where PiT1-mediated P_i transport is regulated by P_i levels and PTH [117]. In rat parathyroid glands, PiT-1 mRNA levels are regulated by plasma vitamin D and P_i levels [99]. At the protein level only limited data are available regarding the tissue and subcellular distribution of PiT-1 and PiT-2. In osteoclasts and macrophages has been shown that transfected protein localizes to the basolateral membrane [118] indicating an involvement of PiT1 in P_i transport in bone-resorbing osteoclasts. PiT proteins may also play a role in P_i transport in the distal segments of the kidney [119]: both PiT-1 and PiT-2 mRNAs are present in immortalized mouse distal convoluted tubule (MDCT) cells and the pH dependence of P_i transport is consistent with PiT-mediated transport. In the liver, PiT-1 and PiT-2 localize to the basolateral membrane in hepatocytes [103], whereas in airway epithelial cells PiT2 is expressed both apically and basolaterally [120].

Finally, it was recently reported that the malaria parasite *Plasmodium falciparum* expresses a homologous PiT protein (*Pf*PiT) in its plasma membrane and that is critical for supplying P_i to the parasite into the erytrocyte. PfPiT-mediated P_i transport is energized by the Na^+ gradient and, because infection causes a gradual increase in intracellular Na^+, there is adequate driving force for P_i uptake via PfPiT [121].

3.2.3.2 Transport mechanism of PiT1 & 2.

Transport mechanism Very limited characterization of the transport kinetics of either PiT1 or PiT2 has been reported [89, 100, 101, 119, 122, 123]. In oocytes expressing rat PiT1 or human PiT2 the concentration dependence of phosphate uptake followed as expected for a solute carrier a Michaelis-Menten kinetics: for PiT1 the P_i apparent affinity (K_m) was 24.1±5.5 μM, and for PiT2 25.3±6.0 μM; in transfected fibroblasts the values were: 70 μM, Km^{P_i} for PiT1, and 200 μM for PiT2 [89]. For PiT2 has been reported also a Km^{Na} of 36.3±19 mM and a Hill coefficient of 1.12 indicating weak cooperativity of Na^+ interaction [100]. Kinetic analysis have been investigated in parathyroid glands: *Xenopus* oocytes have been injected with rat PiT1 or parathyroid poly(A)$^+$RNA showed that the

Km^{P_i} are (89±13) and (123±59) μM, respectively. The kinetic properties of P_i transport in Xenopus oocytes expressing rat PiT1 and rat parathyroid glands was not significantly different (89±13) and (140±20) μM, respectively [99]. In PyMS osteoblast-like cells Km^{P_i} for PiT1 has been evaluated 109±12 μM [101]. For human PiT1 expressed in *Xenopus* oocytes a Km^{P_i} of 322.5±124.5 μM was determined, while for PiT2 Km^{P_i} was 163.5±39.8 μM and the Hill coefficient was n=2 indicating a cooperative substrate binding [122].

Bøttger and coworkers published that PiT1 and PiT2 sustain Na^+/P_i transport function at various pH values without significant modification of the ^{32}P uptake [122], whereas Olah and coworkers discovered an increase of ^{32}P uptake in MDTF cell expressing PiT1 at pH 6.5 and 7.5 [90]. Several groups have consistently reported that PiT1 and 2 show reduced activity at alkaline pH [89, 90, 100].

The possibility of other substrates interacting with PiTs has been investigated by Bøttger et al. [122] but without significant findings.

The relative large variations in kinetic parameters reported in the literature for PiT1 and PiT2 is more than what would be expected for heterologous expression and may reflect the effect of low membrane expression of the specific transporter. For example, although the data reported by Kavanaugh et al. (see fig. 3.7) show a typical P_i induced inward current, the magnitude of this current and uptake are significantly small compared to data published for SLC34 proteins.

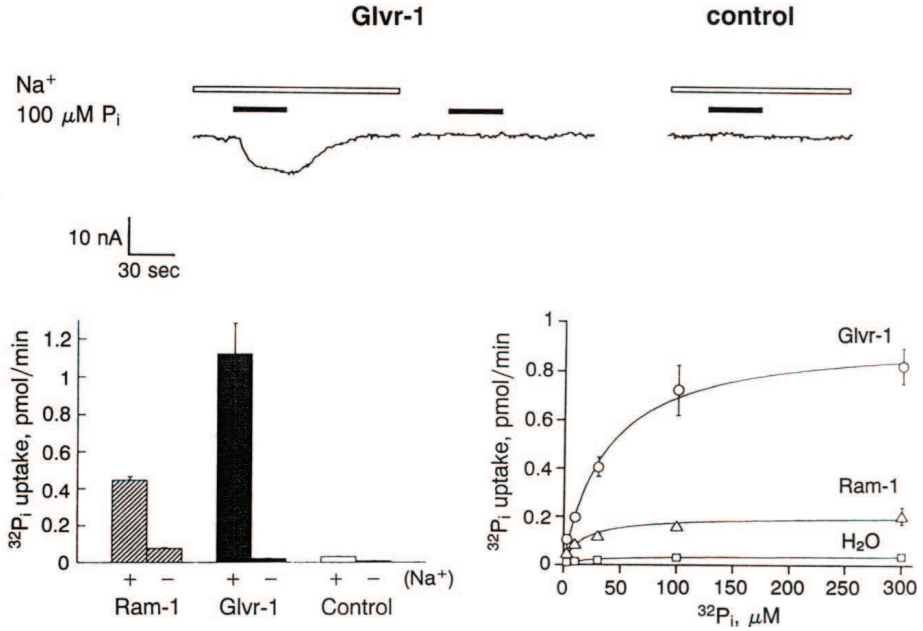

Figure 3.7: Upper panel: two electrode voltage recording of oocytes injected with PiT1 mRNA (left) or H_20 (right). The inward current evoked in the cells expressing PiT1 by application of 100 pM phosphate (solid bar) is dependent on sodium (hollow bar). No P_i-dependent currents were seen in water-injected oocytes (right). Voltage-clamp recordings were performed with a holding potential of -60 mV. Lower panel: ^{32}P uptake in presence or absence of sodium in *Xenopus* oocytes injected with PiT1 or PiT2 mRNA. Oocytes were incubated in recording solution containing ^{32}P for 60 min followed by lysis and scintillation spectroscopy. In the last part of the figure is shown the concentration-dependence of ^{32}P uptake (modified from Kavanaugh et al. 1994 [89].

3.2.3.3 Structure-function.

Structure-function. A search of the ProDom database [124] identified several domains within these proteins (see fig. 3.8). They include domains specific for the mammalian isoforms of PiT1 and PiT2, like the N- and C-terminal extremities and a large central region, and domains that are in common with non mammalian isoforms. These homology domains are called PD1131 and PD7717 in the ProDom database (blue and red colour respectively in fig. 3.8). Domain PD1131 is found in prokaryotes, fungi, yeasts, and plants. Such duplicated sequences probably have similar but inverted topologies. PD1131 homology defines the PiT family of proteins according to a classification proposed by the Transport Commission [125]; the PiT family is also called the Pho-4 family (SwissProt). This family currently includes 37 members and most of them, including mammalian PiT1 and PiT2, PD1131 are duplicated so that proteins contain amino- and carboxy-terminal copies of PD1131. Alignments of the 68 PD1131 homology domains stored in the ProDom database revealed four blocks of highly conserved amino acids [126]. They appear adjacent to predicted transmembrane domains and that conservation among distant species suggests that these regions may be important for

transporter function. Experimental investigations confirmed the predicted topological organization of human PiT2: 12 putative transmembrane domains are hypothesized, the asparagine 81 is glycosylated and that locate the first predicted loop in an extracelluar position. Tags inserted at the NH_2 and COOH termini are accessible from the external side, indicating that both termini are extracellular [126] and the intracellular localization of the large loop 7 was confirmed using an antibody raised against it [112]. Similar topologies have been suggested for the malaria parasite transporter PfPiT [121] and for the related H^+/P_i transporter from the plant *Arabidopsis* [91].

It has been shown that PiT2 retains its retroviral receptor function after deletion of loop 7 as well as transmembrane domains 6-7. Bøettger and co-workers did not investigate the transport function of their truncated protein, and thus it is unknown whether the large loop is essential for substrate transport [127]. The ability of a retrovirus to infect cells via its receptor has been used extensively to investigate which amino acids are crucial for infection with different viruses and thus also serves as a tool for probing the secondary structure of PiTs. Most of the attention has been directed towards loop 8. This shows large sequence variability between different species, and it appears to play a role in determining virus binding [128–130]. Only a few features of PiT topology have been experimentally confirmed, such as the location of the termini and loops 2 and 7 [126]. More experiments are necessary to establish a definitive membrane topology for PiT1 and PiT2.

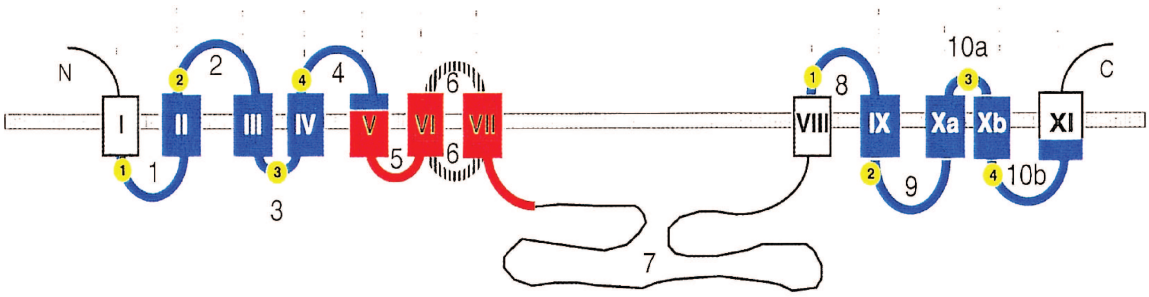

Figure 3.8: Topology proposed by Salaün et al. 2001 for human PiT2 . Blue segments are the N-PD1131 and C-PD1131 homology domains, in which numbers in green circles indicate the conserved amino acid blocks. The red segment is PD7717. As the orientation of loop 6 is still unknown, this segment appears as a striped line (fig. adapted from Salaün [126]).

3.2.3.4 Open questions.

There were many questions that need further investigations such as:

- transport mechanism: pH dependence, binding order, potential substrates and co-substrates, phosphate preferred species or potential inhibitors of PiT.

- structure function: the topology of PiT required experimental validation and identification of the residues involved in the substrate binding-site.
- regulation and localization: the localization (e.g. apical or basolateral in epithelia) of PiT transporters in different organs need to be investigated, to better understand their physiological role, and study which physiological factors regulate their expression levels.

Part II

Projects and Results

Chapter 4

PiT localisation and regulation.

The Na^+-Pi cotransporter PiT-2 (SLC20A2) is expressed in the apical membrane of rat renal proximal tubules and regulated by dietary Pi

[*Am J Physiol Renal Physiol,* **2008***, 296,*F691-699

Silvia Ravera, Ricardo Villa-Bellosta, Victor Sorribas, Gerti Stange, Moshe Levi, Heini Murer, Jurg Biber, and Ian C. Forster

Submitted 19 October 2008; accepted in final form 8 December 2008

Am J Physiol Renal Physiol 296: F691–F699, 2009.
First published December 10, 2008; doi:10.1152/ajprenal.90623.2008.

The Na^+-P_i cotransporter PiT-2 (SLC20A2) is expressed in the apical membrane of rat renal proximal tubules and regulated by dietary P_i

Ricardo Villa-Bellosta,[1]* Silvia Ravera,[2]* Victor Sorribas,[1] Gerti Stange,[2] Moshe Levi,[3] Heini Murer,[2] Jürg Biber,[2] and Ian C. Forster[2]

[1]*Laboratory of Molecular Toxicology, University of Zaragoza, Spain;* [2]*Institute of Physiology and Center for Integrative Human Physiology, University of Zurich, Switzerland; and* [3]*Department of Medicine, University of Colorado Health Sciences Center, Aurora, Colorado*

Submitted 19 October 2008; accepted in final form 8 December 2008

Villa-Bellosta R, Ravera S, Sorribas V, Stange G, Levi M, Murer H, Biber J, Forster IC. The Na^+-P_i cotransporter PiT-2 (SLC20A2) is expressed in the apical membrane of rat renal proximal tubules and regulated by dietary P_i. *Am J Physiol Renal Physiol* 296: F691–F699, 2009. First published December 10, 2008; doi:10.1152/ajprenal.90623.2008.—The principal mediators of renal phosphate (P_i) reabsorption are the SLC34 family proteins NaPi-IIa and NaPi-IIc, localized to the proximal tubule (PT) apical membrane. Their abundance is regulated by circulatory factors and dietary P_i. Although their physiological importance has been confirmed in knockout animal studies, significant P_i reabsorptive capacity remains, which suggests the involvement of other secondary-active P_i transporters along the nephron. Here we show that a member of the SLC20 gene family (PiT-2) is localized to the brush-border membrane (BBM) of the PT epithelia and that its abundance, confirmed by Western blot and immunohistochemistry of rat kidney slices, is regulated by dietary P_i. In rats treated chronically on a high-P_i (1.2%) diet, there was a marked decrease in the apparent abundance of PiT-2 protein in kidney slices compared with those from rats kept on a chronic low-P_i (0.1%) diet. In Western blots of BBM from rats that were switched from a chronic low- to high-P_i diet, NaPi-IIa showed rapid downregulation after 2 h; PiT-2 was also significantly downregulated at 24 h and NaPi-IIc after 48 h. For the converse dietary regime, NaPi-IIa showed adaptation within 8 h, whereas PiT-2 and NaPi-IIc showed a slower adaptive trend. Our findings suggest that PiT-2, until now considered as a ubiquitously expressed P_i housekeeping transporter, is a novel mediator of P_i reabsorption in the PT under conditions of acute P_i deprivation, but with a different adaptive time course from NaPi-IIa and NaPi-IIc.

brush-border membrane; inorganic phosphate; sodium-dependent transport

THE PRINCIPAL MEANS BY WHICH mammals achieve homeostasis of inorganic phosphate (P_i) is through control of P_i reabsorption along the renal proximal tubule (5, 28, 29). The underlying physiological signals include dietary P_i, circulating hormones such as parathyroid hormone and growth hormone, vitamin D, and phosphotonins (e.g., fibroblast growth factor 23, secreted frizzled related protein-4, matrix extracellular phosphoglycoprotein) (for review, see Refs. 4, 12, and 28). In the kidney, the functional protein targets of these factors are two gene products of the solute carrier family SLC34 (SLC34A1, SLC34A3), commonly referred to as type II Na^+-coupled P_i cotransporters (NaPi-IIa, NaPi-IIc), which are expressed in the brush-border membrane (BBM) of proximal tubular epithelia. Another member of the SLC34 family, SLC34A2 (NaPi-IIb), is not expressed in the kidney, but is proposed to mediate P_i transport in the small intestine and other organs (27).

NaPi-IIa and NaPi-IIc mediate apical entry of P_i in the epithelial cell from the primary urine via a secondary-active transport mechanism that couples the movement of Na^+ down their electrochemical gradient to uphill movement of P_i. A wide body of experimental evidence supports the view that the abundance of these proteins in the BBM determines the degree of renal P_i reabsorption. The electrogenic NaPi-IIa and electroneutral NaPi-IIc have been the subject of extensive kinetic studies at the molecular level (reviewed in Ref. 53) and studies on renal tubular P_i handling in vitro and in vivo (reviewed in Refs. 12, 26, and 28). Their physiological importance is underscored by the clear phenotypes observed in animal knockout studies. Mice in which the *Npt2a* gene coding for NaPi-IIa is knocked out exhibit P_i wasting, hypercalcuria, and skeletal abnormalities (3). Moreover, Na^+-dependent P_i uptake in BBM preparations from these mice is reduced by ~70% compared with the tissue from normal animals. However, the incomplete suppression of P_i transport activity in this and other studies (46) also implies that there must be other P_i-selective transport proteins involved. Thus, with the subsequent identification of the third member of the SLC34 family (NaPi-IIc) and its localization to the BBM of proximal tubular epithelia (40), it was generally assumed that the transport activity of NaPi-IIc could account for the remaining 30% P_i transport capacity in *Npt2a*$^{-/-}$ mice (46). This conclusion was further supported by the documentation of increased abundance of NaPi-IIc in the kidneys of *Npt2a*$^{-/-}$ mice as a compensation for the lack of NaPi-IIa (33, 46). Recently, it was reported that knockout of both NaPi-IIa and NaPi-IIc in mice results in severe hypophosphatemia, markedly reduced bone mineralization, and increased urinary P_i and Ca^{2+} compared with single knockout mice (41). Despite this phenotype, it is significant that, even in these animals, some renal P_i reabsorptive capacity remained. Notwithstanding passive paracellular flux of P_i driven by the transepithelial potential, this indicates that there should be other secondary-active transport proteins present in the kidney to mediate P_i transport from the nephron lumen.

Two potential candidates are gene products of the SLC17 and SLC20 families, both known to transport P_i by a secondary-active mechanism. Although originally identified through ex-

* R. Villa-Bellosta and S. Ravera contributed equally to this work.

Address for reprint requests and other correspondence: I. C. Forster, Institute of Physiology, Univ. of Zurich, Winterthurerstrasse 190, CH-8057 Zurich, Switzerland (e-mail: iforster@access.uzh.ch).

The costs of publication of this article were defrayed in part by the payment of page charges. The article must therefore be hereby marked "*advertisement*" in accordance with 18 U.S.C. Section 1734 solely to indicate this fact.

pression cloning as a Na^+-dependent P_i cotransporter (30), localized in the kidney, the role of SLC17A1 in renal P_i handling has been questioned by subsequent studies (7, 28). On the other hand, the two known members of the SLC20 family, SLC20A1 (PiT-1) and SLC20A2 (PiT-2), are generally considered to fulfill a housekeeping role consistent with their ubiquitous expression (2, 14, 17, 18, 31, 45). PiT-1 and PiT-2 were originally identified as cell surface receptors for gibbon ape leukemia virus (Glvr-1) and murine amphotropic leukemia virus, respectively, and were subsequently shown to mediate Na^+-coupled P_i cotransport (18, 34). Both PiT-1 and PiT-2 are electrogenic (17, 18, 36), but unlike NaPi-IIa and NaPi-IIc, they show a preference for monovalent P_i and reduced sensitivity to pH and the P_i transport inhibitor phosphonoformic acid (PFA) compared with NaPi-IIa/c (36, 51). Therefore, with such different functional characteristics compared with SLC34 proteins, one might expect them to subserve unique roles in P_i handling. For example, recent studies that address their potential roles in vascular calcification (15, 22, 23, 51) and bone mineralization (55) suggest that they may be key players in skeletal and vascular pathologies.

SLC20 proteins have also been proposed as housekeeping transporters in basolateral membrane of renal epithelia, although immunohistochemical evidence for basolateral localization has so far been lacking (26, 28). In mouse kidney, the relative abundance of mRNA for PiT-1 and PiT-2 was reported to be >50-fold less than NaPi-IIa, and, in the same study using in situ hybridization with a probe for Glvr-1 (PiT-1), a signal was detected throughout the kidney (47) and, similarly, PiT-2 at the mRNA and protein levels has been detected in rat kidney in all regions (20). Recently, PiT-1 and PiT-2 gene expression was shown to be upregulated in *Npt2a*$^{-/-}$ mice under conditions of metabolic acidosis, which suggests a possible compensatory role for SLC20 proteins (32). Because the localization at the cellular level was not established in these studies, the relative abundance of the candidate P_i transporter mRNAs may not necessarily reflect that of their corresponding proteins or the apical P_i transport rate. Therefore, any conclusions about the roles these proteins may play in P_i handling should be treated with caution without the support of functional expression data. In this respect, several in vitro studies indicate that P_i transport mediated by SLC20 proteins is upregulated by P_i depletion. In 208F rat fibroblasts grown in P_i-free medium, increased P_i uptake and mRNA levels of both PiT-1 and PiT-2 were documented (18). Similarly, in human embryonic kidney cells, P_i deprivation stimulated PiT-1-mediated P_i uptake (11), and stimulation of PiT-2 mRNA and protein levels was reported for two osteosarcoma cell lines (8).

The aims of the present study were to investigate the kidney localization and potential regulatory roles of one member of the SLC20 family, PiT-2, in renal P_i handling under the influence of one of the key regulators of P_i reabsorption, P_i diet. Because both NaPi-IIa and NaPi-IIc show clear phenotypical adaptive responses to changes in P_i diet (24, 25, 35, 42), they were used as benchmarks against which the PiT-2 behavior was compared. In this report, we show for the first time that Pit-2 is localized to the brush border of renal proximal tubules, and its abundance is strongly regulated by P_i diet, but with a slower adaption rate compared with NaPi-IIa. Our findings should prompt a reevaluation of the role played by SLC20 proteins in P_i homeostasis and their potential as regulated targets for renal P_i handling.

MATERIALS AND METHODS

Antibody preparation. Polyclonal antibodies were prepared against synthetic peptides from rat NaPi-IIa (rabbit), rat NaPi-IIc (chicken), and rat PiT-2 (rabbit) (Davids Biotechnologie, Regensburg, Germany). The NaPi-IIa peptide sequence was MMSYSERLGGPAV and corresponds to amino acids 1-13 in the NH_2 terminal; the NaPi-IIc peptide sequence was AHCYENPQVIASQQL (50). The PiT-2 peptide sequence was HCKVGSVVAVGWIRSRKA and corresponds to amino acids 597-614, close to the COOH terminus. The peptides were conjugated to keyhole limpet hemocyanin, mixed in Freund's complete adjuvant, and injected in rabbit or chicken. Two booster injections were given to the animals before sera were collected. A monospecific antibody was affinity purified from serum using the corresponding antigenic peptide.

Animals and diets. Specific diets and the procedure to adapt the animals to chronic diet or acute changes was performed as previously described (19). All animal handling was according to Spanish and Swiss Animal Welfare laws and were approved by the local veterinary authorities. Briefly, for chronic adaptation, male Wistar rats 6–8 wk old (Charles River Laboratories) were first stabilized on a normal diet (0.6% P_i) for 5 days and then placed on either one containing 1.2% P_i (chronic high-P_i diet) or 0.1% P_i (chronic low-P_i diet) for 5 days before being killed. Diets were otherwise identical in their mineral, electrolyte, protein, carbohydrate, fat, and calorie content. For acute experiments, animals were supplied food from 0800 to 1000 AM each day after which they had access to tap water only. They were first conditioned on the high-P_i or low-P_i diets for 3–4 days as above and then switched to the acute dietary regime (0800) [acute low-P_i (0.1%) or acute high-P_i (1.2%)], and subsequently killed in triplicates at the specified time (2, 4, 8, 24, and 48 h) after switching to the acute diet. Each animal consumed the same quantity of food.

BBM preparation and free-flow electrophoresis. BBM were prepared according to the Mg^{2+} precipitation method, with one single precipitation, as previously described (6). Simultaneous isolation of BBM and basolateral membrane was achieved by free-flow electrophoretic separation of the crude membrane fraction obtained from rat kidney cortex (9, 10).

Brush-border membrane vesicle transport assays. Brush-border membrane vesicle (BBMV) ^{32}P uptake was performed as described elsewhere (6, 52). The protein concentration in the BBMV samples was quantitated using a Bio-Rad Protein Assay kit (Bio-Rad). BBMVs prepared from kidneys from five rats previously adapted with the chronic high-P_i diet and from five rats treated with the chronic low-P_i diet were incubated with solutions containing 300 mM mannitol, 20 mM HEPES-Tris, pH 7.4, and 125 mM NaCl. The substrate P_i was made with 0.125 mM K_2HPO_4 and 1 μCi/ml ^{32}P to give a final concentration 0.1 mM close to the expected apparent affinity constant for P_i for Na^+-dependent transport in BBMVs. Trisodium PFA (final concn 6 mM) was added to the same solution with 107 mM NaCl. The stop solution contained 100 mM mannitol, 5 mM Tris·HCl, pH 7.4, 150 mM NaCl, and 5 mM P_i. Na^+ dependence was established by incubating BBMVs in solutions in which KCl replaced NaCl equimolarly. BBMVs were incubated for 1 or 120 min with the uptake solutions and then washed with stop solution on a 45-μm cellulose nitrate filter. $^{32}P_i$ activities of individual filters were counted using a Packard Tri-Carb 2900TR scintillation counter.

Protein detection and relative quantification by Western blot. Immunoblot assays on BBM preparations were performed as previously described (21). In brief, BBM proteins (34 μg/lane) were electrophoresed in Miniprotean III (Bio-Rad). The NaPi-IIa affinity antibody was used at 1:3,000 dilution in PBS, NaPi-IIc at 1:5,000, and

Pit-2 at 1:3,000. Primary antibodies were incubated overnight in the presence of 0.01% $NaNO_3$ and detected with horsedarish peroxidase-conjugated secondary antibodies. Chemiluminescent reaction was performed with a Millipore kit. Densitometric signals were obtained with a Gel-Doc 1000 (Bio-Rad) after exposure to an X-ray film. Specificity of signals was determined with preimmune serum and by blocking the affinity-purified antibodies with the corresponding antigenic peptide using the standard procedure, and 50-fold molar excess of peptide per IgG. NaPi-IIa and Pit-2 antibodies were used at 1:3,000 dilution, and NaPi-IIc at 1:5,000. For all immunoblots, a protein determination was performed (DC Protein Assay Kit; Bio-Rad) to ensure equal loading per lane.

Immunohistochemistry on chronically treated animals. Immunohistochemical assays were performed with Wistar rats (Charles River Laboratories) placed on the chronic high-P_i or low-P_i diets for 5 days. On *day 5*, rats were induced in deep anesthesia by 20 mg xylazine and 100 mg ketamine and perfused through the abdominal aorta with 3% paraformaldehyde in PBS buffer for 5 min and with PBS buffer for a further 5 min. Kidneys were then removed, maintained in ice-cold PBS buffer, cut in 5-mm slices, and frozen using liquid propane. Consecutive 4-μm slices were cut using a Leica Cryostat Microtome, fixed on polylysine-treated slides, and allowed to dry for 2 min. After rehydration using ice-cold PBS buffer, the slices were exposed to 0.1% SDS-PBS solution for 5 min at room temperature, washed two times, 10 min each, in PBS buffer, incubated for 30 min in blocking buffer [10% normal donkey serum (Sigma), 2% BSA (Sigma), PBS buffer] at room temperature, and afterward exposed to the antibodies (dissolved in the blocking buffer) overnight at 4°C. Sections were then washed two times, 10 min each, in PBS buffer and subsequently exposed to the anti-rabbit IgG conjugated with fluorescein (Alexa Fluor 488 donkey anti-rabbit; Molecular Probes) and phalloidin (Texas Red-X; Molecular Probes), both dissolved in the blocking solution, for 1 h at room temperature. Sections were rinsed with PBS buffer and then mounted with Glycergel Mounting Medium (Dako-Cytomation; Denmark) supplied with DABCO and observed by a fluorescent microscope (Nikon Eclipse TE 300 plus Nikon Xenon power supply XPS-100 lamp).

Data analysis. Data for repeated measurements are given as means ± SE. Statistical significance between groups was performed using paired Student's *t*-test.

RESULTS

Functional evidence that Na^+/P_i transport is not mediated exclusively by SLC34 proteins in proximal tubule BBMVs. A functional assay using BBMVs from rat renal tissue offered compelling evidence that SLC34 proteins do not exclusively mediate the Na^+-coupled P_i transport capacity and the remaining transport is under dietary regulation. Here, we compared the P_i uptake of rat BBMVs in the absence and presence of the competitive inhibitor of type II Na^+-coupled P_i transport, PFA (44). BBMVs were prepared from animals treated chronically with high-P_i (1.2%) and low-P_i (0.1%) diets to change the membrane abundance of SLC34 proteins (21, 42). Uptake was measured at 1 min, at which time the transport has typically peaked to give a sensitive measure of any dietary influence on transport activity. From the data (Table 1), with no PFA in the medium, BBMVs from high-P_i animals showed a 52% reduction in P_i uptake compared with vesicles from low-P_i animals, in agreement with previous findings under linear transport velocity conditions (21). BBMVs from both animal groups treated on either diet showed residual uptake with 6 mM PFA in the uptake medium. For chronic high-P_i-treated animals, we documented a 74% inhibition, whereas, for chronic low-P_i-treated animals, the inhibition was 53%, which was statistically different from the high-P_i group. In these assays, Na^+-independent uptake (equimolar K^+ replacement) was negligible, which confirmed that Na^+-coupled P_i transport is the principal mechanism mediating P_i transport at the apical membrane of PT epithelia.

Table 1. *Uptake of BBMV prepared from rat kidney for chronic P_i diets*

	Diet	
BBMV uptake condition	Chronic low P_i (0.1 %)	Chronic high P_i (1.2%)
Control + 0.1 mM P_i	3,947±366 (91±1)	1,911±348 (76±3)
Control + 0.1 mM P_i + 6 mM PFA	1,860±416*	492±172*
Inhibition, %	53	74

Uptake values in pmol P_i/mg protein are given as means ± SE; $n = 3$ experiments. P_i concentration in uptake medium: 0.1 mM, 1 min P_i incubation. Values in parentheses are uptake data in 0 Na^+ (equimolar replacement with K^+, see scap≈materials and methods≈). BBMW, brush-border membrane vesicles; PFA, phosphonoformic acid. *Statistical significance between control and PFA groups for each diet determined by paired *t*-test ($P = 0.022$).

If P_i transport were mediated solely by SLC34 proteins (NaPi-IIa, NaPi-IIc), we would expect the fractional inhibition of uptake by PFA to be independent of dietary condition, since it has been shown by studies using *Xenopus* oocytes that both NaPi-IIc and NaPi-IIa have both comparable apparent affinities for P_i (40, 52) and inhibition constants for PFA (52). The 21% difference in uptake for BBMVs from rats conditioned under two dietary conditions therefore suggests that part of the uptake is mediated by a Na^+-dependent P_i transport system that has a different sensitivity to PFA.

PiT-2 expression in rat kidney cortex. Based on the above findings and given that P_i transport by SLC20 proteins is significantly less sensitive to PFA (36, 50, 51), we focused our attention on one member of the SLC20 gene family (PiT-2, SLC20A2) that previous studies have shown is expressed in the kidney (20, 47). To confirm the specificity of our PiT-2 antibody, we first performed Western blots of HEK-293 cells transfected with the rat PiT-2 clone (data not shown). In Western blots of BBM prepared from rat superficial cortex (SC) and juxtamedullary (JM) material from the same animals under non-reducing conditions, the rat PiT-2 antibody recognized a major polypeptide fragment with an estimated molecular mass ~70 kDa for BBMs from both SC and JM. This corresponds to the expected mass based on the amino acid sequence. NaPi-IIa and NaPi-IIc antibodies were used as positive controls (Fig. 1*A*). In this preparation, we confirmed the specificity of the antibody by peptide protection and by blotting with the preimmune sera of the animals (Fig. 1*B*). For PiT-2, the 70-kDa fragment was comparable with previously published values in basolateral liver plasma membranes (14), osteosarcoma cell lines (8), and overexpression in CHO cells (38). These data strongly suggested that PiT-2 is expressed in the rat kidney BBM. However, because of possible contamination by other membranes, we cannot exclude the possibility that PiT-2 might be expressed in other membrane fractions such as basolateral and intracellular organelles.

Additional confirmation of the protein localization of PiT-2 in BBM was obtained by performing free-flow electrophoresis of apical and basolateral membranes from rat kidney homogenate. Single fractions were analyzed for the

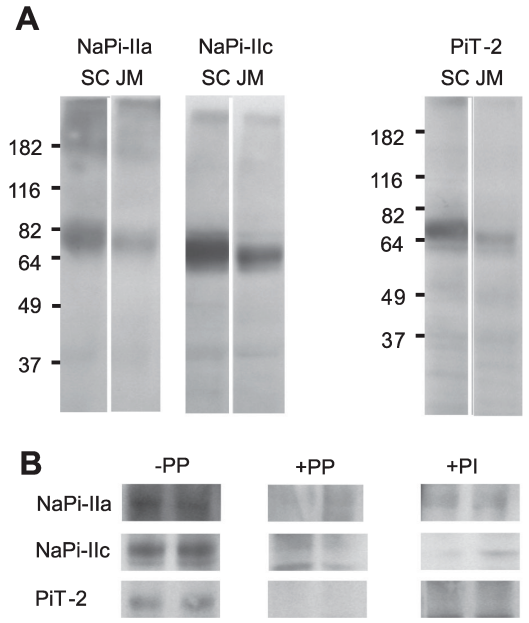

Fig. 1. Detection of Na^+-coupled P_i cotransporter (NaPi)-IIa, NaPi-IIc, and PiT-2 proteins in kidney brush-border membrane (BBM) preparations by immunoblotting. *A*: Western blots of BBM from superficial cortical (SC) and juxtamedullary (JM) regions for NaPi-IIa, NaPi-IIc, and PiT-2 from the same animal. In this and other Western blots, 34 μg protein were loaded per lane. NaPi-IIa affinity antibody was used at 1:3,000 dilution in PBS, NaPi-IIc at 1:5,000, and PiT-2 at 1:3,000. *B*: specificity of the antibodies. −PP, immunoreactive bands in control kidney cortex BBM proteins; +PP, blocking of antibodies with the immunogenic peptide. Affinity purified antibodies were incubated with 50 μg/ml peptide for 5 min at room temperature before the Western blot assay. +PI, blots obtained with preimmune sera of the corresponding animals.

enzymatic activities of leucine aminopeptidase N (an indicator of apical localization) and Na^+-K^+-ATPase (an indicator of basolateral localization) (Fig. 2*A*). Fractions were then probed with the NaPi-IIa and PiT-2 antibody (Fig. 2*B*). The NaPi-IIa and PiT-2 profiles follow that of leucine aminopeptidase N, which provides strong biochemical evidence that PiT-2 is mostly apically localized in the nephron, like NaPi-IIa.

Immunohistochemistry confirms apical localization of PiT-2. We performed immunohistochemistry on rat kidney slices staining for PiT-2 (Fig. 3*A*) and NaPi-IIa as a control (Fig. 3*B*) from the same kidney, obtained from a rat that had previously adapted on a chronic low-P_i (0.1%) diet. As expected, immunoreactive signals corresponding to NaPi-IIa were localized exclusively in the proximal tubule, in agreement with previous studies on rat kidney (9, 42). An immunoreactive signal recognized by the PiT-2 antibody was widely distributed throughout the cortex, predominantly in the early proximal tubules. At higher magnification, PiT-2 staining appears to be exclusively associated with the apical membrane of tubular epithelia and is mostly seen in the brush border of the early proximal tubules (S_1 segment) (Fig. 3*C*, *top*). We also confirmed that the PiT-2 staining was absent when the slice was preincubated using the antigenic peptide (Fig. 3*C*, *bottom*). Figure 3*D* shows colocalization of PiT-2 with the membrane cytoskeleton protein β-actin, confirming the association of the transporter with the BBM.

Chronic P_i diet induces a redistribution of PiT-2. Slices of kidney from rats preconditioned with low-, normal-, or high-P_i diets show a redistribution of the immunoreactive signal of PiT-2 (Fig. 4). For animals fed chronically for 5 days on a high-P_i diet, we were unable to detect PiT-2 (Fig. 4*A*, *top*). However, for animals fed on a normal-P_i (0.6%) and low-P_i (0.1%) diets, clear evidence for PiT-2 localization in the brush-border regions of proximal tubules was obtained (Fig. 4*A*, *center* and *bottom*,). Under chronic low-P_i dietary conditions, the staining was stronger than under normal dietary conditions. These findings provide compelling evidence that the abundance of PiT-2 protein is regulated by P_i dietary conditions. The lack of staining for the chronic high-P_i diet condition suggests that, like NaPi-IIa (24), PiT-2 is not simply redistributed within the proximal tubule cell.

To provide further confirmation of these observations, we performed Western blots of BBM preparations from both superficial and JM cortex material (Fig. 4, *B* and *C*). After 3 days of chronic low-P_i diet, clear bands in the Western blot were obtained for all three proteins in both kidney regions (Fig. 4*B*). Quantification of Western blots from BBM showed that they were all downregulated by >70% (Fig. 4*C*). Exposure to the chronic high-P_i diet led to the disappearance of a band for NaPi-IIa, NaPi-IIc, and PiT-2 in both kidney regions. The behavior of NaPi-IIa and NaPi-IIc confirmed the findings in previous studies (21, 25, 37, 42, 48). Taken together, our data provide compelling evidence that PiT-2 protein level is regulated by chronic P_i dietary manipulations.

Acute response of protein expression to change in dietary P_i. The NaPi-IIa and NaPi-IIc protein abundances in the BBM of proximal tubular epithelia are tightly regulated by acute

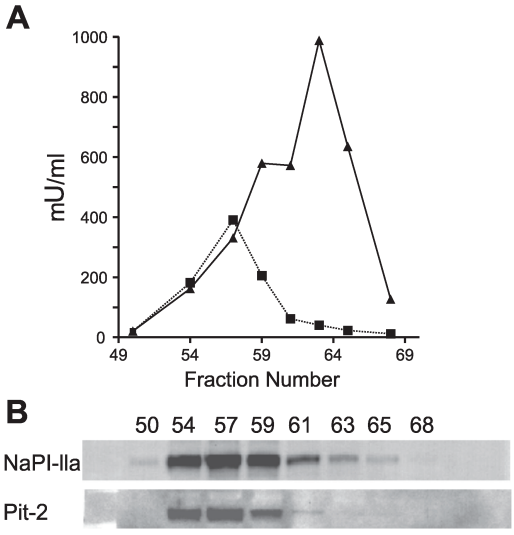

Fig. 2. Free-flow electrophoresis. Free-flow electrophoretic separation of rat kidney cortical BBM and basolateral membranes. Single fractions were analyzed for enzyme activity in leucine aminopeptidase N (■) and Na^+-K^+-ATPase (▲) (*A*) and probed by Western blot analysis for NaPi-IIa and PiT-2 (*B*).

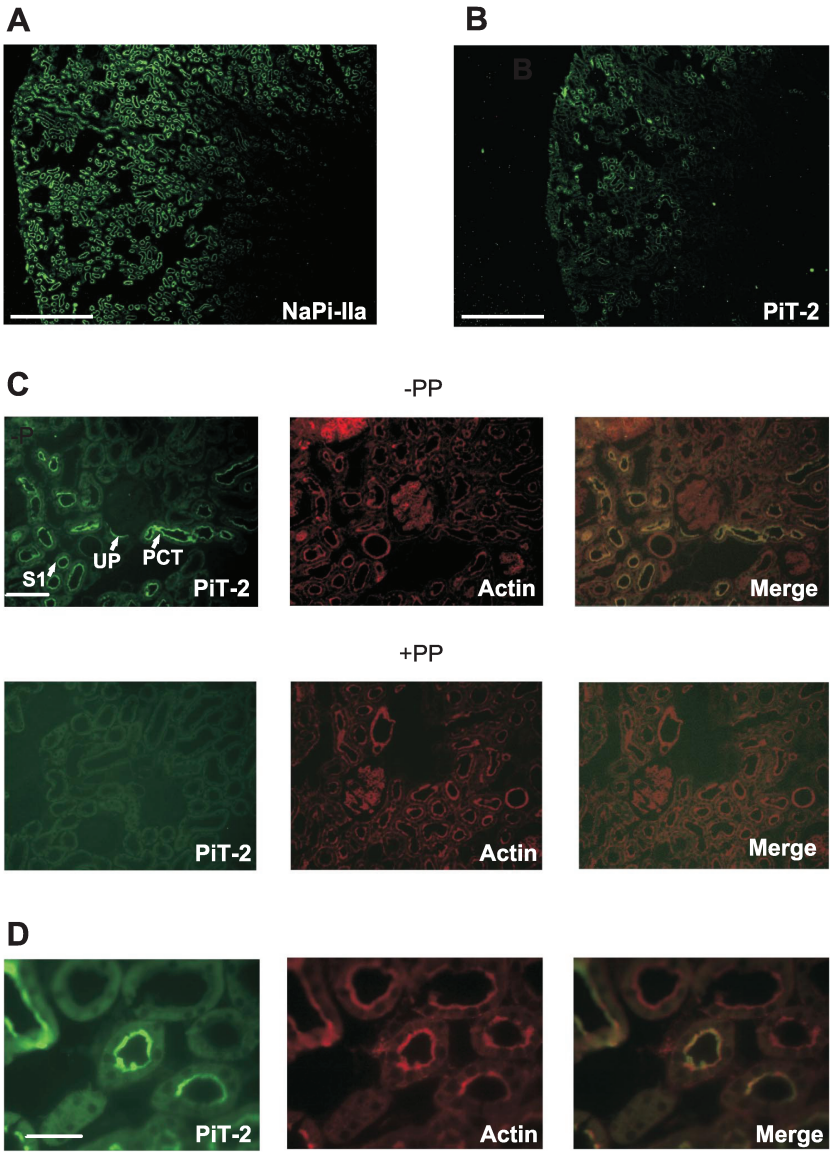

Fig. 3. PiT-2 immunohistochemistry for kidney slices from one animal fed on a chronic low-P_i (0.1%) diet. *A*: immunostaining with PiT-2 antibody indicates expression of PiT-2, particularly in cortical areas. Scale bar: 750 μm. *B*: immunostaining with NaPi-IIa antibody of material from same animal shows more widespread staining in both cortical and JM regions. Scale bar: 750 μm. *C*: immunostaining with PiT-2 antibody of kidney slice at higher magnification shows strong staining in the early part of the proximal tubule, including urinary pole (UP), proximal convoluted tubule (PCT), and S_1 segment of PT (S1). Scale bar: 375 μm. Second row shows images with peptide protection (PP). *D*: higher magnification of S_1 segment staining for PiT-2 (*left*), actin (*center*), and merged images (*right*). Scale bar: 75 μm.

changes to dietary P_i (21, 42). To investigate if PiT-2 protein was also affected by acute dietary manipulations, we fed rats on two complementary dietary regimes. First, for rats fed chronically with a high-P_i (1.2%) diet, and then exposed to a low-P_i (0.1%) diet for 2, 4, 8, 24, and 48 h, NaPi-IIa protein progressively upregulated in the BBM after 2 h and was maintained for 8 h (Fig. 5*A*). NaPi-IIc expression in BBMs followed a similar, but slower, pattern. PiT-2 protein levels in BBM paralleled the changes of NaPi-IIc, i.e., adaptation to the low-P_i diet was slower than NaPi-IIa.

In the converse experiment, animals were chronically adapted to a low-P_i diet for 3 days and then subjected to the high-P_i diet and killed at the same time points as above. As expected, NaPi-IIa showed rapid downregulation within 2 h of exposure to the high-P_i regime, in agreement with previous findings (21, 42). Both NaPi-IIc and PiT-2 were also downregulated; however, the respective time courses were slower. NaPi-IIc did not show a significant change in level until 48 h of exposure to the acute high-P_i diet, whereas the time course of PiT-2 was intermediate between NaPi-IIa and NaPi-IIc. The slow regulation of NaPi-IIc contrasts with the more rapid effect reported for NaPi-IIc (42). The discrepancy in behavior most likely lies in the different dietary conditions used in the previous study, in which animals were adapted on 0.02% P_i for the chronic low-P_i diet. This may have resulted in a higher level of NaPi-IIc protein at the start of the acute low-P_i phase compared with the present study.

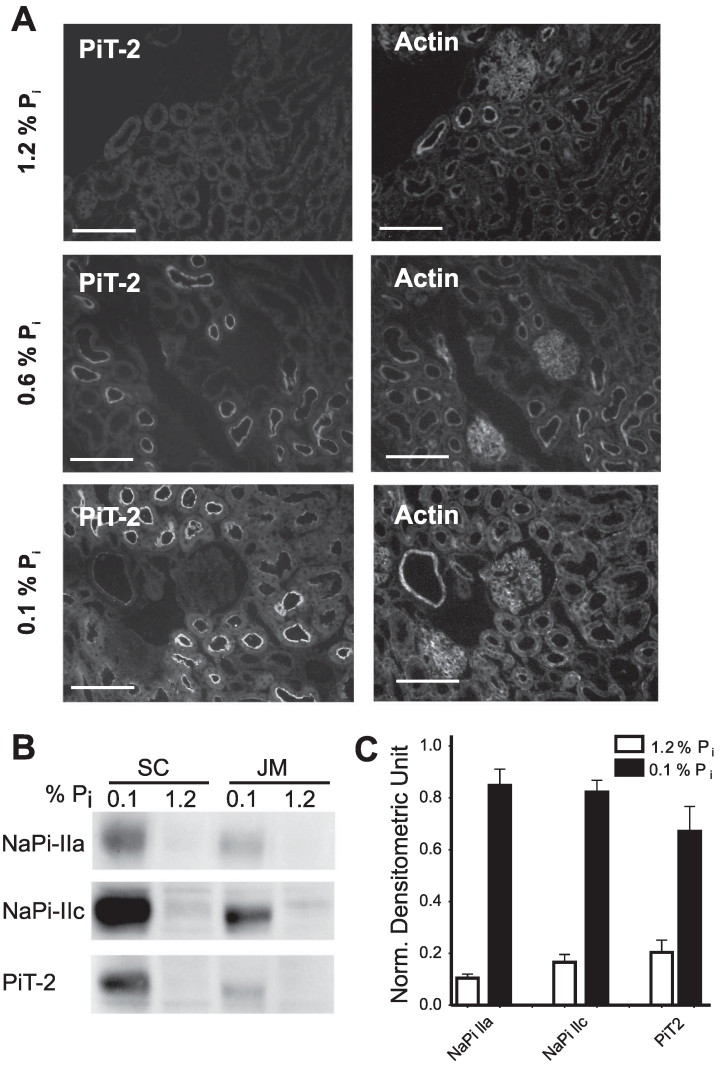

Fig. 4. Response to chronic dietary conditions. *A*: immunohistochemistry of kidney slice stained for PiT-2 (*left*) and for actin (*right*). *Top*: chronic high-P_i (1.2%) diet; *center*: normal-P_i (0.6%) diet; *bottom*: chronic low-P_i (0.1%) diet. Scale bar: 150 μm. *B*: Western blots from SC and JM BBM using material from animals fed on chronic high-P_i and chronic low-P_i diets. *C*: quantitation of Western blots for NaPi-IIa, NaPi-IIc, and PiT-2 indicates that all three transporters respond similarly to chronic changes in P_i concentration in the diet ($n = 5$ experiments). The downregulation, based on densitometric analysis, of material from rats treated on low-P_i and high-P_i diet is 88% for NaPi-IIa ($P < 0.0001$), 84% for NaPi-IIc ($P < 0.0001$), and 70% for PiT-2 ($P = 0.0023$). Normalized densitometric units were calculated by subtracting the background from the signal and corrected using the actin signal.

DISCUSSION

We report for the first time the renal localization and dietary regulation of a member of the SLC20 family, PiT-2. We present immunohistological evidence that PiT-2 is localized to the BBM of rat kidney proximal tubules and therefore potentially offers an additional route for P_i to enter the proximal tubule epithelia from the glomerular filtrate. Moreover, we document that changes in dietary P_i markedly affect the abundance PiT-2 protein in the BBM.

The functional data presented in Table 1 also highlight the effect of diet on two components of Na^+-dependent P_i transport: a "PFA-sensitive" component and a "PFA-resistant" component. In the absence of PFA, the high-P_i diet resulted in a 52% suppression of total P_i uptake relative to the low-P_i diet case, as previously established (21). In the presence of 6 mM PFA, the high-P_i diet led to a 33% suppression of the component of uptake contributed by the PFA-sensitive component (estimated for each dietary condition by subtracting the uptake with PFA from the uptake without PFA). In contrast, for the PFA-resistant component of uptake, the high-P_i diet led to a 74% suppression of Na^+-dependent uptake.

Our findings are also supported indirectly by other functional studies of BBMVs. Consistent with the functional data that we report here for 1-min uptakes (Table 1), Villa-Bellosta et al. (50) have shown that the Na^+-dependent ^{32}P (0.05 mM total P_i) uptake rate of renal cortex BBMVs in the initial constant velocity range is reduced by ~70% in the presence of 6 mM PFA. For this assay, the apparent inhibition constant for PFA (K_i^{PFA}) was estimated to be 2.2 mM, which is approximately twofold greater than values reported for assays involving SLC34 proteins heterologously expressed in *Xenopus* oocytes (50). If NaPi-IIa and NaPi-IIc alone were responsible for mediating Na^+-dependent P_i cotransport and given the similarity of the phenomenological kinetic constants for these

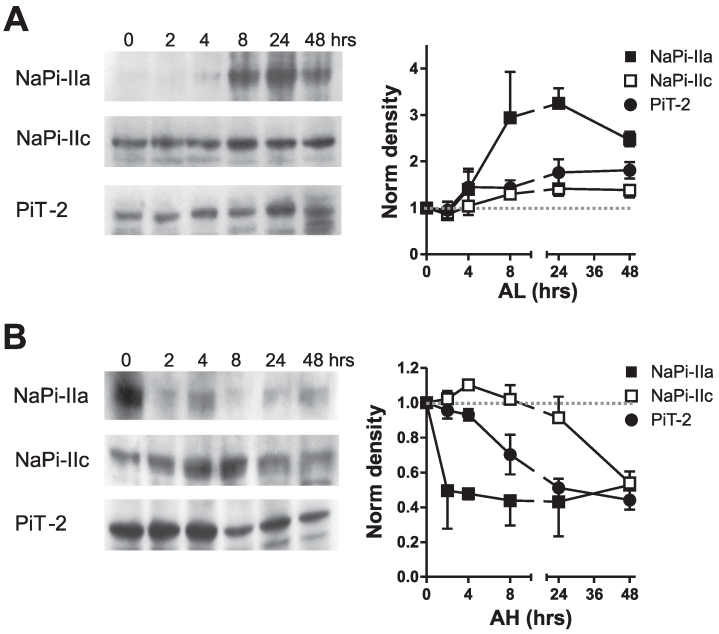

Fig. 5. Acute adaptation of NaPi-IIa, NaPi-IIc, and PiT-2 to dietary conditions. *A*: changes from chronic high-P_i diet to acute low-P_i diet (AL). Western blots from representative animals are shown for NaPi-IIa, NaPi-IIc, and PiT-2. In each case, densitometric quantitation of acute changes shows the mean of measurements on material taken from 3 animals killed at the indicated time point. Whereas NaPi-IIa is up-regulated within 4 h of dietary change to low-P_i diet, NaPi-IIc and PiT-2 require 8 h to increase their abundance at the plasma membrane. *B*: changes from chronic low-P_i diet to acute high-P_i diet (AH) as in *A*. NaPi-IIa is eliminated from the BBM within 2 h, whereas the reduction in NaPi-IIc expression is only clearly seen at 48 h, and PiT-2 at 8 h.

isoforms determined using the *Xenopus* oocyte expression system (52), we predict that the transport rate should be reduced by ~80% for these uptake conditions.[1] Under the tacit assumption that the oocyte data are also valid for the BBMV system, the discrepancy between measured and predicted uptake rate inhibition strongly supports the notion that a component of P_i transport capacity is present in renal BBMs that is either insensitive to PFA or has a significantly higher K_i^{PFA} compared with that for NaPi-IIa/c. The higher value of K_i^{PFA} reported for renal BBMs would therefore result from a mixed inhibitory response of PFA. Moreover, our functional uptake data indicate that this transport component is regulated by P_i diet, but its abundance in the BBM does not parallel the well-characterized dietary regulation of SLC34 proteins (21, 25, 42). Given that SLC20 proteins show significantly reduced (51, 52) or no sensitivity to PFA (36), depending on the expression system and assay conditions, it is therefore tempting to speculate that PiT-2 contributes to at least part of the non-SLC34-mediated Na^+-dependent P_i transport capacity. This conclusion is underscored by the correlated changes in kidney immunostaining and BBM protein abundance documented in the present study. Because no SLC20-specific inhibitor is presently available, it is not possible, based on the present data, to quantitate the relative contribution of PiT-2 to the overall P_i transport at the BBM. Furthermore, it has been reported (51, 52) that Na^+-dependent P_i transport rate of SLC20 proteins is partially suppressed by high concentrations of PFA; therefore, we cannot exclude the possibility that part of the PFA-sensitive uptake results from partial inhibition of PiT-2 itself and that a PFA-insensitive component of transport is mediated by yet another transport protein.

What could the potential role of PiT-2 in the apical membrane of PT epithelia be? First, because the time course of regulation of PiT-2 in response to dietary switching to an acute high-P_i regime is different from both NaPi-IIa and NaPi-IIc, this suggests that the regulatory pathway is different. PiT-2 might therefore play a role in fine tuning overall P_i reabsorption under different dietary conditions. Second, a possible answer may be found from kinetic studies of SLC20 proteins (36) and the related malaria plasmodium falciparum PiT (39) expressed in *Xenopus* oocytes. These studies show conclusively that these transporters prefer monovalent P_i ($H_2PO_4^-$), whereas all three SLC34 family proteins prefer divalent P_i (HPO_4^{2-}) (1, 13, 54). Moreover, the maximum electrogenic transport rate of PiT-1 shows less sensitivity to changes in external pH (36, 39) compared with NaPi-IIa (53), which makes it an ideal candidate for transporting P_i under acidic conditions. Micropuncture studies have shown that the pH in the proximal tubule can fall by up to 0.78 pH units relative to arterial blood in rats previously loaded with NH_4Cl (16, 49). At pH 7.4, the ratio $[HPO_4^{2-}]/[H_2PO_4^-] = 4$, which decreases to 1.6 at pH 6.6, at which the NaPi-IIa/c transport rate will be reduced by ~50% (29, 53). On the other hand, we would expect PiT-2 to be unaffected by these changes in luminal pH so that the presence of both types of transporter will assure the reuptake of the necessary amount of P_i from the primary urine.

In conclusion, until now, P_i reabsorption in the kidney was thought to be solely the responsibility of the SLC34 proteins NaPi-IIa and NaPi-IIc, whereas SLC20 proteins have been generally considered to fulfill general housekeeping roles throughout the organism. Our findings provide compelling

[1] Assuming Michaelis-Menten kinetics and ideal competitive inhibition, the ratio of transport velocities with and without PFA can be expressed as: $([Pi] + K_m^{Pi})/([Pi] + K_m^{Pi}(1 + [PFA]/K_i^{PFA}))$, where K_i^{PFA} is the apparent affinity constant for Pi, K_i^{PFA} is the inhibition constant for PFA (43), and brackets denote concentration. For estimating the ratio for SLC34 proteins, we used $K_i^{PFA} = 0.08$ mM and $K_i^{PFA} = 1$ mM based on the data of Ref. 52.

evidence that it is now time to revise this long-standing renal P_i-handling dogma.

ACKNOWLEDGMENTS

We thank Drs. Beatrice Beck-Schimmer, Martin Schäpfer, B. Stieger, and Paola Capuano for assistance with the animal preparation and Drs. Nati Hernando and Carsten A. Wagner for valuable discussions throughout this project.

GRANTS

This study was supported by financial contributions from the Swiss National Science Foundation to H. Murer (31-065397/1), the Spanish Ministry of Education and Science to V. Sorribas (BFU2006-06284/BFI), a predoctoral fellowship from the Government of Aragón, Spain (B086/2007) to R. Villa-Bellosta, and the National Institute of Diabetes and Digestive and Kidney Diseases to M. Levi (R01 DK-066029).

REFERENCES

1. **Bacconi A, Virkki LV, Biber J, Murer H, Forster IC.** Renouncing electrogenicity is not free of charge: switching on electrogenicity in a Na^+-coupled phosphate cotransporter. *Proc Natl Acad Sci USA* 102: 12606–12611, 2005.
2. **Bai L, Collins JF, Ghishan FK.** Cloning and characterization of a type III Na-dependent phosphate cotransporter from mouse intestine. *Am J Physiol Cell Physiol* 279: C1135–C1143, 2000.
3. **Beck L, Karaplis AC, Amizuka N, Hewson AS, Ozawa H, Tenenhouse HS.** Targeted inactivation of Npt2 in mice leads to severe renal phosphate wasting, hypercalciuria, and skeletal abnormalities. *Proc Natl Acad Sci USA* 95: 5372–5377, 1998.
4. **Berndt T, Kumar R.** Phosphatonins and the regulation of phosphate homeostasis. *Annu Rev Physiol* 69: 341–359, 2007.
5. **Berndt TJ, Kumar R.** Clinical disturbances of phosphate homeostasis. In: *Seldin and Giebisch's The Kidney*, edited by Alpern RJ and Hebert SC. New York, NY: Academic, 2008, p. 1989–2006.
6. **Biber J, Stieger B, Stange G, Murer H.** Isolation of renal proximal tubular brush-border membranes. *Nat Protoc* 2: 1356–1359, 2007.
7. **Broer S, Schuster A, Wagner CA, Broer A, Forster I, Biber J, Murer H, Werner A, Lang F, Busch AE.** Chloride conductance and Pi transport are separate functions induced by the expression of NaPi-1 in Xenopus oocytes. *J Membr Biol* 164: 71–77, 1998.
8. **Chien ML, Foster JL, Douglas JL, Garcia JV.** The amphotropic murine leukemia virus receptor gene encodes a 71-kilodalton protein that is induced by phosphate depletion. *J Virol* 71: 4564–4570, 1997.
9. **Custer M, Lotscher M, Biber J, Murer H, Kaissling B.** Expression of Na-P_i cotransport in rat kidney: localization by RT-PCR and immunohistochemistry. *Am J Physiol Renal Fluid Electrolyte Physiol* 266: F767–F774, 1994.
10. **Cutillas PR, Geering B, Waterfield MD, Vanhaesebroeck B.** Quantification of gel-separated proteins and their phosphorylation sites by LC-MS using unlabeled internal standards: analysis of phosphoprotein dynamics in a B cell lymphoma cell line. *Mol Cell Proteom* 4: 1038–1051, 2005.
11. **Fernandes I, Beliveau R, Friedlander G, Silve C.** $NaPO_4$ cotransport type III (PiT1) expression in human embryonic kidney cells and regulation by PTH. *Am J Physiol Renal Physiol* 277: F543–F551, 1999.
12. **Forster IC, Hernando N, Biber J, Murer H.** Proximal tubular handling of phosphate: a molecular perspective. *Kidney Int* 70: 1548–1559, 2006.
13. **Forster IC, Loo DD, Eskandari S.** Stoichiometry and Na^+ binding cooperativity of rat and flounder renal type II Na^+-P_i cotransporters. *Am J Physiol Renal Physiol* 276: F644–F649, 1999.
14. **Frei P, Gao B, Hagenbuch B, Mate A, Biber J, Murer H, Meier PJ, Stieger B.** Identification and localization of sodium-phosphate cotransporters in hepatocytes and cholangiocytes of rat liver. *Am J Physiol Gastrointest Liver Physiol* 288: G771–G778, 2005.
15. **Giachelli CM, Speer MY, Li X, Rajachar RM, Yang H.** Regulation of vascular calcification: roles of phosphate and osteopontin. *Circ Res* 96: 717–722, 2005.
16. **Gottschalk CW, Lassiter WE, Mylle M.** Localization of urine acidification in the mammalian kidney. *Am J Physiol* 198: 581–585, 1960.
17. **Kavanaugh MP, Kabat D.** Identification and characterization of a widely expressed phosphate transporter/retrovirus receptor family. *Kidney Int* 49: 959–963, 1996.
18. **Kavanaugh MP, Miller DG, Zhang W, Law W, Kozak SL, Kabat D, Miller AD.** Cell-surface receptors for gibbon ape leukemia virus and amphotropic murine retrovirus are inducible sodium-dependent phosphate symporters. *Proc Natl Acad Sci USA* 91: 7071–7075, 1994.
19. **Lanaspa MA, Giral H, Breusegem SY, Halaihel N, Baile G, Catalan J, Carrodeguas JA, Barry NP, Levi M, Sorribas V.** Interaction of MAP17 with NHERF3/4 induces translocation of the renal Na/Pi IIa transporter to the trans-Golgi. *Am J Physiol Renal Physiol* 292: F230–F242, 2007.
20. **Leung JC, Barac-Nieto M, Hering-Smith K, Silverstein DM.** Expression of the rat renal PiT-2 phosphate transporter. *Horm Metab Res* 37: 265–269, 2005.
21. **Levi M, Lotscher M, Sorribas V, Custer M, Arar M, Kaissling B, Murer H, Biber J.** Cellular mechanisms of acute and chronic adaptation of rat renal P_i transporter to alterations in dietary P_i. *Am J Physiol Renal Fluid Electrolyte Physiol* 267: F900–F908, 1994.
22. **Li X, Giachelli CM.** Sodium-dependent phosphate cotransporters and vascular calcification. *Curr Opin Nephrol Hypertens* 16: 325–328, 2007.
23. **Li X, Yang HY, Giachelli CM.** Role of the sodium-dependent phosphate cotransporter, Pit-1, in vascular smooth muscle cell calcification. *Circ Res* 98: 905–912, 2006.
24. **Lotscher M, Kaissling B, Biber J, Murer H, Levi M.** Role of microtubules in the rapid regulation of renal phosphate transport in response to acute alterations in dietary phosphate content. *J Clin Invest* 99: 1302–1312, 1997.
25. **Madjdpour C, Bacic D, Kaissling B, Murer H, Biber J.** Segment-specific expression of sodium-phosphate cotransporters NaPi-IIa and -IIc and interacting proteins in mouse renal proximal tubules. *Pflugers Arch* 448: 402–410, 2004.
26. **Miyamoto K, Ito M, Tatsumi S, Kuwahata M, Segawa H.** New aspect of renal phosphate reabsorption: the type IIc sodium-dependent phosphate transporter. *Am J Nephrol* 27: 503–515, 2007.
27. **Murer H, Forster I, Hilfiker H, Pfister M, Kaissling B, Lotscher M, Biber J.** Cellular/molecular control of renal Na/Pi-cotransport. *Kidney Int Suppl* 65: S2–S10, 1998.
28. **Murer H, Forster IC, Hernando N, Biber J.** Proximal Tubular Handling of Phosphate: Na/Pi-Cotransporters and their Regulation. In: *Seldin and Giebisch's The Kidney*, edited by Alpern RJ and Hebert SC. New York, NY: Acdemic, 2008, p. 1979–1988.
29. **Murer H, Hernando N, Forster I, Biber J.** Proximal tubular phosphate reabsorption: molecular mechanisms. *Physiol Rev* 80: 1373–1409, 2000.
30. **Murer H, Werner A, Reshkin S, Wuarin F, Biber J.** Cellular mechanisms in proximal tubular reabsorption of inorganic phosphate. *Am J Physiol Cell Physiol* 260: C885–C899, 1991.
31. **Nishimura M, Naito S.** Tissue-specific mRNA expression profiles of human solute carrier transporter superfamilies. *Drug Metab Pharmacokinet* 23: 22–44, 2008.
32. **Nowik M, Picard N, Stange G, Capuano P, Tenenhouse HS, Biber J, Murer H, Wagner CA.** Renal phosphaturia during metabolic acidosis revisited: molecular mechanisms for decreased renal phosphate reabsorption. *Pflugers Arch* 457: 539–549, 2008.
33. **Ohkido I, Segawa H, Yanagida R, Nakamura M, Miyamoto K.** Cloning, gene structure and dietary regulation of the type-IIc Na/Pi cotransporter in the mouse kidney. *Pflugers Arch* 446: 106–115, 2003.
34. **Olah Z, Lehel C, Anderson WB, Eiden MV, Wilson CA.** The cellular receptor for gibbon ape leukemia virus is a novel high affinity sodium-dependent phosphate transporter. *J Biol Chem* 269: 25426–25431, 1994.
35. **Pfister MF, Hilfiker H, Forgo J, Lederer E, Biber J, Murer H.** Cellular mechanisms involved in the acute adaptation of OK cell Na/Pi-cotransport to high- or low-Pi medium. *Pflugers Arch* 435: 713–719, 1998.
36. **Ravera S, Virkki LV, Murer H, Forster IC.** Deciphering PiT transport kinetics and substrate specificity using electrophysiology and flux measurements. *Am J Physiol Cell Physiol* 293: C606–C620, 2007.
37. **Ritthaler T, Traebert M, Lotscher M, Biber J, Murer H, Kaissling B.** Effects of phosphate intake on distribution of type II Na/Pi cotransporter mRNA in rat kidney. *Kidney Int* 55: 976–983, 1999.
38. **Salaun C, Rodrigues P, Heard JM.** Transmembrane topology of PiT-2, a phosphate transporter-retrovirus receptor. *J Virol* 75: 5584–5592, 2001.
39. **Saliba KJ, Martin RE, Broer A, Henry RI, McCarthy CS, Downie MJ, Allen RJ, Mullin KA, McFadden GI, Broer S, Kirk K.** Sodium-dependent uptake of inorganic phosphate by the intracellular malaria parasite. *Nature* 443: 582–585, 2006.
40. **Segawa H, Kaneko I, Takahashi A, Kuwahata M, Ito M, Ohkido I, Tatsumi S, Miyamoto K.** Growth-related renal type II Na/Pi cotransporter. *J Biol Chem* 277: 19665–19672, 2002.

41. **Segawa H, Onitsuka A, Aranami F, Tomeo Y, Kaneko I, Furutani J, Ito M, Matsumoto M, Li M, Amizuka N, Kuwahata M, Miyamoto KI.** Npt2a and Npt2c in mice play distinct and synergistic roles in inorganic phosphate metabolism and skeletal development. *J Amer Soc Nephrol* SA-FC101, 2007.
42. **Segawa H, Yamanaka S, Ito M, Kuwahata M, Shono M, Yamamoto T, Miyamoto K.** Internalization of renal type IIc Na-P_i cotransporter in response to a high-phosphate diet. *Am J Physiol Renal Physiol* 288: F587–F596, 2005.
43. **Segel IH.** *Enzyme Kinetics: Behavior and Analysis of Rapid Equilibrium and Steady-state Enzyme Systems*. New York, NY: Wiley, 1975.
44. **Szczepanska-Konkel M, Yusufi AN, VanScoy M, Webster SK, Dousa TP.** Phosphonocarboxylic acids as specific inhibitors of Na+-dependent transport of phosphate across renal brush border membrane. *J Biol Chem* 261: 6375–6383, 1986.
45. **Tatsumi S, Segawa H, Morita K, Haga H, Kouda T, Yamamoto H, Inoue Y, Nii T, Katai K, Taketani Y, Miyamoto KI, Takeda E.** Molecular cloning and hormonal regulation of PiT-1, a sodium-dependent phosphate cotransporter from rat parathyroid glands. *Endocrinology* 139: 1692–1699, 1998.
46. **Tenenhouse HS, Martel J, Gauthier C, Segawa H, Miyamoto K.** Differential effects of Npt2a gene ablation and X-linked Hyp mutation on renal expression of Npt2c. *Am J Physiol Renal Physiol* 285: F1271–F1278, 2003.
47. **Tenenhouse HS, Roy S, Martel J, Gauthier C.** Differential expression, abundance, and regulation of Na^+-phosphate cotransporter genes in murine kidney. *Am J Physiol Renal Physiol* 275: F527–F534, 1998.
48. **Traebert M, Lotscher M, Aschwanden R, Ritthaler T, Biber J, Murer H, Kaissling B.** Distribution of the sodium/phosphate transporter during postnatal ontogeny of the rat kidney. *J Am Soc Nephrol* 10: 1407–1415, 1999.
49. **Vieira FL, Malnic G.** Hydrogen ion secretion by rat renal cortical tubules as studied by an antimony microelectrode. *Am J Physiol* 214: 710–718, 1968.
50. **Villa-Bellosta R, Barac-Nieto M, Breusegem SY, Barry NP, Levi M, Sorribas V.** Interactions of the growth-related, type IIc renal sodium/phosphate cotransporter with PDZ proteins. *Kidney Int* 73: 456–464, 2008.
51. **Villa-Bellosta R, Bogaert YE, Levi M, Sorribas V.** Characterization of phosphate transport in rat vascular smooth muscle cells: implications for vascular calcification. *Arterioscler Thromb Vasc Biol* 27: 1030–1036, 2007.
52. **Villa-Bellosta R, Sorribas V.** Role of rat sodium/phosphate cotransporters in the cell membrane transport of arsenate. *Toxicol Appl Pharmacol* 232: 125–134, 2008.
53. **Virkki LV, Biber J, Murer H, Forster IC.** Phosphate transporters: a tale of two solute carrier families. *Am J Physiol Renal Physiol* 293: F643–F654, 2007.
54. **Virkki LV, Forster IC, Biber J, Murer H.** Substrate interactions in the human type IIa sodium-phosphate cotransporter (NaPi-IIa). *Am J Physiol Renal Physiol* 288: F969–F981, 2005.
55. **Yoshiko Y, Candeliere GA, Maeda N, Aubin JE.** Osteoblast autonomous Pi regulation via Pit1 plays a role in bone mineralization. *Mol Cell Biol* 27: 4465–4474, 2007.

Chapter 5

PiT transport mechanism

Deciphering PiT transport kinetics and substrate specificity using electrophysiology and flux measurements.

[*Am J Physiol Cell Physiol,* **2007**, *293,*C606C620]

Silvia Ravera, Leila V. Virkki, Heini Murer, and Ian C. Forster

Institute of Physiology and Center for Integrative Human Physiology, University of Zurich, Zurich, Switzerland

Am J Physiol Cell Physiol 293: C606–C620, 2007.
First published May 9, 2007; doi:10.1152/ajpcell.00064.2007.

Deciphering PiT transport kinetics and substrate specificity using electrophysiology and flux measurements

Silvia Ravera, Leila V. Virkki, Heini Murer, and Ian C. Forster

Institute of Physiology and Center for Integrative Human Physiology, University of Zurich, Zurich, Switzerland

Submitted 16 February 2007; accepted in final form 28 April 2007

Ravera S, Virkki LV, Murer H, Forster IC. Deciphering PiT transport kinetics and substrate specificity using electrophysiology and flux measurements. *Am J Physiol Cell Physiol* 293: C606–C620, 2007. First published May 9, 2007; doi:10.1152/ajpcell.00064.2007.—Members of the SLC20 family or type III Na^+-coupled P_i cotransporters (PiT-1, PiT-2) are ubiquitously expressed in mammalian tissue and are thought to perform a housekeeping function for intracellular P_i homeostasis. Previous studies have shown that PiT-1 and PiT-2 mediate electrogenic P_i cotransport when expressed in *Xenopus* oocytes, but only limited kinetic characterizations were made. To address this shortcoming, we performed a detailed analysis of SLC20 transport function. Three SLC20 clones (*Xenopus* PiT-1, human PiT-1, and human PiT-2) were expressed in *Xenopus* oocytes. Each clone gave robust Na^+-dependent $^{32}P_i$ uptake, but only *Xenopus* PiT-1 showed sufficient activity for complete kinetic characterization by using two-electrode voltage clamp and radionuclide uptake. Transport activity was also documented with Li^+ substituted for Na^+. The dependence of the P_i-induced current on P_i concentration was Michaelian, and the dependence on Na^+ concentration indicated weak cooperativity. The dependence on external pH was unique: the apparent P_i affinity constant showed a minimum in the pH range 6.2–6.8 of ~0.05 mM and increased to ~0.2 mM at pH 5.0 and pH 8.0. *Xenopus* PiT-1 stoichiometry was determined by dual ^{22}Na-$^{32}P_i$ uptake and suggested a 2:1 Na^+:P_i stoichiometry. A correlation of $^{32}P_i$ uptake and net charge movement indicated one charge translocation per P_i. Changes in oocyte surface pH were consistent with transport of monovalent P_i. On the basis of the kinetics of substrate interdependence, we propose an ordered binding scheme of Na^+:$H_2PO_4^-$:Na^+. Significantly, in contrast to type II Na^+-P_i cotransporters, the transport inhibitor phosphonoformic acid did not inhibit PiT-1 or PiT-2 activity.

Na^+-P_i cotransport; two-electrode voltage clamp; surface pH electrode; SLC20; retroviral receptor

INORGANIC PHOSPHATE (P_i) is fundamental to many metabolic processes, and it is a component of many biological structures. As a negatively charged anion, P_i has to be actively transported into the cell via an active transport process. In mammals, this task is carried out by two unrelated Na^+-P_i cotransporter families. The well-characterized type II Na^+-coupled P_i cotransporter family (SLC34) has been shown to be instrumental for P_i absorption and reabsorption at the apical membrane of many epithelia (20, 25, 28, 29, 40). The type III Na^+-P_i or PiT cotransporters (SLC20) were initially identified as retroviral receptors and later shown to be Na^+-P_i cotransporters (33, 41, 60). PiT proteins are present in all kingdoms and use either the transmembrane Na^+ (animals, fungi) or H^+ (plants, bacteria) gradients to drive P_i transport.

The two known mammalian PiT members, PiT-1 and PiT-2, have a broad tissue distribution (3, 30, 33, 50). This suggests that they may play a housekeeping role for P_i homeostasis in cells, but other roles for PiT proteins are also emerging. For example, PiT-mediated P_i transport appears to play an important role in providing P_i for the formation of mineralized bone (8, 46, 62). Furthermore, PiT proteins have been strongly implicated in pathological calcification of vascular tissue in response to hyperphosphatemia (31, 34, 39). Recently it was shown (43) that the malaria parasite *Plasmodium falciparum* expresses a PiT protein that is essential for providing the parasite with P_i for growth.

Although P_i plays a central role in cell metabolism as well as in normal and pathological calcification, the PiT transporters that provide cells with P_i have not been well characterized. Most studies have relied on radionuclide uptake measurements, where lack of membrane-potential control makes interpretation of kinetic studies of electrogenic transport processes difficult. Data analysis is further complicated by the low transport rates attained when expressing mammalian PiT-1 and PiT-2 heterologously. This may explain why, apart from the initial reports by Kavanaugh et al. (32, 33), no further electrophysiological characterization has been done.

We reasoned that *Xenopus* oocytes might express a *Xenopus* protein better than mammalian ones and decided to express a *Xenopus* homolog (XlPiT-1) as well as human PiT (hPiT)-1 and hPiT-2 in *Xenopus* oocytes. The P_i transport attained with XlPiT-1 far exceeded that of either mammalian isoform, and therefore most of our kinetic characterization was done using XlPiT-1. Using electrophysiology, radiotracer flux, and surface pH measurements, we show that PiT transports two Na^+ ions for each P_i and that the preferred P_i species is monovalent $H_2PO_4^-$. PiT transport is affected by pH because of the dependence of the $H_2PO_4^-$:HPO_4^{2-} ratio on pH, and between pH 6.2 and 8.0 there is no effect of H^+ per se on PiT function. On the basis of the kinetics of substrate interdependence, we propose an ordered binding scheme of Na^+:$H_2PO_4^-$:Na^+; however, the lack of significant pre-steady-state current precludes the assignment of voltage dependence to a particular partial reaction in the transport cycle.

During the preparation of this manuscript, a report on PiT-mediated P_i transport in vascular smooth muscle cells appeared (53). This study, based on $^{32}P_i$-uptake assays, provides confirmation of our findings concerning phosphonoformic acid (PFA), Li^+, and pH dependence. However, because PiT-mediated P_i transport is electrogenic, controlling the membrane potential (V_m) is essential for determining transport kinetics, and thus the electrophysiological findings that we

Address for reprint requests and other correspondence: I. C. Forster, Institute of Physiology, Univ. of Zurich, Winterthurerstrasse 190, CH-8057 Zurich, Switzerland (e-mail: Iforster@access.uzh.ch).

The costs of publication of this article were defrayed in part by the payment of page charges. The article must therefore be hereby marked "*advertisement*" in accordance with 18 U.S.C. Section 1734 solely to indicate this fact.

report herein both complement and extend those of Ref. 53 and previous tracer-flux studies.

MATERIALS AND METHODS

Molecular Biology and Oocyte Expression

cDNAs encoding hPiT-1, XlPiT-1, and hPiT-2 from the German Resource Center for Genome Research (RZPD) were subcloned into a KSM expression vector (56) to improve expression in *Xenopus laevis* oocytes. In some experiments, we used a type II Na^+-P_i transporter cloned from flounder (flounder NaPi-IIb) for comparison. The plasmids were linearized and were used as a template for the synthesis of capped cRNA by using the mMESSAGE mMACHINE T3 kit (Ambion).

Stage V–VI defolliculated oocytes from *X. laevis* were isolated and maintained as described previously (57). Oocytes were injected with 50 nl of cRNA (50 ng). Control oocytes were either injected with 50 nl of water or not injected. Oocytes were incubated at 16°C in modified Barth's solution, containing (in mM) 88 NaCl, 1 KC1, 0.41 $CaCl_2$, 0.82 $MgSO_4$, 2.5 $NaHCO_3$, 2 $Ca(NO_3)_2$, and 7.5 HEPES, pH 7.4, adjusted with Tris. The solution was supplemented with 5 mg/l doxycycline.

Electrophysiology and radiotracer flux experiments were performed 2–5 days after injection. Each data set was obtained from at least two batches of oocytes from two different donor frogs.

Reagents and Solutions

The solution compositions were as follows. Control superfusate (ND100) contained (in mM) 100 NaCl, 2 KCl, 1.8 $CaCl_2$, 1 $MgCl_2$, and 10 HEPES adjusted to pH 7.4 using Tris, unless otherwise stated (different pHs, different concentration of Ca^{2+} or Mg^{2+}). For pH ≤ 6.2, MES was substituted for HEPES. Na^+-free superfusate composition was as for ND100 with isosmotic substitution of choline chloride for NaCl (ND0) or LiCl (LD100). Solutions with intermediate Na^+ concentrations were prepared by mixing ND0 and ND100 in appropriate proportions. For substrate test solutions, P_i was added from 1 M K_2HPO_4 and KH_2PO_4 stocks premixed to give the required pH. PFA was added from 100 mM stock; arsenate and sulfate were added from 1 M stocks.

Radiotracer Uptake

A group of oocytes (7–10 oocytes/group) was first allowed to equilibrate in uptake solution without tracer. After aspiration of this solution, we added 100 μl uptake solution containing radiotracer ($^{32}P_i$ alone or both $^{32}P_i$ and ^{22}Na). The uptake was allowed to proceed for 15–20 min before it was stopped by washing the oocytes four times with 4 ml ice-cold ND0 solution containing 0.5 mM cold P_i. Uptake of $^{32}P_i$ alone was carried out by using ND100 solution and 1 mM cold P_i, to which $^{32}P_i$ (specific activity 10–20 mCi/mmol P_i) was added. Simultaneous uptake of $^{32}P_i$ and ^{22}Na was done in ND50 solution (50 mM NaCl; pH 6.2 or pH 7.4) with 2 mM cold P_i. These concentrations of cold P_i and Na^+ were used to balance the specific activities of the two radionuclides. $^{32}P_i$ was added to obtain 7 mCi/mmol P_i, and ^{22}Na was added to obtain 1.4 mCi/mmol Na. After being washed, oocytes were placed individually in a scintillation vial and lysed in 250 μl 10% SDS. $^{32}P_i$ activities of individual oocytes were counted by using a Packard Tri-Carb 2900TR scintillation counter. To separate the counts of $^{32}P_i$ and ^{22}Na, we programmed the counter for dual DPM assay with quench curves. Net P_i and Na^+ uptakes for each individual oocyte were plotted, and linear regression analysis was performed to obtain the Na:P_i transport stoichiometry.

Electrophysiology

Standard two-electrode voltage-clamp hardware was used [GeneClamp, Model 500 (Molecular Devices) or a laboratory-built clamp (17)]. Clamp hardware was controlled and data were acquired by using pClamp 8 software (Molecular Devices), which also controlled valves for solution switching. At the onset of each experiment, the oocyte was clamped to a holding potential (V_h) = −50 mV and was superfused with ND100 solution. To measure P_i-induced currents (I_{Pi}), the superfusate was switched to one containing P_i and the change in the holding current was monitored. When the current had reached a steady state, the perfusate was switched back and washout of P_i was monitored by observing the return of holding current to baseline.

Rundown of Electrogenic Activity and Estimation of Membrane Capacitance

Repeated application of P_i to voltage-clamped oocytes often resulted in a progressive loss of activity, which in severe cases amounted to >50% loss by the end of an experiment (see Fig. 2*A*). To take account of rundown in those experiments where repeated P_i applications induced a reduction in I_{Pi}, successive test applications were bracketed with control substrate applications (1 mM P_i in ND100). These were normalized to the response at *time 0* and were fitted with a single exponential that satisfactorily described the time course of rundown. The test values were then rescaled by a factor derived from the fit. To obtain a mechanistic insight into the rundown of I_{Pi}, we correlated changes in the oocyte membrane capacitance (C_m, indicative of changes in membrane area), with the decrease in I_{Pi} documented with repeated exposure of P_i. C_m was determined by measuring the current transient in response to voltage steps from −50 mV to −60 mV and to −40 mV, integrating the capacitive transients and calculating the mean from the magnitude of the two charge estimates (23).

Measurement of Apparent P_i and Na^+ Affinities

The oocyte was voltage clamped to V_h = −50 mV, and the holding current was continuously recorded. To measure I_{Pi}, the superfusate was switched to one containing P_i and change in the holding current was monitored. When the current had ′reached a steady state, the superfusate was switched back and washout of P_i was monitored by observing the return of holding current to baseline. When I_{Pi} was recorded for another Na^+ concentration or pH, the holding current was first allowed to stabilize at the new reference solution before being switched to one containing P_i. To control for current rundown, each P_i test pulse was bracketed by a control (1 mM P_i) application, which was used to correct the measurements. To determine the apparent affinity constant for P_i ($K^{P_i}_{0.5}$), I_{Pi} was measured by using different P_i concentrations while keeping the Na^+ concentration constant. For determining the apparent affinity constant for Na^+ ($K^{Na}_{0.5}$), the oocyte was first perfused with a specific concentration of Na^+ before being switched to one containing P_i (i.e., the P_i concentration was kept constant throughout the experiment). Estimates of $K^{Pi}_{0.5}$ and $K^{Na}_{0.5}$ were obtained by fitting data with the modified Hill equation given by

$$I_{P_i} = I^{max}_{P_i}[S]_{n_H}/([S]_{n_H} + (K^{S}_{0.5n_H}) + I_{OFF} \quad (1)$$

where $I^{max}_{P_i}$ is the maximum current attainable, I_{OFF} is a variable offset (see below), [S] is the variable substrate concentration, and n_H is the Hill coefficient.

The voltage dependence of I_{Pi} was measured by applying potentials from −160 or −140 mV to +40 mV and subtracting the current records for the same potential in the presence and absence of P_i, as described previously (17, 55). To account for the differences in expression levels between individual oocytes, data obtained from each oocyte were normalized to I_{Pi} recorded at −100 mV with 100 mM Na^+ and 1 mM P_i in the bath at pH 7.4 before the data was fitted with *Eq. 1*. The offset was included to account for the leak current that we have documented in NaPi-IIa-expressing oocytes in the absence of P_i but that is blocked by P_i with an unknown affinity (12, 55).

Pre-Steady-State Current Measurements

Pre-steady-state currents were recorded by applying voltage steps from $V_h = -60$ mV to test potentials. To improve the signal resolution without distorting the current during the membrane-charging phase when exogenous charge movements might occur, the endogenous capacitive transient was partially suppressed by using a capacitive transient simulator.

Simultaneous Voltage Clamp and $^{32}P_i$ Uptake

These experiments were carried out as previously described (2, 55). Briefly, an oocyte was placed in a superfusion chamber and the membrane voltage was clamped to −80 mV. After the holding current had stabilized, the superfusate was switched from ND100 (pH 7.4 or pH 6.2) to ND100 solution (with the same pH) containing 1 mM cold P_i and $^{32}P_i$ at a specific activity of 5 mCi/mmol P_i. After ~5 min, the perfusate was switched back to ND100 solution, and washout of P_i was monitored by following the return of the current to baseline. The oocyte was then removed from the chamber and lysed in 10% SDS, and oocyte radioactivity was counted by using a scintillation counter.

The net charge (Q) translocated by the transporter was calculated by first subtracting the baseline holding current and then by integrating the I_{Pi}. Net P_i uptake and Q were plotted for each individual oocyte, and linear regression analysis was used to obtain the P_i:Q translocation ratio.

Surface pH Measurements

pH-sensitive microelectrodes of the liquid-membrane type (1) were manufactured as previously described (19). For surface pH measurements, we used electrodes with a large tip diameter (~20 μM) that were fire polished to obtain a smooth surface. The pH electrode potential was measured by using a laboratory-built unity-gain electrometer amplifier. The signal from the pH electrode was electronically subtracted from that of the V_m electrode of the two-electrode voltage clamp. Because the V_m electrode was intracellular and the pH electrode extracellular, the V_h (intracellular − bath) was then subtracted from the signal to obtain extracellular pH. The pH electrodes were calibrated by using a two-point calibration (pH 8.0 and 6.0).

Continuous current and pH recordings were obtained from voltage-clamped ($V_h = -10$ mV, −50 mV, or −100 mV) control oocytes or oocytes expressing XlPiT-1 or flounder NaPi-IIb. In these experiments, the buffering power of the ND100 solution was decreased by reducing the amount of HEPES from 10 to 2 mM. The response of the pH electrode to application of 1 mM P_i was recorded with the pH electrode either in the bath or pressed firmly against the oocyte surface. Because applying P_i with the pH electrode in the bath caused a deflection in the pH signal of 5–8 mV, possibly due to an unspecific interaction of the P_i ion with the liquid membrane, we subtracted the P_i-induced deflection obtained with the electrode in the bath from the one obtained with the electrode pressed against the oocyte surface.

RESULTS

Expression of Type III Na-P_i Cotransporter Isoforms in Xenopus Oocytes and Basic Transport Characteristics

We first investigated the P_i transport capabilities of the different clones by performing $^{32}P_i$ uptake in 100 mM Na, 100 mM choline, and 100 mM lithium. Figure 1*A* shows P_i uptake measured in oocytes expressing hPiT-1, XlPiT-1, and hPiT-2 and in uninjected oocytes. P_i uptake was much higher in oocytes expressing XlPiT-1 than in either human isoform. P_i uptake was highest in the presence of Na^+ for all isoforms, but we also observed P_i uptake in choline and Li^+ that was significantly larger than in control oocytes (except for hPiT-1 in choline solution).

Next, we investigated the electrogenic response of hPiT-1, XlPiT-1, and hPiT-2 to 1 mM P_i in ND100 solution. First we recorded a continuous current response to 1 mM P_i by using $V_h = -50$ mV (Fig. 1*B*). Application of 1 mM P_i induced an inward current, which indicated transport of positive charge into the cell. The magnitude of the I_{Pi} was highest in oocytes expressing XlPiT-1, intermediate in hPiT-2, and lowest in hPiT-1, which paralleled the P_i uptake results documented in Fig. 1*A*. It is conceivable that the difference in $^{32}P_i$ transport and I_{Pi} results from different expression levels of the three isoforms; however, because the turnover rate and the number of active transporters in the membrane are not known for any of the isoforms, this remains speculative. Uninjected oocytes from the same batch did not show P_i-induced inward current (data not shown).

The voltage dependence of I_{Pi} in XlPiT-1 and hPiT-2 is shown in Fig. 1*C*. Again, XlPiT-1-expressing oocytes showed a higher I_{Pi} than the human isoform, but the voltage dependence of I_{Pi} was similar for the two clones. We were unable to

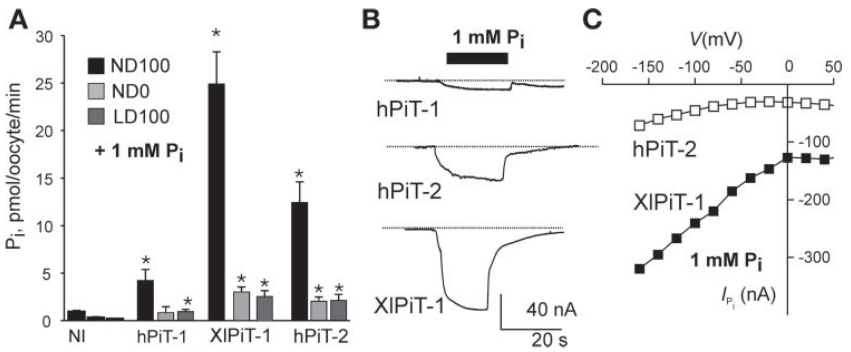

Fig. 1. P_i transport mediated by different type III Na^+-coupled P_i cotransporter (PiT) isoforms. *A*: $^{32}P_i$ uptake performed on control, noninjected oocytes (NI) and oocytes expressing human (h) PiT-1, *Xenopus* (Xl) PiT-1, or hPiT-2 in superfusates containing 100 mM Na^+ (ND100), 100 mM choline (ND0), or 100 mM Li^+ (LD100). *B*: original current traces obtained from 3 oocytes from the same batch expressing hPiT-1, hPiT-2, and XlPiT-1 in response to 1 mM P_i at −50 mV. *C*: voltage dependence of the P_i-induced current (I_{Pi}) induced by 1 mM P_i in oocytes from the same batch expressing hPiT-2 (□) and XlPiT-1 (■). Data points are joined for visualization only. Asterisks indicate statistically significant uptake compared with NI oocytes under same external bath conditions (Student's *t*-test, $P < 0.05$).

determine with confidence the voltage dependence of I_{Pi} in oocytes expressing hPiT-1 because of the small currents.

Rundown of I_{Pi}. On repeated and continuous P_i application, we observed that I_{Pi} in XlPiT-1-expressing oocytes decreased. This phenomenon was particularly severe in oocytes giving large I_{Pi} (≤ -100 nA at $V_h = -50$ mV). Figure 2*A* shows a current recording from a representative oocyte where we applied 1 mM P_i for 20 s at 1-min intervals. Such a loss of activity could result from accumulation of substrate of the *trans* side of the membrane, resulting in inhibition of the forward transport rate. Alternatively, it could result from a reduction in the number of active cotransporters in the membrane due to endocytosis (23). To investigate the latter hypothesis, we investigated whether changes in the oocyte whole cell capacitance accompanied the decrease in I_{Pi} . The capacitance was taken as a measure of the oocyte membrane area, and a decrease in capacitance (C_m) would indicate that endocytosis had occurred. Figure 2*B* shows I_{Pi} plotted against the change in C_m (ΔC_m) induced by repeated P_i applications. The decrease in I_{Pi} was accompanied by a decrease in C_m that strongly suggested that endocytosis of transporters was induced by repeated P_i exposure. However, the correlation between the decrease in I_{Pi} and ΔC_m was not linear, and therefore other mechanisms must also play a role.[1]

P_i Dependence of XlPiT-1 at pH 7.4

To investigate the electrogenic response of XlPiT-1 to P_i in more detail, we determined the P_i dependence at different V_m. Pooled current-voltage (*I-V*) data are shown in Fig. 3*A* for P_i varying from 0.01 mM to 1 mM with 100 mM Na^+, pH 7.4. At the lowest P_i concentration tested (0.01 mM), the slope of the *I-V* data was positive and reversed direction in the range -30 mV to -50 mV. The response to 0.01 mM P_i varied between batches of oocytes and suggested that a P_i-dependent leak component was also present, as previously reported for the type II Na^+-P_i cotransporter (17). For all other P_i concentrations, the currents did not reverse, even up to +60 mV, for those oocytes where endogenous activating currents were judged to be negligible (data not shown). By transposing the *I-V* data, we obtained the P_i dependence at each test potential (Fig. 3*B*). The data were well described analytically by fitting them with a form of the Michaelis-Menten function (*Eq. 1*, with $n_H = 1$) for test potentials $\leq$0 mV. We accounted for the putative P_i-inhibitable leak component by including a variable offset in the fit function (see *Measurement of Apparent P_i and Na^+Affinities*) as previously described (12, 55). For potentials >0 mV, the P_i dependence was prone to contamination by endogenous activating currents, which precluded analysis in this region. The Michaelian behavior suggested that there was one P_i interaction site for each XlPiT-1 transporter. These fits yielded an estimate for the apparent $K_{0.5}^{P_i}$ that was independent of the test potential (Fig. 3*F*), and the predicted maximum electrogenic activity ($I_{P_i}^{max}$) showed a curvilinear voltage dependence with no evidence of rate-limiting behavior at the hyperpolarizing limit (Fig. 3*E*). The lack of voltage dependence of $K_{0.5}^{P_i}$with 100 mM Na^+ superfusion suggested that P_i did not interact with the transmembrane electric field.

To determine the nature of the substrate interaction (i.e., ordered vs. random binding), we repeated this assay by superfusing oocytes in 50 and 25 mM Na^+. To aid comparison, we normalized the data to the response to 1 mM P_i at -100 mV and 100 mM Na^+. Reducing external Na^+ led to a concomitant reduction in currents at all potentials, as illustrated for 25 mM Na^+ superfusion (Fig. 3*C*), and we also observed a P_i dependence. Like the behavior in 100 mM Na^+, these data were well described by fitting with *Eq. 1* to yield estimates for $K_{0.5}^{P_i}$ and $I_{P_i}^{max}$. The predicted $K_{0.5}^{P_i}$ at 50 mM Na^+ exceeded $K_{0.5}^{P_i}$ at 100 mM Na^+ slightly and deviated at depolarizing potentials. This trend was even more obvious for 25 mM Na^+; at -100 mV, $K_{0.5}^{P_i}$ doubled and the voltage dependence was clearly evident in the depolarizing direction (Fig. 3*F*). The behavior suggested that voltage-dependent transitions in the transport cycle were rate determining and dependent on Na^+ ion availability. The maximum P_i-induced current ($I_{P_i}^{max}$) obtained from the fits was also dependent on external Na^+ (Fig. 3*E*), which implied that the interaction of Na^+ and P_i with XlPiT-1 was ordered (45). Moreover, if we assume that I_{Pi} is a measure of the number of carrier proteins with fully bound substrate the dependence of $I_{P_i}^{max}$ on Na^+ would be consistent with Na^+ ions being the last substrate to bind before translocation (45).

Na^+ Dependence of XlPiT-1 at pH 7.4

To investigate the dependence of I_{Pi} on external Na^+, we determined the *I-V* relationship for I_{Pi} by varying the external Na^+ from 0 to 100 mM, with $P_i = 1$ mM (Fig. 4*A*). As expected, at all test potentials, I_{Pi} decreased in a concentration-dependent manner with decreasing external Na^+. *I-V* data were pooled and normalized to I_{Pi} induced by 1 mM P_i at -100 mV, to take account of different expression levels. As for the P_i-dependence assays, for $V_m > 0$ mV, the data were less reliable due to contamination from endogenous activating currents, and analysis was only performed for $V \leq 0$ mV. The data were transposed into a Na^+-dependence relationship that showed obvious saturation at all test potentials. Together with our finding of a saturable P_i dependence of the electrogenic response (Fig. 3*B*), the Na^+ dependence provided complementary evidence for carrier-type behavior for XlPiT-1 with respect to Na^+ as the variable substrate. The Na^+-dependence data were well described by fitting with the modified Hill equation (*Eq. 1*; Fig. 4*B*). With all four fit parameters unconstrained, the fits predicted a n_H close to unity. An *F*-test that compared the fits for the unconstrained case (n_H as a free parameter) with the Michaelian model ($n_H = 1$) indicated that there was no statistical difference ($P > 0.3$) between the two models for all test potentials. All subsequent fitting for determination of the apparent affinity constant for Na^+ ($K_{0.5}^{Na}$) and maximum P_i-inducible current ($I_{P_i}^{max}$) was therefore constrained with $n_H = 1$ to reduce the uncertainty in estimating these parameters. If we assume that more than one Na^+ ion is translocated per transport cycle, which would be the most straightforward explanation for the observed electrogenicity, the Michaelian behavior of the Na^+ dependence suggests that there was little cooperativity for the interaction of Na^+ ions with the transporter.

[1] Rundown of response has also been reported for the SLC5A8 Na^+-monocarboxylate cotransporter (9), and these authors suggested that it resulted from *trans* inhibition, because it was not observed at low substrate concentrations. We have also documented rundown behavior for oocytes expressing the flounder NaPi-IIb, where a decrease in C_m was also found (I. C. Forster, unpublished data). The phenomenon also appeared to depend on the batch of oocytes and, in the case of PiTs, suggested that internalization of transporters occurs as a result of P_i-activated oocyte-signaling pathways.

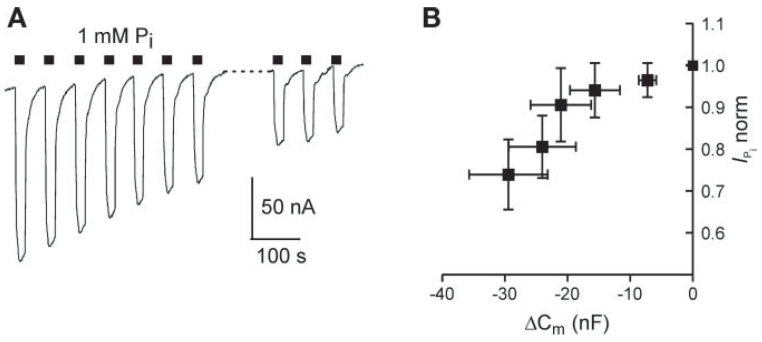

Fig. 2. Current rundown induced by repeated P_i exposure in XlPiT-1-expressing oocytes. *A*: original trace from an oocyte expressing XlPiT-1 repeatedly exposed to 1 mM P_i for 20 s at 1-min intervals, showing a decrease in I_{Pi} of 60% at the end of the experiment. *B*: decrease in I_{Pi} as a function of change in membrane capacitance (ΔC_m). I_{Pi} was recorded during repeated exposures to 1 mM P_i, normalized to the first application of P_i, and plotted against ΔC_m accumulated since the start of the experiment.

We obtained further insight into the nature of substrate interactions by studying the Na^+ dependence at P_i concentrations close to the predicted apparent $K_{0.5}^{Pi}$. For 0.3 mM total P_i (data not shown) and 0.1 mM total P_i (Fig. 4*C*), we also observed a monotonic dependence of I_{P_i} on Na^+. To compare the different P_i conditions, we normalized each data point to I_{Pi} induced by 1 mM P_i at −100 mV and superfusion in 100 mM Na^+. After transposition of these data, saturation with respect to Na^+ was also evident, and the data were similarly well described by a Michaelian relationship (Fig. 4*D*) for test potentials ≤−40 mV. The normalized $I_{P_i}^{max}$ was obviously dependent on P_i (Fig. 4*E*). The apparent affinity for Na^+ was also voltage dependent, and $K_{0.5}^{Na}$ increased with membrane hyperpolarization (Fig. 4*F*). There was no statistical difference for $K_{0.5}^{Na}$ with P_i = 1 and 0.3 mM; however, for P_i = 0.1 mM, $K_{0.5}^{Na}$ increased markedly in the depolarizing direction. At hyperpolarizing potentials, the $K_{0.5}^{Na}$ data suggested that there was an asymptotic limit for this parameter that was independent of P_i and V_m.

Transport Stoichiometry of XlPiT-1

Simultaneous voltage clamp and uptake of $^{32}P_i$. We measured the Q transferred for each P_i molecule transported by performing simultaneous voltage clamp and $^{32}P_i$ uptake measurements in oocytes expressing XlPiT-1. Uninjected oocytes served as controls. This assay was performed at two pH values (6.2 and 7.4) to determine whether the transporter has a preference for mono- or divalent P_i. For a pK_a of 6.8, the ratio $H_2PO_4^-$:HPO_4^{2-} at pH 6.2 is 4:1, whereas at pH 7.4 it is 1:4. If

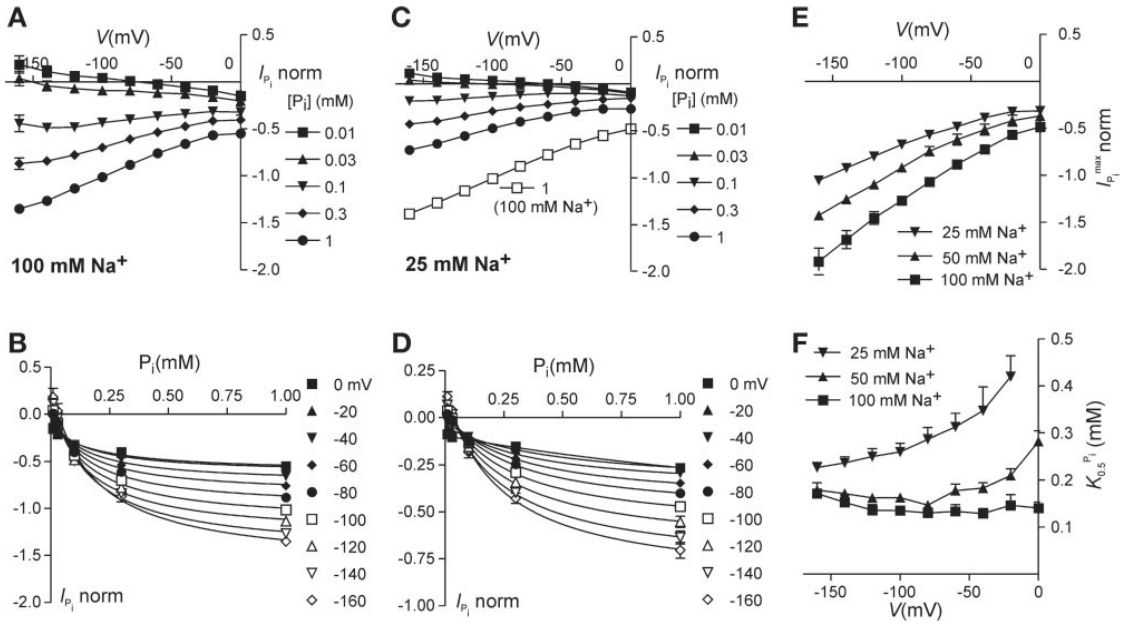

Fig. 3. P_i dependence of XlPiT-1 at pH 7.4. *A*: current-voltage (*I-V*) data for I_{Pi} with total P_i as the variable substrate and Na^+ fixed at 100 mM, normalized to the response to 1 mM P_i at −100 mV in 100 mM Na^+ (n = 7). Data points are joined for visualization only. *B*: transformation of data in *A* to show P_i dependence at each test potential. Continuous lines are fits using *Eq. 1*. *C*: *I-V* data obtained in 25 mM Na^+ and normalized as in *A* (n = 9). *D*: transformation of data in *C* fitted with *Eq. 1*. *E*: voltage dependence of maximum P_i-induced current (I_{Pi}) reported by fitting *Eq. 1* to the P_i dependencies for the 3 Na^+ concentrations indicated. *F*: voltage dependence of apparent affinity constant of P_i ($K_{0.5}^{Pi}$) reported by curve fitting for 3 Na^+ concentrations indicated. Error bars in *E* and *F* indicate SE of fit. For Na^+ = 50 mM, data were pooled from n = 5 oocytes.

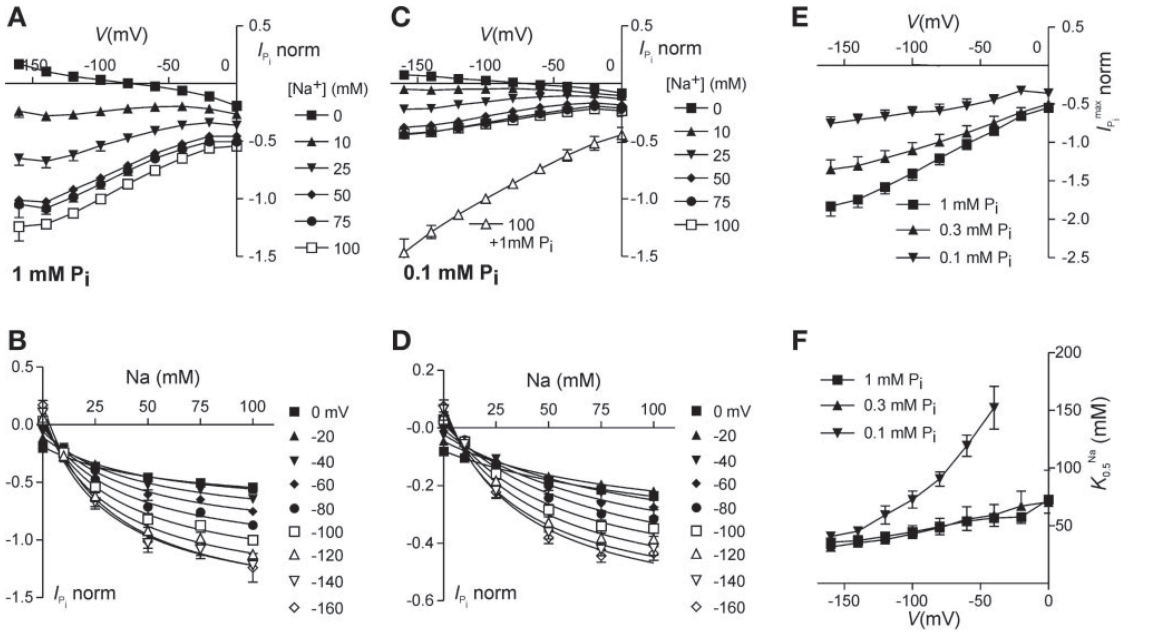

Fig. 4. Na^+ dependence of XlPiT-1 at pH 7.4. *A*: *I-V* data for I_{Pi} with Na^+ as the variable substrate and P_i fixed at 1 mM (total), normalized to the response to 1 mM P_i at −100 mV in 100 mM Na^+ ($n = 7$). Data points are joined for visualization only. *B*: transformation of the data in *A* to show Na^+ dependence at each test potential. Continuous lines are fits using *Eq. 1*. *C*: *I-V* data obtained with 0.1 mM P_i (total) and normalized as in *A* ($n = 6$). *D*: transformation of the data in *C* and fitted with *Eq. 1*. *E*: voltage dependence of I_{Pi} reported by fitting *Eq. 1* to the Na^+ dependencies for the 3 P_i concentrations indicated. *F*: voltage dependence of apparent affinity constant of Na ($K_{0.5}^{Na}$) reported by curve fitting for 3 P_i concentrations indicated. Error bars in *E* and *F* indicate SE of fit. For $P_i = 0.3$ mM, data were pooled from $n = 7$ oocytes.

both species were transported with similar efficiencies, we would expect the Q:P_i ratio to change with different pH (assuming that the number of Na^+ ions transported per P_i remain unchanged). Figure 5*A* shows an original current trace of and oocyte expressing XlPiT-1 and held at $V_h = -80$ mV. The oocyte was initially superfused with ND100 solution; then 1 mM P_i with $^{32}P_i$ as a tracer was applied as indicated. After washout of P_i, the holding current was allowed to return to baseline before the oocyte was removed and lysed for scintillation counting to measure intracellular $^{32}P_i$. The Q moved was calculated by integrating the area under the I_{Pi} trace.

Figure 5*B* shows transferred Q plotted against the amount of transported P_i for each individual oocyte. Linear regression analysis showed that the ratio of charge to P_i was close to unity for both pH values tested (0.93 ± 0.04 at pH 7.4 and 0.82 ± 0.03 at pH 6.2), indicating that one charge is moved for each transported P_i. In control oocytes exposed to the same experimental manipulation as oocytes expressing XlPiT-1, no I_{Pi} were observed and the amount of P_i taken up was minimal.

Dual uptake of $^{32}P_i$ and ^{22}Na. Next we performed simultaneous uptake of $^{32}P_i$ and ^{22}Na at pH 6.2 and 7.4 to measure the Na:P_i transport stoichiometry. These experiments were per-

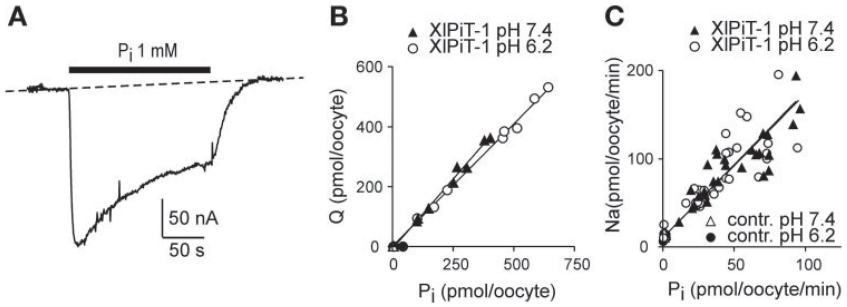

Fig. 5. Transport stoichiometry of XlPiT-1. *A*: original trace showing I_{Pi} in an oocyte expressing XlPiT-1 at a holding potential (V_h) of −80 mV. Dashed line indicates baseline. *B*: transferred charge Q was obtained by integrating I_{Pi} from recordings similar to *A* and plotted as a function of P_i uptake (measured using $^{32}P_i$) into the same oocyte. The slope of Q:P_i was obtained by using linear regression and was 0.93 ± 0.04 for pH 7.4 and 0.82 ± 0.03 for pH 6.2. *C*: unidirectional Na^+ uptake (measured using ^{22}Na) was plotted against P_i uptake (measured using $^{32}P_i$) for each oocyte. The slope of Na:P_i was obtained by using linear regression and was 1.6 ± 0.1 for pH 7.4 and 1.7 ± 0.1 for pH 6.2. The regression lines were forced through the values measured for noninjected oocytes.

formed without voltage clamping the oocytes. We reduced the Na^+ concentration in the solution to 50 mM and increased the P_i concentration to 2 mM to ensure that the energy spectra of the radioactive isotopes were well separated by the scintillation counter. The amount of Na^+ and P_i taken up by each oocyte was calculated from the amount of radioactivity accumulated in each cell. Figure 5*C* shows a plot of Na^+ uptake as a function of P_i uptake for each individual cell. Using linear regression analysis, we obtained a Na:P_i ratio of 1.6 ± 0.1 for pH 7.4 and 1.7 ± 0.1 for pH 6.2, suggesting that the Na:P_i stoichiometry is 2:1. However, because the measured Na:P_i ratio was not exactly an integer, it is possible that another substrate, for example H^+, may substitute for Na^+. However, because there was no difference between the slopes of the regression lines measured at pH 6.2 and 7.4, representing a 16-fold difference in H^+ concentration, it seems unlikely that H^+ would play a significant role as transported substrate.

Surface pH measurements. Finally, we made surface pH measurements to determine if XlPiT-1 preferentially transported monovalent or divalent P_i. If the transporter were to remove monovalent $H_2PO_4^-$ from the extracellular solution, we would expect an alkalinization to occur, because excess HPO_4^{2-} left behind would combine with H^+ to form $H_2PO_4^-$, thus causing an increase in pH. On the other hand, if divalent HPO_4^{2-} were the preferred species, we would expect to observe an acidification. Inside the oocyte, the pH changes would be reversed. However, we did not see any P_i-induced changes in intracellular pH in oocytes expressing NaPi-IIb (I. C. Forster, unpublished observations) or in XlPiT-1-expressing oocytes (data not shown). This is most likely due to the low transport rate accomplished when expressing these transporters in oocytes and the high buffering capacity of the oocyte [~20 mM/ΔpH (e.g., Ref. 10)].

To observe pH changes in the bath solutions due to XlPiT-1 transport activity, we fabricated pH-sensitive microelectrodes with a large tip area and fire-polished them to be very smooth, so that they did not damage the oocyte surface. Pressing the tip of such an electrode onto the top of an oocyte creates a microenvironment to which diffusion of substrate from the bulk medium is slowed down (but not blocked). This enables pH changes caused by P_i transport to be recorded, provided that the P_i removal rate by the transporter exceeds the H^+ diffusion rate to or from the bulk medium. To magnify any pH change occurring, we reduced the buffering power of the ND100 solution from 7.2 to 1.4 mM/ΔpH by reducing the HEPES concentration from 10 to 2 mM.

Figure 6*A* shows surface pH recording from a control oocyte, an oocyte expressing XlPiT-1, and an oocyte expressing flounder NaPi-IIb, along with the corresponding current recordings. Application of 1 mM P_i caused a small deflection in the voltage signal from the pH electrode, which translated into an apparent decrease in pH of 0.02–0.05 pH units. We believe, however, that this may be an artifact caused by interaction of P_i ions with the liquid membrane electrode, because we observed no difference in pH between the two solutions with a glass electrode. When we repeated the P_i application with the pH electrode pressed against the surface of a control oocyte ("ON") we observed an identical deflection in the signal from the pH electrode. However, when the pH electrode was pressed against the surface of an XlPiT-1-expressing oocyte, the direction of the pH change was reversed, showing that an alkalinization occurred on the surface of the oocyte. This would be consistent with transport of monovalent $H_2PO_4^-$ by XlPiT-1. In contrast, when we pressed the pH electrode onto the surface of an oocyte expressing flounder NaPi-IIb, the magnitude of the pH deflection was increased. This acidification of the oocyte surface indicated that NaPi-IIb transports divalent HPO_4^{2-}, which is in excellent agreement with previous studies (2, 22, 55) on the stoichiometry and substrate specificity of the type II Na^+-P_i cotransporter family.

Figure 6*B* summarizes surface pH changes recorded in control oocytes and in oocytes expressing XlPiT-1 or NaPi-IIb at three different potentials. The pH change was calculated from the difference in the P_i-induced change in pH observed with the pH electrode pressed onto the oocyte surface (ON) and with the pH electrode freely in the bath (OFF). No pH changes were observed on the surface of control oocytes at any V_h. In contrast, we consistently observed alkalinization on the surface of XlPiT-1-expressing oocytes, whereas acidification was observed for NaPi-IIb. Both responses were statistically different

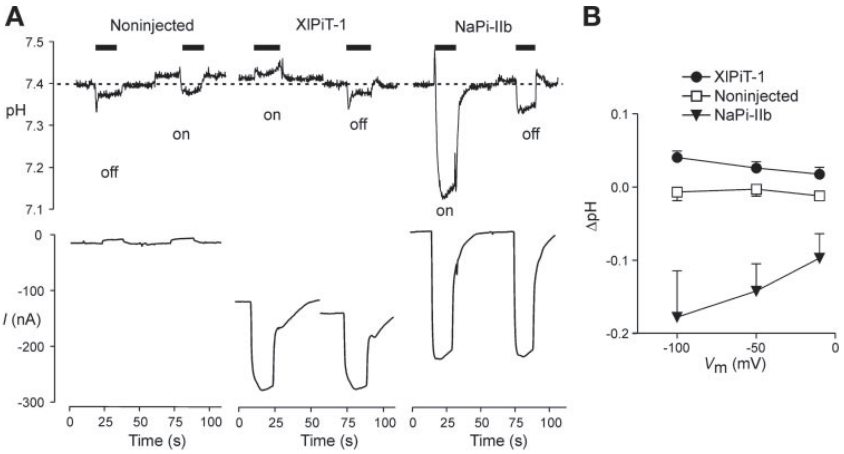

Fig. 6. Surface pH measurements. *A*: original tracings showing extracellular pH (*top*) and current (*bottom*) recorded from a control oocyte and an oocyte expressing XlPiT-1 or flounder type II Na-P_i cotransporter (NaPi-IIb). Black bars above the pH trace indicate application of 1 mM P_i. OFF and ON denote when pH electrode was freely in bath or firmly pressed onto surface of oocyte, respectively, during P_i exposure. Dashed line indicates pH 7.4 measured with electrode in bath. *B*: summary of the differences between the P_i-induced change in pH for ON and OFF (ΔpH) recorded at different V_h in different oocytes; $n = 5$ for control and XlPiT-1, and $n = 3$ for NaPi-IIb. ΔpH recorded from oocytes expressing XlPiT-1 and NaPi-IIb differed significantly from controls (2-way ANOVA).

from the values obtained in control oocytes, as determined by using two-way ANOVA. The magnitude of the pH change tended to increase with increasing hyperpolarization (which increases the transport rate); however, this trend did not reach statistical significance.

Role of metal-ion complexes. Bottger et al. (4) recently reported that $^{32}P_i$ uptake into oocytes expressing hPiT-1 and hPiT-2 was reduced by ~46 and ~42%, respectively, when Ca^{2+} and Mg^{2+} were omitted from the incubation medium. They suggested that divalent cations modulate the P_i-transport capacities of the proteins rather than P_i being transported as a metal complex, as has been reported for some bacterial P_i transporters (51, 52). We addressed the role of divalents by measuring the current induced by 1 mM P_i in oocytes expressing XlPiT-1. We found that I_{Pi} was reduced by 29 ± 2% when both Ca^{2+} and Mg^{2+} were removed and by 15 ± 2 and 12 ± 1% when either Ca^{2+} or Mg^{2+} was removed, respectively (n = 6). These values were significantly smaller than reported by Bottger et al. (4).

pH Dependence of P_i Transport in XlPiT-1

To determine the pH dependence of P_i transport by PiT-1, we measured the apparent affinity constant for P_i ($K_{0.5}^{P_i}$) in XlPiT-1-expressing oocytes at seven pH values in the range 5.0–8.0. The V_m was held at −50 mV, and deflections in I_{Pi} induced by application of P_i at different concentrations were monitored. The oocyte responses were normalized to I_{Pi} obtained with 1 mM P_i, pH 7.4, to allow pooling of data from oocytes with different expression levels. We plotted I_{Pi} as a function of P_i concentration (Fig. 7*A*) and fitted the data with *Eq. 1* (n_H was constrained to 1). For clarity, only four pH conditions are shown. Figure 7*B* shows the fitted parameters $K_{0.5}^{P_i}$ (*left axis*) and $I_{P_i}^{max}$ (*right axis*) as a function of pH. The data show that $I_{P_i}^{max}$ is unaffected by a change in pH between 5 and 7.4. $I_{P_i}^{max}$ slightly decreased only when pH increased to 8.0. In contrast, large changes were documented for the apparent P_i affinity. $K_{0.5}^{P_i}$ increased both when pH was lowered below pH 6.2 or increased above pH 6.8 (Fig. 7*B*). However, given a pK_a for $H_2PO_4^-$:HPO_4^{2-} of 6.8, and because the preferred substrate for XlPiT-1 is $H_2PO_4^-$ (Fig. 6), it would appear that the increase in $K_{0.5}^{P_i}$ seen when pH was increased above pH 6.8 resulted from a reduced availability of monovalent $H_2PO_4^-$. Indeed, if we calculate the apparent affinity constant for $H_2PO_4^-$ ($K_{0.5}^{H_2PO_4^-}$) instead of for P_i (Fig. 7*B*), we see essentially no change in $K_{0.5}^{H_2PO_4^-}$ for pH values >6.8.

To investigate whether protons alter the Na^+ dependence, for example by substituting for Na^+ or modulating the kinetics of Na^+ interaction, we repeated the Na^+-dependence assay at pH 6.2 and 8.0 for V_m in the range from −140 mV to 0 mV by using 1 mM P_i. Na^+ dose dependencies were fitted with *Eq. 1* as before to obtain estimates for $K_{0.5}^{Na}$ and I_{Pi}. As shown in Fig. 7*C*, the normalized maximum attainable current showed the same voltage dependence for all pH values. Furthermore, for pH 7.4 and 8.0, we documented no significant alteration in

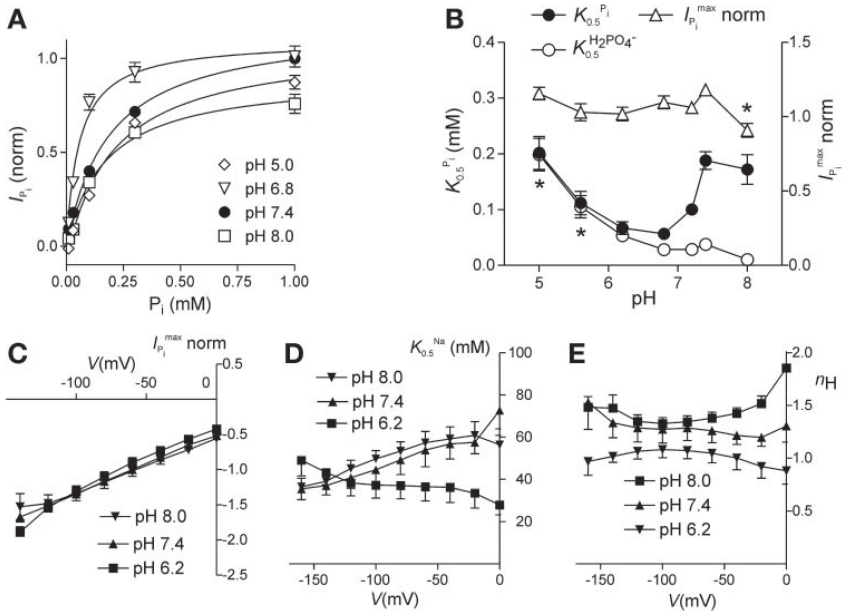

Fig. 7. pH dependence of P_i transport by XlPiT-1. *A*: I_{Pi} at −50 mV were determined at different concentrations of P_i over the pH range 5.0–8.0. Data obtained from each oocyte were normalized to I_{Pi} measured at pH 7.4, 1 mM P_i. Pooled data were fit with *Eq. 1* [Hill coefficient (n_H) constrained to 1; continuous lines]. For clarity, only data for 4 of the 7 different pH conditions are shown. *B*: fit parameters from data in *A* were plotted as a function of pH. Since $H_2PO_4^-$ concentration changes with pH, we calculated both $K_{0.5}^{P_i}$ and $K_{0.5}^{H_2PO_4^-}$. *Left axis*, $K_{0.5}^{P_i}$ and $K_{0.5}^{H_2PO_4^-}$; *right axis*, I_{Pi}. Asterisk indicates that value differs significantly ($P < 0.05$, ANOVA) from corresponding value at pH 7.4. No statistics were calculated for $K_{0.5}^{P_i}$; n = 4–8 in *A* and *B*. *C*: I_{Pi} plotted as a function of voltage for 3 pH values. There was no statistical difference between points over range of voltages shown. *D*: $K_{0.5}^{Na}$ plotted as a function of voltage for 3 pH values. Data for pH 7.4 and 8.0 were not statistically different, but pH 6.2 data were significantly different. *E*: n_H of Na^+ dependence fits plotted as a function of voltage for 3 pH values. Two-way ANOVA indicated that n_H was significantly influenced by pH but not by voltage. In *C*, *D*, and *E*, data are shown as means ± SE; pH 6.2 (n= 8); pH 7.4 (n = 10); pH 8.0 (n = 9).

either the magnitude or voltage dependence of $K_{0.5}^{Na}$, whereas at pH 6.2, $K_{0.5}^{Na}$ showed little variation with voltage and the apparent affinity for Na^+ increased. This behavior reflects the interdependence of substrates in determining their apparent affinities because at pH 6.2, there is an increased availability of the preferred species, $H_2PO_4^-$. We also observed that at pH 8.0, fits to the Na^+-dependence data with n_H as a free parameter were improved compared with those by fixing $n_H = 1$. This behavior suggested that at the higher pH the cooperativity of Na^+ interaction increased.

Substrate Specificity

Arsenate is structurally similar to P_i and is a known substrate for members of the SLC34 family of Na^+-P_i cotransporters (7, 27). To investigate whether arsenate is also a substrate for the type III family, we performed $^{32}P_i$ uptake and electrophysiology assays. First, we performed $^{32}P_i$ uptake on uninjected oocytes and oocytes expressing hPiT-1, XlPiT-1, and hPiT-2 by using 0.3 mM cold P_i with or without 1 mM arsenate. Arsenate induced a significant reduction in P_i transport in the two PiT-1 isoforms. However, arsenate did not affect P_i transport by hPiT-2 (Fig. 8).

The reduction in $^{32}P_i$ uptake in the presence of arsenate may have resulted from inhibition or substitution of arsenate for P_i. To investigate these possibilities further, we studied the transport behavior by electrophysiology. Under voltage clamp, arsenate induced currents in oocytes expressing XlPiT-1. Applying 1 mM arsenate elicited an inward current that was ~40% of current induced by 1 mM P_i (Fig. 8*B*). This suggested that arsenate is indeed transported by XlPiT-1. In contrast, no significant change in the holding current was observed when applying sulfate (1 mM; Fig. 8*B*). We then measured the apparent arsenate affinity constant ($K_{0.5}^{arsenate}$) in XlPiT-1-expressing oocytes and normalized the current response to that obtained with 1 mM P_i for each oocyte. Fitting the data in Fig. 8*C* with *Eq. 1* gave a $K_{0.5}^{arsenate}$ of 0.83 ± 0.10 mM, which indicated that the arsenate affinity of XlPiT-1 was significantly smaller than its affinity for P_i (0.19 ± 0.02 mM at pH 7.4 in Fig. 7*A*). In addition, the maximum attainable arsenate current ($I_{arsenate}^{max}$), as reported by the fit of Eq. 1 to the arsenate data, was smaller compared with P_i (0.74 compared with 1.2 for similarly normalized data), which indicated that the transporter transports arsenate at a slower rate than P_i.

Lithium is known to support transport in some Na^+-coupled transporters such as the Na^+-dicarboxylate transporter (42) and Na^+-driven Cl^-/HCO_3^- exchanger (54). Our results from the $^{32}P_i$ uptake experiment (Fig. 1*A*) and others (6, 53) indicated that P_i transport through PiT isoforms could be driven by Li^+. We revisited this question by using electrophysiology in oocytes expressing XlPiT-1. We recorded currents induced by 1 mM P_i in 100 mM Na^+, 100 mM Li^+, and 100 mM choline$^+$ solutions at $V_h = -50$ mV. Under these conditions, P_i elicited a current response in Li^+ that was ~15 ± 1% of the response seen in Na^+, whereas in 100 mM choline, P_i did not elicit inward currents (data not shown). Thus it appears that Li^+ also can act as a substrate for PiT, whereas choline is excluded.

Inhibitors of PiT

PFA is a well-documented competitive inhibitor of the type II Na^+-P_i cotransporter (7, 47) and has also been reported to inhibit PiT-mediated P_i uptake (3, 49). Recently, Villa-Bellosta et al. (53) showed by using $^{32}P_i$ uptake assays that PFA is a very poor inhibitor of P_i uptake mediated by rat PiT-1 and PiT-2 both in oocytes and in native rat vascular smooth muscle cells. We investigated the effect of PFA at a concentration of 1 mM on oocytes expressing PiT proteins by means of $^{32}P_i$ uptake and electrophysiology. First, we measured $^{32}P_i$ uptake in uninjected oocytes and oocytes expressing hPiT-1, XlPiT-1, or hPiT-2 with 0.3 mM cold P_i with or without 1 mM PFA. Figure 9A shows that PFA did not cause any statistically significant differences in P_i uptake in any of the isoforms studied.

Similarly, under voltage clamp at −50 mV, XlPiT-1-expressing oocytes showed no difference in electrogenic activity when 1 mM PFA was applied in the presence of 0.3, 0.1, or 0.03 mM P_i compared with the response to P_i alone (Fig. 9, *B* and *C*). PFA induced a small upward deflection of the holding current that we also observed for uninjected oocytes. We also

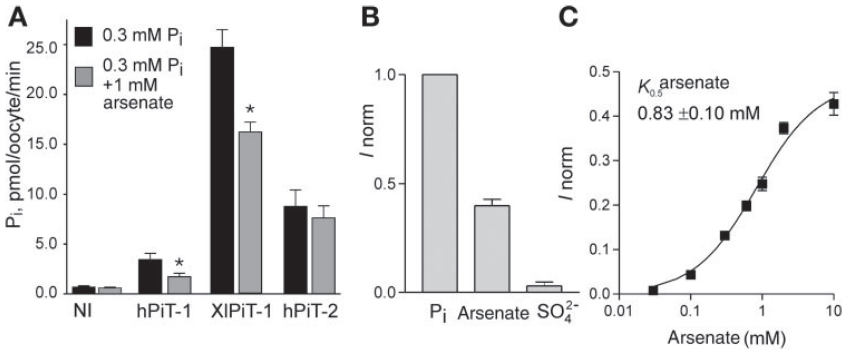

Fig. 8. Arsenate and sulfate (SO_4^{2-}) as potential PiT substrates. *A*: $^{32}P_i$ uptake was performed in control oocytes (NI) and in oocytes expressing hPiT-1, XlPiT-1, or hPiT-2 by using ND100 solution with 0.3 mM P_i with or without 1 mM arsenate. Arsenate significantly decreased P_i uptake for both PiT-1 clones but not for hPiT-2. *B*: current response to 1 mM P_i, 1 mM arsenate, and 1 mM SO_4^{2-} was measured in oocytes expressing XlPiT-1 at $V_h = -50$ mV. Data from each oocyte were normalized to current response in 1 mM P_i. *C*: current response to different concentrations of arsenate was measured in oocytes expressing XlPiT-1 at $V_h = -50$ mV. Arsenate-induced current was normalized to value obtained with 1 mM P_i for each oocyte and was plotted as a function of arsenate concentration. Solid line indicates fit with *Eq. 1*.

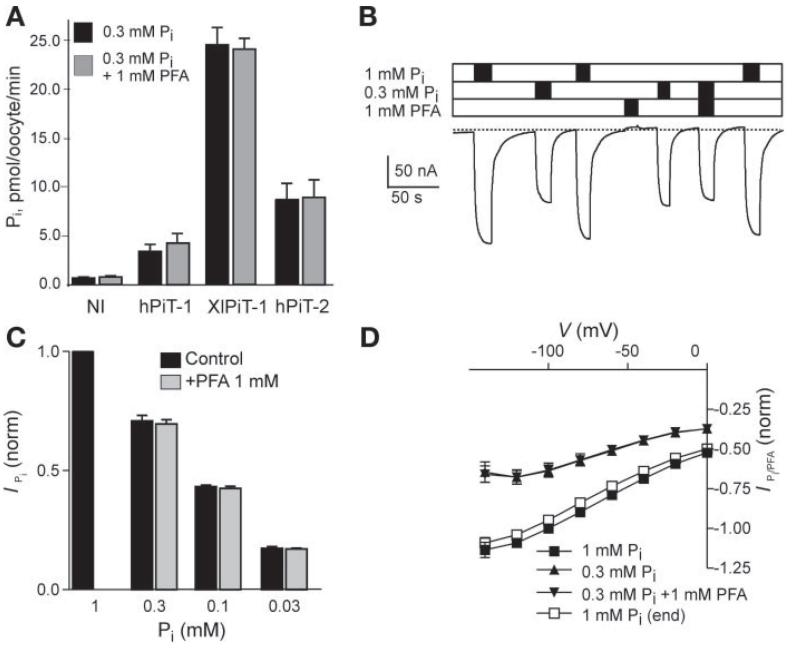

Fig. 9. Phosphonoformic acid (PFA) does not alter transport activity of PiT-1 and -2 isoforms. *A*: $^{32}P_i$ uptake performed in control oocytes and in oocytes expressing hPiT-1, XlPiT-1, or hPiT-2 by using ND100 solution with 0.3 mM P_i with or without 1 mM PFA. No statistically significant effect of PFA was observed for any groups. *B*: original recording from an XlPiT-1-expressing oocyte, with $V_h = -50$ mV. Bars indicate period of application of substrates as indicated. Response to 1 mM P_i was repeated at end to test for response rundown, which for this cell was <10% of initial response. *C*: oocytes expressing XlPiT-1 were clamped to $V_h = -50$ mV, and currents elicited by different concentrations of P_i, applied with or without 1 mM PFA, were recorded. Data were normalized with respect to current response recorded at 1 mM P_i. *D*: *I-V* data showing I_{Pi} for XlPiT-1-expressing oocytes. P_i was applied either alone or together with 1 mM PFA ($n = 4$).

observed no effect of PFA on currents elicited by 0.3 mM P_i in voltage-jump experiments, which extended the voltage range examined (Fig. 9*D*). As a positive control, an oocyte from the same donor frog that expressed the flounder NaPi-IIb gave 75% inhibition at −100 mV (data not shown). Thus we can conclude that, in contrast to its action as a competitive inhibitor of type II Na^+-P_i cotransporters, PFA does not inhibit P_i transport mediated by PiT.

Technetium-99m dimercaptosuccinic acid [^{99m}Tc-(V)-DMSA] is a radiopharmaceutical agent with potential in the medical imaging of tumors. Recently, Denoyer et al. (11) reported that entry of ^{99m}Tc-(V)-DMSA in tumor cell lines is mediated by PiT transporters. We investigated whether DMSA could affect I_{Pi} or whether we could observe DMSA-induced currents in XlPiT-1-expressing oocytes. We observed no effect of 1 mM DMSA alone nor any effect of 1 mM DMSA on currents induced by 0.1 mM P_i in XlPiT-1-expressing oocytes at either pH 6.2 or 7.4 (data not shown), indicating that DMSA is neither transported by nor able to block P_i transport mediated by XlPiT-1. It is, however, possible that an interaction of DMSA with PiT transporters requires chelation with technetium [Denoyer et al. (11) only used ^{99m}Tc-(V)-DMSA, not DMSA alone, in their studies]. This question will remain open for further studies.

Pre-Steady-State Kinetics

Pre-steady-state current relaxations induced by voltage steps are a common property of electrogenic members of the SLC34 Na^+-P_i cotransporter family (NaPi-IIa/b; reviewed in Ref. 21), and relaxations in the millisecond range are readily observed superimposed on the oocyte capacitive-charging transient. We applied the same experimental protocols to XlPiT-1-expressing oocytes (e.g., Refs. 17 and 55); however, from the raw data alone for oocytes exhibiting comparable I_{Pi} (−200 nA) as observed for the type II cotransporters, we were unable to distinguish pre-steady-state relaxations from the endogenous response either in ND100 or ND0 (not shown).

At saturating concentrations, P_i is known to suppress pre-steady-state charge movements (17), and therefore, in a further attempt to detect charge movements, we subtracted records in ND100 from the corresponding traces in ND100 + 1 mM P_i and then examined the time course of currents at the voltage-step onset at high time resolution (Fig. 10*A*). The current did not change immediately at the onset of the voltage step, and we observed a finite time dependence as the current settled to the new steady-state value. This was qualitatively similar to the time course documented for the type II Na^+-P_i cotransporter (e.g., Ref. 24) under similar experimental conditions. Moreover, the relaxations extended beyond the range of the membrane-charging time (1–2 ms) and were therefore unlikely to have originated from a voltage-clamp artifact. For uninjected oocytes from the same donor frog, no relaxations were observed under the same experimental conditions (data not shown). Interestingly, the apparent charge movements were not balanced, i.e., the area under the relaxation curve was not the same for the ON and OFF steps as illustrated in Fig. 10*B* for two traces at extreme hyper- and hypopolarizing potentials. Under the assumption that we had detected all transient charges for both steps, the lack of charge balance suggested that the relaxations do not arise from a conserved charge movement within the transmembrane field. Nevertheless, the apparent charge associated with the ON transition correlated with I_{Pi} over a wide range of expression levels ($n = 12$), which strongly suggested that the relaxations were associated with the presence of XlPiT-1 in the membrane (Fig. 10*C*).

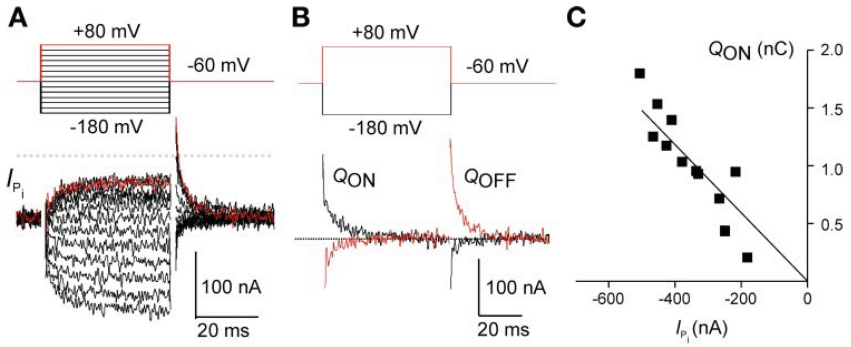

Fig. 10. Pre-steady-state relaxations of XlPiT-1. *A*: I_{Pi} in response to voltage steps from $V_h = -60$ mV to test potentials from −180 mV to +80 mV. Each trace is difference between recording with ND100 + 1 mM P_i and ND100. Dashed line indicates 0 current level. A 1.6-ms interval after each step onset was blanked, during which membrane potential was undefined due to finite voltage-clamp speed. Red trace indicates data for a voltage step from −60 mV to −180 mV. Recording bandwidth was 1 kHz. *B*: extracted traces from data set in *A* for steps to −180 mV and +80 mV with baseline removed to illustrate putative P_i-dependent charge movement associated with XlPiT-1. Note lack of charge balance for ON and OFF steps. *C*: correlation between steady-state I_{Pi} for a step to −140 mV and apparent net on charge (Q_{ON}) for same step found by integrating under relaxation ($n = 12$). Linear regression line was arbitrarily forced through the origin.

DISCUSSION

We have performed a thorough characterization of the transport kinetics of PiT. Previous studies used mammalian PiT-1 and PiT-2 isoforms expressed in *Xenopus* oocytes or various cell lines and assayed transport activity by radionuclide uptake. The apparent $K_{0.5}^{P_i}$ reported in these studies lay between 50 and 500 μM for measurements in cell lines (14, 33, 41, 48, 49, 60) and between 40 and 300 μM in oocytes (3, 4, 48). Whereas cell-specific environmental issues might influence $K_{0.5}^{P_i}$ measured in different environments, it is also most likely that the lack of membrane-potential control as well as contamination from endogenous P_i-transport systems may have contributed to the spread in the measurements. The problem is further exacerbated by the low P_i-transport levels attained in these systems, possibly explaining why only limited electrophysiological characterization has previously been carried out (32, 33).

Reasoning that *Xenopus* oocytes might express a *Xenopus* protein better than a mammalian one, we compared the P_i transport levels of XlPiT-1, hPiT-1, and hPiT-2 by heterologous expression in *Xenopus* oocytes. Indeed, our results show that XlPiT-1 expressed far better than either of the mammalian isoforms, and therefore we performed most of our kinetic characterization on XlPiT-1. At the amino acid level, XlPiT-1 is ~78% identical to hPiT-1 and ~60% identical to hPiT-2, and it is possible that the isoforms differ to some extent in their kinetic profiles. However, the main transport-function characteristics, such as substrate specificity, binding order, transport stoichiometry, pH sensitivity, and voltage dependence are probably very similar in the different isoforms, given the high degree of amino acid identity, thus validating the use of XlPiT-1 as a model for vertebrate PiT-1 characteristics in general.

Transport Stoichiometry Determination

Our results from the simultaneous ^{22}Na vs. $^{32}P_i$ and charge vs. $^{32}P_i$ uptake experiments strongly suggest that the transport cycle of XlPiT-1 involves the transport of 2 Na^+ ions, one P_i in the form of the monovalent $H_2PO_4^-$ ion, and one net positive charge. Because the transport stoichiometries were the same, whether measured at pH 6.2 ($H_2PO_4^-$:HPO_4^{2-} ratio 4:1) or at pH 7.4 ($H_2PO_4^-$:HPO_4^{2-} ratio 1:4), it appears that the transporter has an absolute preference for monovalent P_i. Furthermore, pH changes recorded at the oocyte surface are consistent with transport of $H_2PO_4^-$. This contrasts with the behavior of the flounder NaPi-IIb, for which surface pH changes were consistent with transport of HPO_4^{2-}. Thus the results from the surface pH measurements are in excellent agreement with the stoichiometry measurements from simultaneous radionuclide uptake and voltage-clamp experiments both for type II (22, 55) and type III (this study) Na^+-P_i cotransporters.

A 2:1 Na:P_i transport stoichiometry for PiT was initially proposed by Kavanaugh and Kabat (32), but the experimental data were never published. Using $^{32}P_i$ uptake experiments in oocytes expressing mouse PiT-2, Bai et al. (3) observed that the Na^+ dependence of P_i transport showed a very weak positive cooperativity with a n_H of 1.1. This low cooperativity agrees with our electrophysiological findings for XlPiT-1, in which the cooperativity of Na^+ binding became apparent only at pH 8.0, where the $H_2PO_4^-$ concentration is 0.059 mM. At higher $H_2PO_4^-$ concentrations, we observed no cooperativity for the Na^+ dependence (see Fig. 3), and fitting the data with a Michaelian function was statistically indistinguishable from a free fit to the Hill equation. Recently, Saliba et al. (43) showed elegantly that the intraerythrocytic malaria parasite *Plasmodium falciparum* uses a type III Na^+-P_i cotransporter (PfPiT) to mediate Na^+-driven P_i uptake. By using isolated parasites, they estimated a n_H of 2.1 for the Na^+ dependence of $^{32}P_i$ influx, and by using a "static head" experiment, they confirmed the 2:1 Na^+:P_i stoichiometry.

Thus the 2:1 Na^+:$H_2PO_4^-$ stoichiometry of PiT has been unequivocally demonstrated in these studies. Because PiT proteins transport $H_2PO_4^-$, we would expect that this would cause a concomitant acid loading of the cell. In contrast, type II Na^+-P_i cotransporters, which mediate HPO_4^{2-} transport, would alkalinize the cell. Whether the transport rates of type II or type III Na^+-P_i cotransporters in their natural environments are high enough to affect cell pH is not known and has not, to our knowledge, been studied in any cell system. Our own

experience with expressing type II and type III Na^+-P_i cotransporters in *Xenopus* oocytes would suggest that the pH changes would be minimal at most. However, with respect to acid-base regulation in general, the question as to which P_i species is preferential might be of some consequence. For example, in the average human body, ~70% of filtered P_i is reabsorbed in the form of divalent HPO_4^{2-} in the kidney proximal tubule via type II Na^+-P_i cotransporters. Because $H_2PO_4^-$ remains, this effectively constitutes a "secretion" of H^+ into the primary urine. For a glomerular filtration rate of 180 l/day, a serum P_i concentration of 1 mM, and a pH of 7.4 in the lumen of the proximal tubule, we estimate that ~40 mmol of H^+ a day is "excreted" into the proximal tubular lumen this way.

Other Substrates

Anions. In addition to Na^+ and $H_2PO_4^-$, it appears that PiT-1 and PiT-2 transport few other substrates, with the exception of arsenate. Arsenate is a phosphate mimetic and is highly toxic to cells because it can substitute for P_i in glycolytic and cellular respiration pathways. Accordingly, it is transported both by type II Na^+-P_i cotransporters (7, 27) and PiT (this study). In both transporter families, $K_{0.5}^{arsenate}$ is three to four times higher than $K_{0.5}^{P_i}$ and the transport rate of arsenate is slower than that for P_i, showing that it is not a perfect P_i substitute. In contrast to arsenate, SO_4 did not induce any currents in XlPiT-1-expressing oocytes.

Cations. In PiT proteins, Li^+ ions can act as cosubstrates, as evidenced by both tracer flux (6, 53) and electrophysiology, but the transport rate is much lower than for Na^+ (the magnitude of the I_{Pi} in XlPiT-1 using 1 mM P_i in 100 mM Li^+ solution was only ~15% of that in 100 mM Na^+). We do not know if this is because the affinity for Li^+ is much lower than that for Na^+ or because Li^+ is transported less efficiently than Na^+, because the currents were too small to carry out a dose-dependence measurement. Other cations, such as choline or K^+ (53), do not support P_i transport.

Protons. Protons serve as the driving ion in PiT family members from plants and bacteria (5), whereas in vertebrates the driving force of PiT is provided by Na^+. Bottger et al. (4) first reported Na^+-independent P_i transport via hPiT-2. Their finding was recently confirmed by Villa-Bellosta et al. (53), who reported that in oocytes expressing rat PiT-2, lowering pH from 7.5 to 6.0 in choline solution resulted in small (~7% of that observed in Na^+) but statistically significant P_i uptake. These findings indicate that in PiT-2 protons may, to some extent, substitute for Na^+. No such effect was seen for rat PiT-1 in their study, which indicated that this effect is specific for PiT-2. For XlPiT-1, we observed identical Na:P_i and charge:P_i ratios at pH 6.2 and 7.4 despite a 16-fold difference in the H^+ gradient, indicating that in XlPiT-1 H^+ does not substitute for Na^+.

Previous studies have shown that PiT-mediated P_i transport is reduced at alkaline pH when measured at a constant total P_i concentration (3, 4, 53). However, protons do not appear to have a strong effect on PiT per se (see Fig. 7), and thus the mechanism by which changes in H^+ concentration affect the transport rate of PiT-1 is mainly through alteration of the $H_2PO_4^-$:HPO_4^{2-} ratio. In XlPiT-1, we observed a decrease in the apparent $H_2PO_4^-$ affinity at pH < 6.2 (Fig. 7*B*); however, the maximum attainable transport rate was unaffected.

This contrasts with the type II Na^+-P_i cotransporters, where increasing H^+ reduces the P_i transport rate via several mechanisms, including modulation of the state occupancy of the empty carrier and competitive interaction with Na^+ binding (19, 24, 55). Thus the two families of P_i transporters respond differently to changes in pH, and these differences in the pH dependence may serve as a useful tool to identify the dominant P_i transport system in a system where the molecular identity of the transporter is unknown.

Divalent cations. Divalent cations are essential for some P_i-transport systems in bacteria (51, 52), where P_i is transported as a neutral metal-ion ($MeHPO_4$) complex driven by the proton-motive force. Recently, Bottger et al. (4) reported that P_i transport rates for hPiT-1 and hPiT-2 were decreased by ~46 and ~42%, respectively, when both Ca^{2+} and Mg^{2+} ions were removed from the medium, and they suggested that this is because divalent cations modulate PiT function. We replicated their experiment by using electrophysiology and found that removing all divalent cations from the solution decreased P_i-dependent currents in XlPiT-1-expressing oocytes by ~30%. This result indicated that both P_i transport and net charge transfer were reduced when divalent cations were omitted, which suggested that the cotransport, charge-transferring transport cycle was affected and not a bacteria-like $MeHPO_4$ leak pathway. The Ca^{2+}/Mg^{2+} dependence of P_i transport could be explained by, for example, modulation of surface charge of a membrane by divalent cations, and they have been shown to allosterically modulate the transport activity of the vitamin C transporter SVCT2 (26).

PFA does not inhibit PiT

PFA is a well-known competitive inhibitor of Na^+-dependent P_i transport (35, 47). Inhibition studies using heterologously expressed type II Na^+-P_i cotransporters have unequivocally shown that PFA inhibits NaPi-II-mediated P_i transport (7, 61). In contrast, only limited data is available on the effect of PFA on PiT proteins. Bai et al. (3) expressed mouse PiT-2 in *Xenopus* oocytes and documented a 40% decrease in $^{32}P_i$ uptake by using a 50-fold excess of PFA (5 mM). Recently, Villa-Bellosta et al. (53) reported that high concentrations of PFA (≥2.5 mM, ≥50-fold excess of PFA) reduced P_i uptake in vascular smooth muscle cells and in oocytes expressing PiT-1 or PiT-2.

We found no effect of PFA on $^{32}P_i$ uptake in any of the PiT isoforms studied and no effect of PFA on I_{Pi} mediated by XlPiT-1 (Fig. 9*C*), which confirms the findings of Villa-Bellosta et al. (53) with 1 mM PFA found by uptake assays alone. To avoid nonspecific effects, we did not use concentrations of PFA > 1 mM, because these usually increase the oocyte endogenous leak (I. C. Forster, unpublished experiments). Recently, it was reported that PFA inhibits P_i-induced calcification in smooth muscle cells (31, 34) and that that it inhibits matrix calcification in osteoblast-like cells (46). Although other experiments carried out by Li et al. (34) and Suzuki et al. (46) point to an important role of PiT in the calcification process, the effect of PFA in inhibiting calcification is probably more related to the ability of phosphonates and bisphosphonates to inhibit the formation of calcium phosphate crystals (15, 16, 59) than to inhibition of P_i transport through PiT. Alternatively, perhaps PFA-inhibitable type II Na^+-P_i

cotransporters play a more important role in mineral formation than previously thought (37).

PiT-1 Substrate-Binding Scheme

Our substrate-dependence data strongly suggest that XlPiT-1 binds substrates in an ordered manner, as indicated by the dependence of $K_{0.5}^{P_i}$ on Na^+ concentration (Fig. 3*F*) and $K_{0.5}^{Na}$ on P_i (Fig. 4*F*) (45). For P_i as the variable substrate, the dependence of $I_{P_i}^{max}$ on Na^+ is consistent with Na^+ being the last substrate to bind. Consistent with the 2:1 Na^+:P_i stoichiometry, a possible binding order, based on analogy with the electrogenic SLC34 transporters, might therefore be Na^+:$H_2PO_4^-$:Na^+. The increase in apparent cooperativity for Na^+ interaction observed at pH 8.0 would also support this scheme, whereby the decreased availability of $H_2PO_4^-$ at pH 8.0 would increase the apparent dissociation constant associated with the proposed first Na^+-binding step, thus conferring a greater cooperativity to the overall Na^+ interaction. On the other hand, the "V_{max}" effect observed for P_i, with Na^+ as the variable substrate (Fig. 4*F*), would not be consistent with this scheme and suggests that a more complex binding/debinding mechanism exists that may involve both ordered and random partial reactions.

The voltage dependence of PiT requires that at least one partial reaction in the transport cycle is V_m dependent. This implies that mobile charges must sense the V_m, for example charged amino acid residues intrinsic to the protein or charged substrates (e.g., Na^+) moving within the transmembrane electric field. For example, the decrease of $K_{0.5}^{Na}$ with hyperpolarizing potentials (Fig. 4*F*) suggests that Na^+ interaction with the transporter is voltage dependent, whereby a more negative V_m would increase the likelihood of Na^+ binding. Alternatively, Saliba et al. (43) have proposed a model for PfPiT whereby the empty carrier translocation from inward- to outward-facing conformations involves movement of an intrinsic negative charge; however, they provided no direct experimental evidence in support of this proposal. Indeed, for many cation-driven cotransport systems, pre-steady-state measurements in the absence of one or both substrates have revealed transporter-associated charge movements, which provide convincing evidence of voltage-dependent partial reactions in the transport cycle (13, 18, 36, 38, 44, 55, 58). For XlPiT-1, our inability to resolve pre-steady-state relaxations in oocytes expressing XlPiT-1 means that we cannot assign voltage dependence to either the empty carrier or first Na^+-binding partial reactions in the transport cycle.[2] However, we cannot exclude the possibility that pre-steady-state currents in XlPiT-1-expressing oocytes were too small or too fast to be detected and so remain buried in the oocyte capacitive-charging transient. Typically, type II Na^+-P_i cotransporters that exhibit similar steady-state transport activity show ~10-fold larger charge movements (e.g., Ref. 21). Based on our findings, we therefore propose a kinetic scheme for PiT in which the reorientation of the empty carrier and the interaction of the first Na^+ ion are electrically silent, and we tentatively conclude that voltage dependence arises from either the second Na^+ interaction, the final translocation of the fully loaded carrier, or both.

[2] The origin of the time-dependent response of I_{Pi} that we observed (Fig. 10) remains unclear, given that the extracted pre-steady-state charge appears not to satisfy the basic criterion of charge balance. These relaxations may also arise from the time-dependent closure of a P_i-gated leak pathway associated with XlPiT-1 or endogenous anion conductances that also show P_i sensitivity (L.V. Virkki and I. C. Forster, unpublished observations) and that are proportionately upregulated by XlPiT-1 expression.

Conclusions

The novel electrogenic kinetics of the members of the PiT family present a contrasting view of Na^+-driven P_i cotransport with respect to that of the well-characterized members of the SLC34 family (NaPi-IIa/b), and these kinetic differences are underscored by the lack of sequence homology at the molecular level. First, the 2:1 vs. 3:1 Na^+:P_i stoichiometry indicates a 10-fold weaker concentrating ability of SLC20 compared with electrogenic SLC34 family members. Second, the preference of PiT for monovalent over divalent P_i implies that P_i transport by the two transporter families have opposite effects on intra- and extracellular pH. Third, the relative insensitivity to pH compared with members of the SLC34 family suggests that the PiT are more tolerant of the physiological conditions, and this may also reflect their ubiquitous housekeeping role. Finally, the finding that PFA does not inhibit PiT underscores the need for a more efficacious blocker that, ultimately, could be used in the treatment of patients with hyperphosphatemia-induced vascular calcification.

ACKNOWLEDGMENTS

We thank Eva Hänsenberger for the oocyte preparation.

GRANTS

This work was supported financially by the Swiss National Science Foundation and Gebert-Rüf Stiftung (http://www.grstiftung.ch) (to H. Murer).

REFERENCES

1. **Ammann D, Lanter F, Steiner RA, Schulthess P, Shijo Y, Simon W.** Neutral carrier based hydrogen ion selective microelectrode for extra- and intracellular studies. *Anal Chem* 53: 2267–2269, 1981.
2. **Bacconi A, Virkki LV, Biber J, Murer H, Forster IC.** Renouncing electrogenicity is not free of charge: switching on electrogenicity in a Na^+-coupled phosphate cotransporter. *Proc Natl Acad Sci USA* 102: 12606–12611, 2005.
3. **Bai L, Collins JF, Ghishan FK.** Cloning and characterization of a type III Na-dependent phosphate cotransporter from mouse intestine. *Am J Physiol Cell Physiol* 279: C1135–C1143, 2000.
4. **Bottger P, Hede SE, Grunnet M, Hoyer B, Klaerke DA, Pedersen L.** Characterization of transport mechanisms and determinants critical for Na^+-dependent P_i symport of the PiT-family paralogs, human PiT1 and PiT2. *Am J Physiol Cell Physiol* 291: C1377–C1387, 2006.
5. **Bottger P, Pedersen L.** Evolutionary and experimental analyses of inorganic phosphate transporter PiT family reveals two related signature sequences harboring highly conserved aspartic acids critical for sodium-dependent phosphate transport function of human PiT2. *FEBS J* 272: 3060–3074, 2005.
6. **Bottger P, Pedersen L.** Two highly conserved glutamate residues critical for type III sodium-dependent phosphate transport revealed by uncoupling transport function from retroviral receptor function. *J Biol Chem* 277: 42741–42747, 2002.
7. **Busch AE, Wagner CA, Schuster A, Waldegger S, Biber J, Murer H, Lang F.** Properties of electrogenic P_i transport by a human renal brush border Na^+/P_i transporter. *J Am Soc Nephrol* 6: 1547–1551, 1995.
8. **Caverzasio J, Bonjour JP.** Characteristics and regulation of Pi transport in osteogenic cells for bone metabolism. *Kidney Int* 49: 975–980, 1996.
9. **Coady MJ, Chang MH, Charron FM, Plata C, Wallendorff B, Sah JF, Markowitz SD, Romero MF, Lapointe JY.** The human tumour suppressor gene SLC5A8 expresses a Na^+-monocarboxylate cotransporter. *J Physiol* 557: 719–731, 2004.

10. **Cooper GJ, Boron WF.** Effect of PCMBS on CO_2 permeability of *Xenopus* oocytes expressing aquaporin 1 or its C189S mutant. *Am J Physiol Cell Physiol* 275: C1481–C1486, 1998.
11. **Denoyer D, Perek N, Le Jeune N, Frere D, Dubois F.** Evidence that 99mTc-(V)-DMSA uptake is mediated by NaPi cotransporter type III in tumour cell lines. *Eur J Nucl Med Mol Imaging* 31: 77–84, 2004.
12. **Ehnes C, Forster IC, Bacconi A, Kohler K, Biber J, Murer H.** Structure-function relations of the first and fourth extracellular linkers of the type IIa Na^+/P_i cotransporter: II. Substrate interaction and voltage dependency of two functionally important sites. *J Gen Physiol* 124: 489–503, 2004.
13. **Eskandari S, Loo DD, Dai G, Levy O, Wright EM, Carrasco N.** Thyroid Na^+/I symporter. Mechanism, stoichiometry, specificity. *J Biol Chem* 272: 27230–27238, 1997.
14. **Fernandes I, Beliveau R, Friedlander G, Silve C.** $NaPO_4$ cotransport type III (PiT1) expression in human embryonic kidney cells and regulation by PTH. *Am J Physiol Renal Physiol* 277: F543–F551, 1999.
15. **Fleisch H.** Bisphosphonates: mechanisms of action. *Endocr Rev* 19: 80–100, 1998.
16. **Fleisch HA, Russell RG, Bisaz S, Muhlbauer RC, Williams DA.** The inhibitory effect of phosphonates on the formation of calcium phosphate crystals in vitro and on aortic and kidney calcification in vivo. *Eur J Clin Invest* 1: 12–18, 1970.
17. **Forster I, Hernando N, Biber J, Murer H.** The voltage dependence of a cloned mammalian renal type II Na^+/P_i cotransporter (NaPi-2). *J Gen Physiol* 112: 1–18, 1998.
18. **Forster IC.** Towards an understanding of electrogenic cotransporters: structure-function relationships. *Pflügers Arch* 443: 163–165, 2001.
19. **Forster IC, Biber J, Murer H.** Proton-sensitive transitions of renal type II Na^+-coupled phosphate cotransporter kinetics. *Biophys J* 79: 215–230, 2000.
20. **Forster IC, Hernando N, Biber J, Murer H.** Proximal tubular handling of phosphate: a molecular perspective. *Kidney Int* 70: 1548–1559, 2006.
21. **Forster IC, Kohler K, Biber J, Murer H.** Forging the link between structure and function of electrogenic cotransporters: the renal type IIa Na^+/P_i cotransporter as a case study. *Prog Biophys Mol Biol* 80: 69–108, 2002.
22. **Forster IC, Loo DD, Eskandari S.** Stoichiometry and Na^+ binding cooperativity of rat and flounder renal type II Na^+-P_i cotransporters. *Am J Physiol Renal Physiol* 276: F644–F649, 1999.
23. **Forster IC, Traebert M, Jankowski M, Stange G, Biber J, Murer H.** Protein kinase C activators induce membrane retrieval of type II Na^+-phosphate cotransporters expressed in *Xenopus* oocytes. *J Physiol* 517: 327–340, 1999.
24. **Forster IC, Virkki LV, Bossi E, Murer H, Biber J.** Electrogenic kinetics of a mammalian intestinal Na^+/P_i-cotransporter. *J Membr Biol* 212: 177–190, 2006.
25. **Frei P, Gao B, Hagenbuch B, Mate A, Biber J, Murer H, Meier PJ, Stieger B.** Identification and localization of sodium-phosphate cotransporters in hepatocytes and cholangiocytes of rat liver. *Am J Physiol Gastrointest Liver Physiol* 288: G771–G778, 2005.
26. **Godoy A, Ormazabal V, Moraga-Cid G, Zuniga FA, Sotomayor P, Barra V, Vasquez O, Montecinos V, Mardones L, Guzman C, Villagran M, Aguayo L, Onate S, Reyes AM, Carcamo JG, Rivas CI, Vera JC.** Mechanistic insights and functional determinants of the transport cycle of the ascorbic acid transporter SVCT2: activation by sodium and absolute dependence on bivalent cations. *J Biol Chem* 282: 615–624, 2006.
27. **Hartmann CM, Wagner CA, Busch AE, Markovich D, Biber J, Lang F, Murer H.** Transport characteristics of a murine renal Na/Pi-cotransporter. *Pflügers Arch* 430: 830–836, 1995.
28. **Hilfiker H, Hattenhauer O, Traebert M, Forster I, Murer H, Biber J.** Characterization of a murine type II sodium-phosphate cotransporter expressed in mammalian small intestine. *Proc Natl Acad Sci USA* 95: 14564–14569, 1998.
29. **Homann V, Rosin-Steiner S, Stratmann T, Arnold WH, Gaengler P, Kinne RK.** Sodium-phosphate cotransporter in human salivary glands: molecular evidence for the involvement of NPT2b in acinar phosphate secretion and ductal phosphate reabsorption. *Arch Oral Biol* 50: 759–768, 2005.
30. **Johann SV, Gibbons JJ, O'Hara B.** GLVR1, a receptor for gibbon ape leukemia virus, is homologous to a phosphate permease of *Neurospora crassa* and is expressed at high levels in the brain and thymus. *J Virol* 66: 1635–1640, 1992.
31. **Jono S, McKee MD, Murry CE, Shioi A, Nishizawa Y, Mori K, Morii H, Giachelli CM.** Phosphate regulation of vascular smooth muscle cell calcification. *Circ Res* 87: E10–E17, 2000.
32. **Kavanaugh MP, Kabat D.** Identification and characterization of a widely expressed phosphate transporter/retrovirus receptor family. *Kidney Int* 49: 959–963, 1996.
33. **Kavanaugh MP, Miller DG, Zhang W, Law W, Kozak SL, Kabat D, Miller AD.** Cell-surface receptors for gibbon ape leukemia virus and amphotropic murine retrovirus are inducible sodium-dependent phosphate symporters. *Proc Natl Acad Sci USA* 91: 7071–7075, 1994.
34. **Li X, Yang HY, Giachelli CM.** Role of the sodium-dependent phosphate cotransporter, Pit-1, in vascular smooth muscle cell calcification. *Circ Res* 98: 905–912, 2006.
35. **Loghman-Adham M.** Use of phosphonocarboxylic acids as inhibitors of sodium-phosphate cotransport. *Gen Pharmacol* 27: 305–312, 1996.
36. **Loo DD, Hazama A, Supplisson S, Turk E, Wright EM.** Relaxation kinetics of the Na^+/glucose cotransporter. *Proc Natl Acad Sci USA* 90: 5767–5771, 1993.
37. **Lundquist P, Biber J, Murer H.** Type II Na^+-P_i cotransporters in osteoblast mineral formation: regulation by inorganic phosphate. *Cell Physiol Biochem* 19: 43–56, 2007.
38. **Mager S, Naeve J, Quick M, Labarca C, Davidson N, Lester HA.** Steady states, charge movements, and rates for a cloned GABA transporter expressed in *Xenopus* oocytes. *Neuron* 10: 177–188, 1993.
39. **Mizobuchi M, Ogata H, Hatamura I, Koiwa F, Saji F, Shiizaki K, Negi S, Kinugasa E, Ooshima A, Koshikawa S, Akizawa T.** Up-regulation of Cbfa1 and Pit-1 in calcified artery of uraemic rats with severe hyperphosphataemia and secondary hyperparathyroidism. *Nephrol Dial Transplant* 21: 911–916, 2006.
40. **Murer H, Hernando N, Forster I, Biber J.** Proximal tubular phosphate reabsorption: molecular mechanisms. *Physiol Rev* 80: 1373–1409, 2000.
41. **Olah Z, Lehel C, Anderson WB, Eiden MV, Wilson CA.** The cellular receptor for gibbon ape leukemia virus is a novel high affinity sodium-dependent phosphate transporter. *J Biol Chem* 269: 25426–25431, 1994.
42. **Pajor AM, Hirayama BA, Loo DD.** Sodium and lithium interactions with the Na^+/dicarboxylate cotransporter. *J Biol Chem* 273: 18923–18929, 1998.
43. **Saliba KJ, Martin RE, Broer A, Henry RI, McCarthy CS, Downie MJ, Allen RJ, Mullin KA, McFadden GI, Broer S, Kirk K.** Sodium-dependent uptake of inorganic phosphate by the intracellular malaria parasite. *Nature* 443: 582–585, 2006.
44. **Smith KM, Ng AM, Yao SY, Labedz KA, Knaus EE, Wiebe LI, Cass CE, Barldwin SA, Chen XZ, Karpinski E, Young JD.** Electrophysiological characterization of a recombinant human Na-coupled nucleoside transporter (hCNT1) produced in *Xenopus* oocytes. *J Physiol* 558: 807–823, 2004.
45. **Stein WD.** *Channels, carriers and pumps. An introduction to membrane transport.* San Diego, CA: Academic, 1990.
46. **Suzuki A, Ghayor C, Guicheux J, Magne D, Quillard S, Kakita A, Ono Y, Miura Y, Oiso Y, Itoh M, Caverzasio J.** Enhanced expression of the inorganic phosphate transporter Pit-1 is involved in BMP-2-induced matrix mineralization in osteoblast-like cells. *J Bone Miner Res* 21: 674–683, 2006.
47. **Szczepanska-Konkel M, Yusufi AN, VanScoy M, Webster SK, Dousa TP.** Phosphonocarboxylic acids as specific inhibitors of Na^+-dependent transport of phosphate across renal brush border membrane. *J Biol Chem* 261: 6375–6383, 1986.
48. **Tatsumi S, Segawa H, Morita K, Haga H, Kouda T, Yamamoto H, Inoue Y, Nii T, Katai K, Taketani Y, Miyamoto KI, Takeda E.** Molecular cloning and hormonal regulation of PiT-1, a sodium-dependent phosphate cotransporter from rat parathyroid glands. *Endocrinology* 139: 1692–1699, 1998.
49. **Tenenhouse HS, Gauthier C, Martel J, Gesek FA, Coutermarsh BA, Friedman PA.** Na^+-phosphate cotransport in mouse distal convoluted tubule cells: evidence for Glvr-1 and Ram-1 gene expression. *J Bone Miner Res* 13: 590–597, 1998.
50. **Uckert W, Willimsky G, Pedersen FS, Blankenstein T, Pedersen L.** RNA levels of human retrovirus receptors Pit1 and Pit2 do not correlate with infectibility by three retroviral vector pseudotypes. *Hum Gene Ther* 9: 2619–2627, 1998.
51. **van Veen HW, Abee T, Kortstee GJ, Konings WN, Zehnder AJ.** Substrate specificity of the two phosphate transport systems of *Acinetobacter johnsonii* 210A in relation to phosphate speciation in its aquatic environment. *J Biol Chem* 269: 16212–16216, 1994.
52. **van Veen HW, Abee T, Kortstee GJ, Konings WN, Zehnder AJ.** Translocation of metal phosphate via the phosphate inorganic transport system of *Escherichia coli*. *Biochemistry* 33: 1766–1770, 1994.

53. **Villa-Bellosta R, Bogaert YE, Levi M, Sorribas V.** Characterization of phosphate transport in rat vascular smooth muscle cells. Implications for vascular calcification. *Arterioscler Thromb Vasc Biol* 27: 1030–1036, 2007.
54. **Virkki LV, Choi I, Davis BA, Boron WF.** Cloning of a Na^+-driven Cl/HCO_3 exchanger from squid giant fiber lobe. *Am J Physiol Cell Physiol* 285: C771–C780, 2003.
55. **Virkki LV, Forster IC, Biber J, Murer H.** Substrate interactions in the human type IIa sodium-phosphate cotransporter (NaPi-IIa). *Am J Physiol Renal Physiol* 288: F969–F981, 2005.
56. **Virkki LV, Forster IC, Hernando N, Biber J, Murer H.** Functional characterization of two naturally occurring mutations in the human sodium-phosphate cotransporter type IIa. *J Bone Miner Res* 18: 2135–2141, 2003.
57. **Virkki LV, Murer H, Forster IC.** Voltage clamp fluorometric measurements on a type II Na^+-coupled P_i cotransporter: shedding light on substrate binding order. *J Gen Physiol* 127: 539–555, 2006.
58. **Wadiche JI, Arriza JL, Amara SG, Kavanaugh MP.** Kinetics of a human glutamate transporter. *Neuron* 14: 1019–1027, 1995.
59. **Williams G, Sallis JD.** Structure-activity relationship of inhibitors of hydroxyapatite formation. *Biochem J* 184: 181–184, 1979.
60. **Wilson CA, Eiden MV, Anderson WB, Lehel C, Olah Z.** The dual-function hamster receptor for amphotropic murine leukemia virus (MuLV), 10A1 MuLV, and gibbon ape leukemia virus is a phosphate symporter. *J Virol* 69: 534–537, 1995.
61. **Xu H, Inouye M, Missey T, Collins JF, Ghishan FK.** Functional characterization of the human intestinal NaPi-IIb cotransporter in hamster fibroblasts and *Xenopus* oocytes. *Biochim Biophys Acta* 1567: 97–105, 2002.
62. **Zoidis E, Ghirlanda-Keller C, Gosteli-Peter M, Zapf J, Schmid C.** Regulation of phosphate (P_i) transport and NaPi-III transporter (Pit-1) mRNA in rat osteoblasts. *J Endocrinol* 181: 531–540, 2004.

Chapter 6

PiT structure-function studies.

6.1 Structure-function investigation of the first predicted extracellular loop of *Xl*PiT1.

6.1.1 Aim of the study.

The main topological information about PiT has been published by Salaün et al. [126] and a topology of 12 transmembrane domains was hypothesized. In 2005 Bøttger and co-workers investigated the importance of some charged residues in PiT2 [131]. These residues are highly conserved, also in *Xl*PiT1. Some of them like the Glu-68 and the Asp-76 resulted important for the transporter activity. Using a topological model of *Xl*PiT1 we verify the surface accessibility of the protein according to the model starting from the first predicted loop. This loop contains the corresponding residues investigated by Bøettger and colleagues, respectively Glu-87 and Asp-95. Using the the Substitute Cysteine Accessibility Method (SCAM) we specifically wanted to verify the extracellular location of the loop, define its boundaries, and study the structure-function relationships of this region.

6.1.2 Materials and methods.

Mutated proteins. Mutations were introduced following the Quickchange Site-Directed Mutagenesis Kit manual (Stratagene Inc.). In brief, 15 ng of the plasmid containing the *Xenopus* PiT1 cDNA cloned into KSM vector [132] were amplified with 2.5 U PfuUltra (Strategene Inc.) DNA polymerase in the presence of 250 nM of primers. PCR amplification was performed with 25 cycles of 95 °C(30 s), 55 °C (1 min), and 72 °C (12 min). Next, 10 U of DpnI were added directly to the amplification reaction and the sample was incubated for 1 h at 37 °C to digest the parental, methylated DNA. Top10 Ultracompetent cells (Invitrogen) were transformed with 1 μl reaction mixture and plated on LB-ampicillin plates. The

sequence was verified by sequencing (Microsynth). The plasmids were linearized by NotI and used as a template for the synthesis of capped cRNA by mMESSAGE mMACHINE T3 kit (Ambion) [133]. Stage V–VI defolliculated oocytes from *Xenopus laevis* frogs were isolated and maintained as described previously [70]. Oocytes were injected with 50 nl of cRNA (50 ng). Control oocytes were not injected. Oocytes were incubated at 16 °C in modified Barth's solution.

Solutions. All standard chemicals and reagents were obtained from either Sigma Chemical Co. or Fluka AG. The MTS reagents, MTSET, [2-(trimethylammonium)ethyl]methanethiosulfonate was obtained form Toronto Research Biochemicals. The solution compositions (mM) were as follows. (a) Oocyte incubation (modified Barth's solution in mM): 88 NaCl, 1 KC1, 0.41 $CaCl_2$, 0.82 $MgSO_4$, 2.5 $NaHCO_3$, 2 $Ca(NO_3)_2$, and 7.5 HEPES, pH 7.4, adjusted with Tris. The solution was supplemented with 5 mg/l doxycycline and 5mg/l gentamicin. (b) Control superfusate (ND100, in mM): 100 NaCl, 2 KCl, 1.8 $CaCl_2$, 1$MgCl_2$, and 5 HEPES, titrated to pH 7.4 with Tris. (c) Stop solution (ND0): as for ND100, but with choline chloride replacing NaCl to maintain the same osmolarity. Solutions were titrated with HCl and Tris to pH 7.4. (d) Substrate test solutions: inorganic phosphate (P_i) was added to ND100 from a K_2HPO_4/KH_2PO_4 stock preadjusted to pH 7.4.

Radiotracer Uptake. For each mutant two groups of oocytes (8–10 oocytes/ group) were analyzed. The first group was incubated for 5 minutes in ND100 with 1mM MTSET added, then washed in ND100 for 3 minutes. After aspiration of this solution, we added 100 μl uptake solution containing ^{32}P 10 μCi/ml. The second group of oocytes was preincubated in ND100 for 3 minutes and then exposed to the ^{32}P solution. The uptake was allowed to proceed for 15 min before it was stopped by washing the oocytes four times with 3 ml ice-cold ND0 solution containing 0.5 mM cold P_i. Uptake of ^{32}P alone was carried out by using ND100 solution and 1 mM cold P_i, to which ^{32}P (specific activity 10–20 μCi/ml P_i) was added. After washing, oocytes were placed individually in a scintillation vial and lysed in 250 μl 20% SDS. ^{32}P activities of individual oocytes were counted by using a Packard Tri-Carb 2900TR scintillation counter.

Electrophysiology. Standard two-electrode voltage clamp hardware (GeneClamp, Model 500 - Molecular Devices) was used as previously described [132] Clamp hardware was controlled and data were acquired by using pClamp 8 software (Molecular Devices), which also controlled valves for solution exchange. At the start of each experiment, the oocyte was clamped to a holding potential of -50 mV and was superfused with ND100 solution. To measure P_i-induced currents (I_{P_i}), the superfusate was switched to one containing P_i and

the change in the holding current was monitored. When the current had reached a steady state, the perfusate was switched back and washout of P_i was monitored by observing the return of holding current to baseline. To measure the MTSET-induced current inhibition, the superfusate was switched to one containing 1mM MTSET for 3 minutes and then the oocyte was washed for 2 minutes in ND100. To control the reduction in phosphate-induced current 1mM P_i was applied again. If a mutant showed reduction in P_i-induced current or in ^{32}P uptake to evaluate the rate of the interaction between protein and MTSET, the current was continuously measured alternating the superfusate: 30 sec 1mM P_i, 1 min ND100, 1 min MTSET, 1 min ND100, until the current induced by P_i reached zero or a steady state value. Data were fitted with an exponential decay equation (eqn.6.1) and an apparent reaction rate was extracted and used to compare the mutants (eqn.6.2).

$$I(t) = I_{max} \cdot e^{-Kt} + I_0 \tag{6.1}$$

$$K = K^* \cdot [MTSET] \tag{6.2}$$

where K is a rate constant that when corrected with the value of the MTSET concentration used in the reaction will give K*, the apparent second-order rate constant. I_t is the measured current, $I_{\max}$ is is the maximum current attainable and I_0 a variable offset.

Measurement of apparent P_i and Na^+ affinities. The oocyte was voltage clamped at -50 mV, and the holding current was continuously recorded. To measure I_{P_i}, the superfusate was switched to one containing P_i and change in the holding current was monitored. When the current had reached a steady state, the superfusate was switched back and washout of P_i was monitored by observing the return of holding current to baseline. When I_{P_i} was recorded for another Na^+concentration or pH, the holding current was first allowed to stabilize at the new reference solution before being switched to one containing P_i. To determine the apparent affinity constant for P_i ($K_{0.5}^{P_i}$), I_{P_i} was measured by using different P_i concentrations while keeping the Na^+ concentration constant. Estimates of $K_{0.5}^{P_i}$ was obtained by fitting data with the modified Hill equation (eq.6.3)

$$I_{P_i} = \frac{I_{P_i}^{\max} \cdot [S]^{n_H}}{[S]^{n_H} + K_{0.5}^{n_H}} + I_{\mathrm{OFF}} \tag{6.3}$$

where $I_{P_i}^{\max}$ is the maximum current attainable, I_{OFF} is a variable offset, [S] is the variable substrate concentration, and n_H is the Hill coefficient. The voltage dependence of I_{P_i} was measured by applying potentials from -160 to -40 mV and subtracting the current records for the same potential in the presence and absence of P_i, as described previously (17, 55). To account for the differences in expression levels between individual oocytes, data obtained from each oocyte were normalized to I_{P_i} recorded at -100 mV with 100 mM Na^+ and 1mM P_i in the bath at pH 7.4 before the data was fitted with eq.6.3.

6.1.3 Preliminary results.

Topology model.

Topology prediction from the primary sequence. We used algorithms (Prediction of Transmembrane Regions and Orientation - TMpred [134]) to analyze the hydrophobicity of *Xl*PiT1 and hypothesize the secondary structure elements present in the protein to build a topology model of *Xl*PiT1.

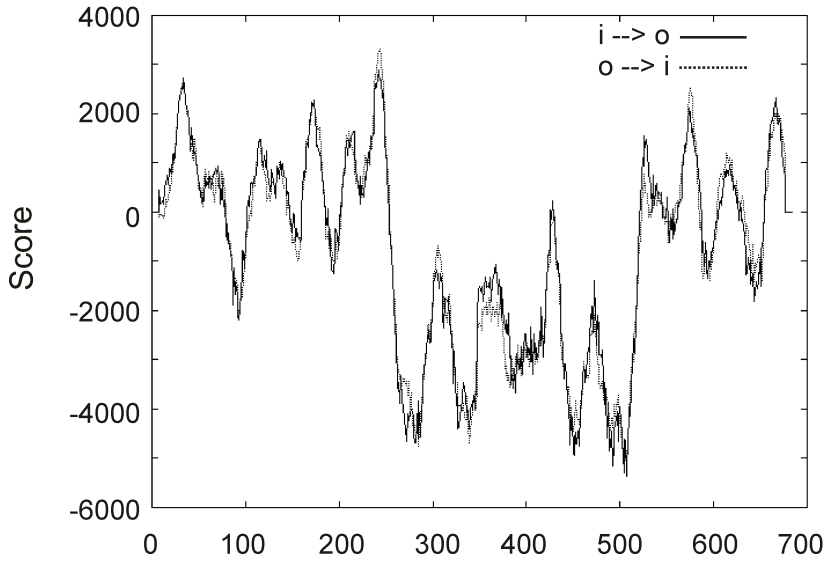

Figure 6.1: Hydropathy plot of *Xl*PiT1 obtained with TMpred (http://www.ch.embnet.org/cgi-bin/TMPRED).

From the TMpred prediction we can hypothesize 10-12 transmembrane domains (see an example in tab.6.1). Some of the possible predictions are in contrast with experimental data published by in 2001 from Salaün et al. [126] for PiT2 where they tagged both -NH_2 and -COOH terminus and they showed that they are extracellular. From the PROSITE motif search four potential N-glycosylation sites have been identified, one of them, the Arg-100, is the corresponding residue in PiT2 of Arg-81 that has been shown by Salaün et al. [126] to be glycosylated.

	from	to	length	score	orientation
1	25	41	(17)	2645	o-i
2	57	81	(25)	948	i-o
3	105	126	(22)	1461	o-i
4	129	151	(23)	1038	i-o
5	166	184	(19)	2243	o-i
6	205	227	(23)	1658	i-o
7	235	255	(21)	3343	o-i
8	519	535	(17)	1553	i-o
9	568	584	(17)	2511	o-i
10	608	626	(19)	957	i-o
11	655	683	(29)	2029	o-i

Table 6.1: Prediction of *Xl*PiT1 transmembrane domains.

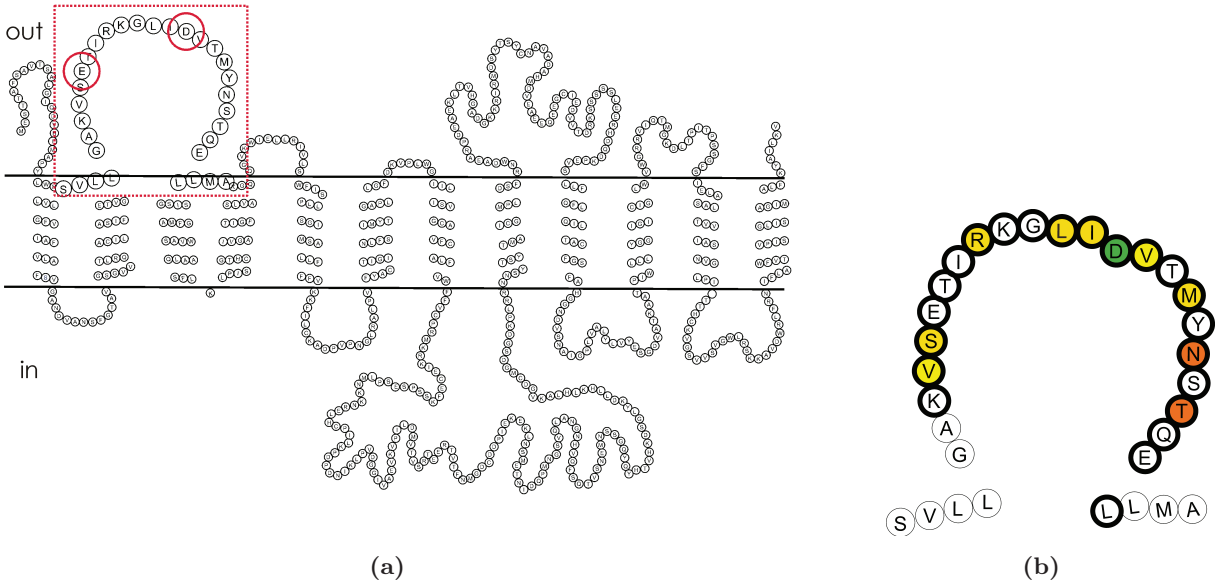

(a) **(b)**

Figure 6.2: Proposed topology for *Xl*PiT1; (a) *Xl*PiT1 proposed topology, the first predicted loop is boxed and shown in detail in (b). Coloured residues correspond to the coloured bars in the fig. 6.3.

Preparation of mutants.

Nineteen mutants were prepared by substituting one by one the native residues of the first predicted loop of the wild type *Xl*PiT1 with a cysteine from Lys-84 to Leu-105 (see panel b in fig. 6.5a) .

^{32}P screening of the mutants.

All the mutants were expressed in *Xenopus* oocytes and screened by ^{32}P uptake for functional expression with or without 5 min pre-incubation with MTSET 1 mM. Seven mutants showed a reduced ^{32}P uptake after the pre-incubation of MTSET 1 mM while two mutants showed an increase in ^{32}P uptake. The oocytes expressing the mutant D95C showed a ^{32}P uptake comparable with the non-injected oocytes, from these data it is not possible to determine if the mutant is non-functional or not expressed. These data are in agreement with the findings of Bøettger et al. [131].

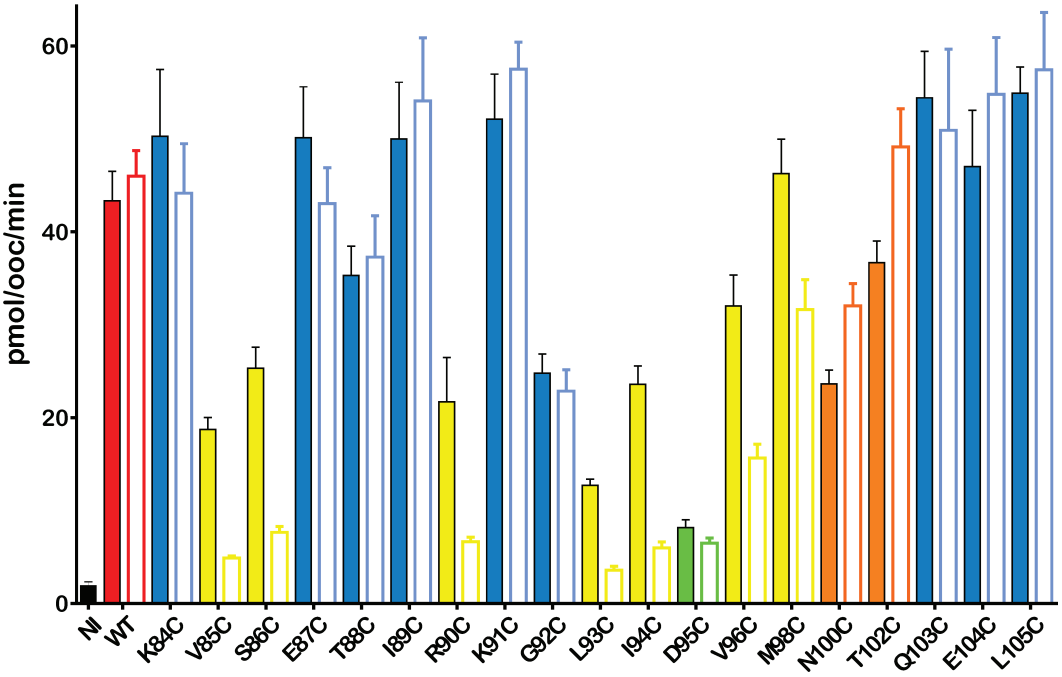

Figure 6.3: ^{32}P screening of the mutants. Oocytes exposed to 0.1 mM P_i (coloured bars); oocytes exposed to 0.1 mM P_i pre-incubated with 1 mM MTSET in ND100 (open bars). Light blue bar: mutants that were not modified after the incubation with MTSET; yellow: mutants that show reduced uptake after exposure; orange: mutants that show an increased ^{32}P uptake; green: mutant D95C that shows a strongly reduced uptake compared with the wild type.

Electrophysiological screening of mutants. All mutants were expressed in *Xenopus* oocytes and tested by two-electrode voltage clamp to compare their electrogenicity, voltage dependence, substrate and co-substrate apparent affinity with the wild type. We started with the mutant that showed a reduced ^{32}P uptake after the pre-incubation with MTSET. All the mutants were electrogenic. D95C that showed a low ^{32}P uptake also gave a small P_i-induced current, dependent on the membrane voltage. We have not compared expression levels, thus the reduced P_i-induced current and the reduced ^{32}P uptake may result from low expression levels or altered kinetics. We tested the mutants with or without pre-incubation with MTSET and we verified that the modification induced by MTSET was reversible using a DTT (dithiothreitol) solution 1mM that breaks the disulfide bridge and restores the sulfhydryl group (data not shown). Fig. 6.4 details the electrophysiological characterization of mutant S86C and compares its P_i- dependence and the phenomenological parameters $I_{P_i}^{max}$, $K_{0.5}^{P_i}$ (the apparent affinity for P_i) with the wild type whereas voltage dependence of $I_{P_i}^{max}$ was unchanged, $K_{0.5}^{P_i}$ was significantly altered by the Cys substitution. This suggests that this site is a critical determinant of P_i interaction with the protein.

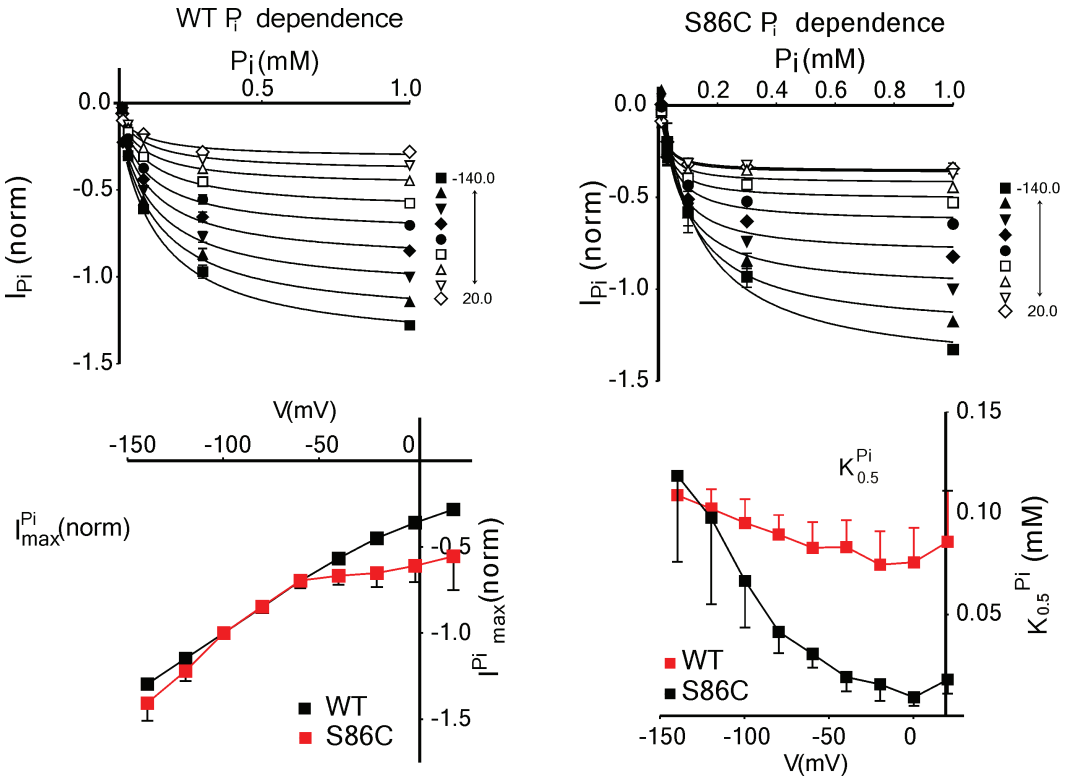

Figure 6.4: Data obtained by two-electrode voltage clamp on oocytes expressing *Xl*PiT1 and the mutant S86C.

Determining the rate of Cys-modification.

To quantitate the rate of Cys-modification by MTSET for each mutant, we exposed the oocytes expressing the mutants to a low dose of thiol reagent and we quantitated the progressive reduction in current induced by P_i until a plateau was reached. We fitted the data with an exponential equation (eqn.6.1). The constant K obtained was corrected using the concentration of MTEST employed in the reaction, to gave K* the apparent second order rate constant, used to compare the mutants. A high K* can be interpreted as high accessibility of the residue from the external solution.

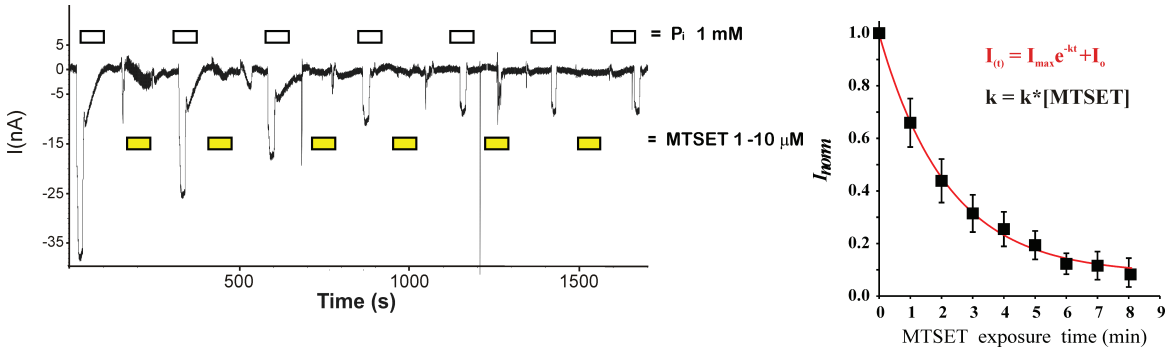

Figure 6.5: Example of determination of Cys-modification reaction rate: a: recording of P_i-induced current after consecutive applications of MTSET; b: normalized value of current-induced by phosphate after exposure to MTSET for exposition for 1 min. The values have been fitted with the eqn.6.1.

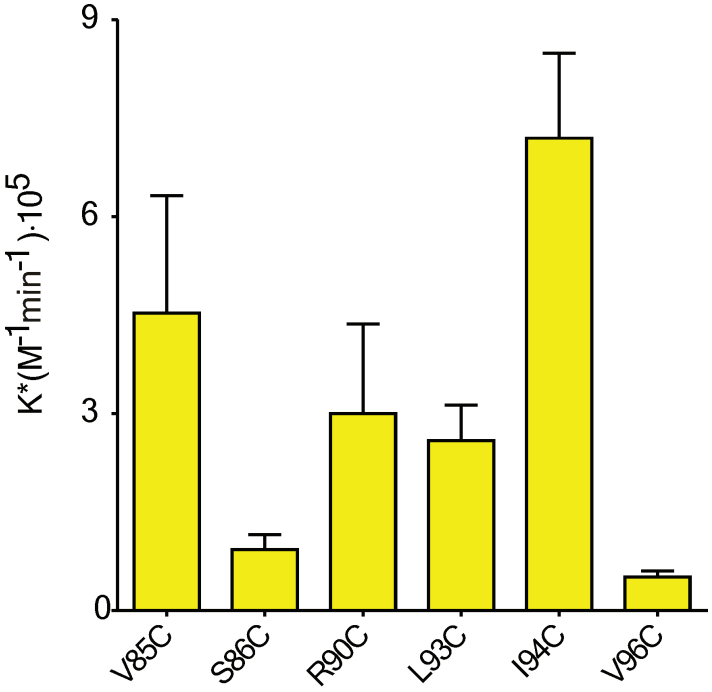

Figure 6.6: K* values calculated for the mutants that showed reduced ^{32}P uptake in presence of MTSET

Summary The data obtained so far allow us to locate this region extracellularly and to hypothesize its role in the transport function due to reduced ^{32}P uptake and P_i-induced current when this region is buried by MTS reagents. So far we cannot determine if it is involved directly in the coordination of the substrates or if it is involved in the conformational changes that occur during the transport cycle.

Chapter 7

Other Publications

Temperature dependence of steady-State and presteady-state kinetics of a type IIb Na^+/P_i cotransporter.

J Membrane Biol, **2007**, *215,*8192

Institute of Physiology and Center for Integrative Human Physiology,
University of Zurich, Zurich, Switzerland

J Membrane Biol (2007) 215:81–92
DOI 10.1007/s00232-007-9008-1

Temperature Dependence of Steady-State and Presteady-State Kinetics of a Type IIb Na^+/P_i Cotransporter

Andrea Bacconi · Silvia Ravera · Leila V. Virkki · Heini Murer · Ian C. Forster

Received: 11 October 2006 / Accepted: 6 January 2007 / Published online: 19 April 2007

Abstract The temperature dependence of the transport kinetics of flounder Na^+-coupled inorganic phosphate (P_i) cotransporters (NaPi-IIb) expressed in *Xenopus* oocytes was investigated using radiotracer and electrophysiological assays. $^{32}P_i$ uptake was strongly temperature-dependent and decreased by ~80% at a temperature change from 25°C to 5°C. The corresponding activation energy (E_a) was ~14 kcal mol^{-1} for the cotransport mode. The temperature dependence of the cotransport and leak modes was determined from electrogenic responses to 1 mM P_i and phosphonoformic acid (PFA), respectively, under voltage clamp. The magnitude of the P_i- and PFA-induced changes in holding current decreased with temperature. E_a at –100 m*V* for the cotransport and leak modes was ~16 kcal mol^{-1} and ~11 kcal mol^{-1}, respectively, which suggested that the leak is mediated by a carrier, rather than a channel, mechanism. Moreover, E_a for cotransport was voltage-independent, suggesting that a major conformational change in the transport cycle is electroneutral. To identify partial reactions that confer temperature dependence, we acquired presteady-state currents at different temperatures with 0 mM P_i over a range of external Na^+. The relaxation time constants increased, and the peak time constant shifted toward more positive potentials with decreasing temperature. Likewise, there was a depolarizing shift of the charge distribution, whereas the total available charge and apparent valency predicted from single Boltzmann fits were temperature-independent. These effects were explained by an increased temperature sensitivity of the Na^+-debinding rate compared with the other voltage-dependent rate constants.

Keywords P_i cotransport · Uncoupled leak · Temperature · Presteady-state · Activation energy

A. Bacconi · S. Ravera · L. V. Virkki · H. Murer · I. C. Forster (✉)
Institute of Physiology and Center for Integrative Human Physiology, University of Zurich, Winterthurerstrasse 190 CH-8057 Zurich, Switzerland
e-mail: IForster@access.unizh.ch

Introduction

Secondary active transporters are solute carrier proteins that mediate the uphill movement of a specific solute by coupling this to the downhill movement of a specific ion (e.g., H^+, K^+ or Na^+) according to the free energy available from the driving ion's own electrochemical gradient. The coupling confers a strict stoichiometric ratio between the driven and driving species. This contrasts with the traditional view of ion channels, which, when in the conducting or open state, allow solute movement through their pore according to an electrodiffusive mechanism, thereby resulting in transport rates up to five orders of magnitude faster than for carriers. The kinetic and molecular models proposed to account for the functional data also reflect these differences between carriers and channels, and the activation energy for movement of an ion through a channel is much less than that associated with the transport cycle of a carrier (Van Winkle 1995). This underscores a thermodynamically based distinction between channels and carriers that is reflected in the greater apparent complexity of the conformational changes involved in the translocation process in the latter case, where ordered substrate binding/debinding and alternating accessibility of substrates to their respective binding sites are features of the currently postulated carrier mechanisms. Recently, the distinction between carriers and channels has become less clear as

evidenced by a number of studies on cotransporters that have identified leak modes in the absence of substrate and which exhibit channel-like properties (DeFelice 2004; Sonders and Amara 1996). Moreover, studies on the serotonin transporter (SERT) indicate that at high substrate concentrations SERT exhibits transport behavior more consistent with a channel rather than a carrier (Adams and DeFelice 2002). Finally, functional studies on a bacterial homolog of the ClC channel have revealed that a single-amino acid substitution can switch the mode of operation from that of an H^+:Cl^- antiporter with strict stoichiometric coupling to the characteristic ClC channel mode (Accardi and Miller 2004).

Electrogenic type II Na^+-coupled inorganic phosphate (P_i) cotransporters (NaPi-II), encoded by members of the solute carrier *SLC34* gene family (http://www.biopara-digms.org), also possess the expected strict stoichiometrically coupled cotransport mode behavior of a carrier (Forster, Loo and Eskandari 1999; Virkki et al. 2005b) as well as leak-mode behavior (Forster et al. 2002). A Na^+-dependent leak mode for the rat NaPi-IIa cotransporter was proposed from the finding that the P_i transport inhibitor phosphonoformic acid (foscarnet or PFA), applied in the absence of P_i to NaPi-IIa-expressing *Xenopus* oocytes under voltage-clamp conditions, led to a decrease in the holding current (Forster et al. 1998). The magnitude of the PFA-induced change in holding current was proportional to the cotransport mode activity, which suggested a direct association of this pathway with functional expression of the cotransporter. Moreover, its reversal potential was reported to shift in a Nernstian manner according to the external Na^+ concentration (Forster et al. 1998). The NaPi-IIa Na^+-leak mode was incorporated into a kinetic scheme as a ''uniporter'' pathway (Forster et al. 1998), similar to that proposed for other Na^+-driven cotransporters (e.g., the sodium glucose cotransporter [SGLT1] [Birnir, Loo and Wright 1991; Chen et al. 1997], the thyroid Na^+/I^- cotransporter [Eskandari et al. 1997] and the Na^+-dependent dicarboxylate cotransporter [Yao and Pajor 2000]). This scheme indicates that the leak and cotransport modes are mutually exclusive but share the same empty carrier and Na^+ binding transitions. Studies involving both wild-type and mutant NaPi-IIa constructs (Kohler et al. 2002a, b; Virkki et al. 2005b) have also provided experimental evidence in support of this idea. Nevertheless, the reversal potential of I_{PFA} lies far to the left (typically –20 m*V* with external 100 mM Na^+) of what would be predicted if Na^+ were the only ion involved, and this observation therefore suggests that I_{PFA} is more complex than originally proposed. Moreover, recent observations (A. Bacconi, L. V. Virkki and I. C. Forster, unpublished results) indicate that Cl^- ions may also be involved, which adds further weight to the concept, proposed for excitatory amino acid cotransporters, that a transporter-associated, substrate-gated, channel-like pathway could also be present (e.g., Otis and Jahr 1998).

The distinction between carrier and leak modes can be experimentally demonstrated by determining their temperature dependence, based on the property that the activation energy for translocating solutes according to a carrier mechanism is significantly greater than that associated with ionic electrodiffusion for a channel (Van Winkle 1995). This hypothesis is supported by studies on a serotonin transporter (dSERT) (Beckman and Quick 2001) and a γ–aminobutyric acid (GABA) transporter isoform (GAT4) (Karakossian et al. 2005), in which significantly different temperature coefficients for the respective cotransport and leak modes were reported.

The aims of the present study were twofold. First, to gain further insight into the mechanism of the NaPi-II cotransport and leak modes, we determined the temperature dependence of the respective transport rates. We used the type IIb Na^+/P_i cotransporter (NaPi-IIb) cloned from flounder because of its 5- to 10-fold higher expression in *Xenopus* oocytes (Forster et al. 1997) compared with its mammalian cousins. We have previously shown that flounder NaPi-IIb exhibits leak and cotransport modes (Forster, Biber and Murer 2000) and displays similar kinetic features associated with the mammalian NaPi-IIa (Forster et al. 1997, 1999, 2000; Virkki, Murer and Forster 2006a, b). Therefore, our findings should be applicable to mammalian members of the SLC34 family. Second, to identify the contributions of resolvable partial reactions that comprise the overall cotransport cycle, we characterized the temperature dependence of presteady-state relaxations under different external superfusion conditions. Analysis of presteady-state relaxations allowed us to compare the temperature dependence of voltage-dependent partial reactions that precede P_i binding.

Materials and Methods

Reagents and Solutions

All reagents were obtained from Sigma (Buchs, Switzerland) or Fluka (Buchs, Switzerland).

The compositions of the solutions used (in mM) were as follows: oocyte incubation (modified Barth's solution), NaCl (88), KCl (1), $CaCl_2$ (0.41), $MgSO_4$ (0.82), $NaHCO_3$ (2.5), $Ca(NO_3)_2$(0.33) and 4-(2-hydroxyethyl)-1-piperazineethanesulfonic acid (HEPES, 7.5), adjusted to pH 7.6 with tris(hydroxymethyl)aminomethane (TRIS) and supplemented with antibiotics (10 mg/liter gentamycin or streptomycin or 5 mg/liter doxycyclin); control superfusate (ND100), NaCl (100), KCl (2), $CaCl_2$ (1.8), $MgCl_2$ (1) and

HEPES (10), adjusted to pH 7.4 with TRIS at room temperature; control superfusate (ND0), as for ND100 but with *N*-methyl-D-glucamine or choline chloride used to replace Na^+ (intermediate Na^+ concentrations were achieved by proportionate mixing of the ND100 and ND0 solutions); substrate test solutions, P_i added to ND100 from 1 M K_2HPO_4 and KH_2PO_4 stocks that were mixed to give pH 7.4.

For a change in temperature from 25°C to 2°C, the superfusate solution pH increased by 0.25 pH units, due to the $\log_{10}$ of acid dissociation constant (pKa) temperature dependence of the HEPES-TRIS buffer. Based on previous studies of the pH dependence of NaPi-IIa/b (Forster et al. 2000; Virkki et al. 2005a), this would result in a negligible change in electrogenic transport activity. Therefore, no pH adjustment was considered necessary in the present study.

Molecular Biology and Expression in *Xenopus laevis* Oocytes

The cDNA encoding for flounder NaPi-IIb was subcloned into a KSM expression vector to improve its expression in *X. laevis* oocytes, as described previously (Virkki et al. 2003). The plasmid was linearized using *Xba*1 (Promega, Madison, WI) and used as a template for the synthesis of capped cRNA using the Message Machine T3 kit (Ambion, Austin, TX). Stage V-VI defolliculated oocytes from *X. laevis* were isolated and maintained as described previously (Virkki et al. 2006b). Oocytes were injected with 50 nl of cRNA (0.2 μg/μl) encoding NaPi-IIb. Oocytes were incubated at 17°C in modified Barth's solution. Transport assays were performed 3–5 days after injection.

Tracer Uptake

The temperature dependence of P_i transport was determined by performing $^{32}P_i$ uptake assays at five different temperatures. Control oocytes and oocytes expressing NaPi-IIb (10–12 oocytes/group) were first allowed to equilibrate in ND100 solution without tracer at the appropriate temperature. After aspiration of this solution, we added 150 μl of ND100 solution containing 1 mM P_i and $^{32}P_i$ (specific activity 10 mCi/mmol P_i). After 30 min, the uptake was stopped by washing the oocytes four times with 3 ml ice-cold ND0 solution containing 0.5 mM cold P_i. Oocytes were then placed individually in scintillation vials and lysed in 250 μl 10% sodium dodecyl sulfate. $^{32}P_i$ activities of individual oocytes were measured using scintillation counting.

Electrophysiology

Electrophysiology was performed using a two-electrode voltage clamp (Geneclamp 500; Molecular Devices, Sunnyvale, CA). Oocytes were mounted in a small recording chamber (100 μl volume) and continuously superfused (~0.2 ml/min) with test solutions supplied using a peristaltic pump. The recording chamber was machined from a block of thermally conductive epoxy (ER2074; Electrolube, UK), which was mounted on a Peltier thermoelement (CP1.4–127–045L; Melcor, NJ). The chamber temperature was controlled by a laboratory-built electronic regulator. Data were acquired online using Digidata 1200 hardware and compatible pClamp8 software (Molecular Devices). Currents were prefiltered at a bandwidth less than twice the sampling rate appropriate for the signals being acquired. Steady-state and presteady-state currents were acquired using voltage steps from a holding potential V_h = –60 m*V* to test potentials in the range –180 to +80 m*V*. Presteady-state records were acquired with fourfold signal averaging. To account for the significant slowing of the presteady-state relaxations with temperature, the test pulse width was extended to ensure that the relaxations were complete before returning to the holding potential.

Data Analysis

Presteady Relaxations and Modeling

Relaxations induced by voltage steps were quantified by fitting a decaying double exponential function using a fitting algorithm (Clampfit, v. 8.0; Molecular Devices). To resolve the charge movement associated with the exogenous protein, a component subtraction method (Hazama, Loo and Wright 1997) was employed: the fast component, assumed to represent the oocyte capacitive charging, was extrapolated to the step onset and subtracted from the total transient current. The slower component was numerically integrated to give the charge attributable to the exogenous protein.

For a voltage step from a holding potential (V_h) to a test potential (V) that induces the movement of a charge Q, the Q-V data were fitted with a form of the Boltzmann equation:

$$Q = Q_{hyp} + Q_{max}/(1 + \exp(-ze(V - V_{0.5})/kT)) \quad (1)$$

The voltage dependence of the time constant (τ) of the slower relaxation induced by the voltage step was fitted as follows:

$$\tau = 1/(k_f \exp(-ze\,V/2kT) + k_b \exp(ze\,V/2kT)) \quad (2)$$

Eqs. 1 and 2 are derived from a simple Eyring transition rate model for a two-state system that describes the distribution and rate of movement of mobile charged particles (of effective valence, z) that move across the membrane over a symmetrical energy barrier, according to the direction and magnitude of the transmembrane electric field. For Eq. 1, Q_{max} is the maximum charge translocated, Q_{hyp} is

the steady-state charge at the hyperpolarizing limit and depends on V_h, $V_{0.5}$ is the voltage at which the charge is distributed equally between the two states, e is the elementary charge, k is Boltzmann's constant and T is the absolute temperature. For Eq. 2, k_f and k_b are the zero voltage forward and backward transition rates, respectively, for the relocation of the hypothetical particles according to a clockwise movement around the transport cycle. Based on this model, it can be shown that $V_{0.5} = -kT/ze \ln (k_b/k_f)$. Eqs.1 and 2 were fit to the Q-V and τ–V data, respectively, by nonlinear regression analysis with Q_{hyp}, Q_{max}, z, $V_{0.5}$, k_f and k_b as free parameters, for $T = 278$, 283, 288, 293 K. All curve fitting using Eqs. 1 and 2 was performed using the nonlinear regression analysis algorithms in GraphPad (San Diego, CA) Prism version 3.02/4.02 for Windows (http://www.graphpad.com).

Temperature Dependence

The Arrhenius equation (Segel 1976) was used for determining the temperature dependence of the transport kinetics:

$$k_r = A\exp(-E_a/RT) \quad (3a)$$

where k_r is the rate (uptake rate, substrate-induced current or partial reaction rate constant), A is a constant, R is the gas constant and E_a is the activation energy (in kcal mol^{-1}). Fitting with a single exponential function yields an estimate for E_a. Commonly, Eq. 3a can be recast in a logarithmic form and linear regression analysis applied to the experimental data to obtain E_a:

$$\log k_r = -E_a/(2.303R)(1/T) + \log A \quad (3b)$$

Both methods yield similar estimates for E_a, and we used the logarithmic graphical representation for consistency with other studies.

The temperature coefficient for a 10°C change, Q_{10}, is related to E_a as follows:

$$\log Q_{10} = 10E_a/(2.303RT1T2) \quad (4)$$

where T_1 and T_2 are the two temperatures (K).

Results

Temperature Dependence of Flounder NaPi-IIb in the Steady State

We first determined the temperature dependence of $^{32}P_i$ uptake for oocytes injected with flounder NaPi-IIb cRNA. Figure 1A shows that $^{32}P_i$ uptake exhibited a strong temperature dependence with an approximately fivefold increase with increasing temperature over the 20°C range used in these experiments. The uptake levels for noninjected oocytes were at least 50–100 times smaller than those for NaPI-IIb-expressing cells and showed no systematic temperature dependence. We therefore ignored the contribution of any endogenous uptake in the subsequent analysis. Figure 1B shows the same data for the NaPi-IIb-expressing oocytes replotted in the form of an Arrhenius plot (Segel 1976). The dependence of uptake rate (scaled logarithmically) on the reciprocal of absolute temperature

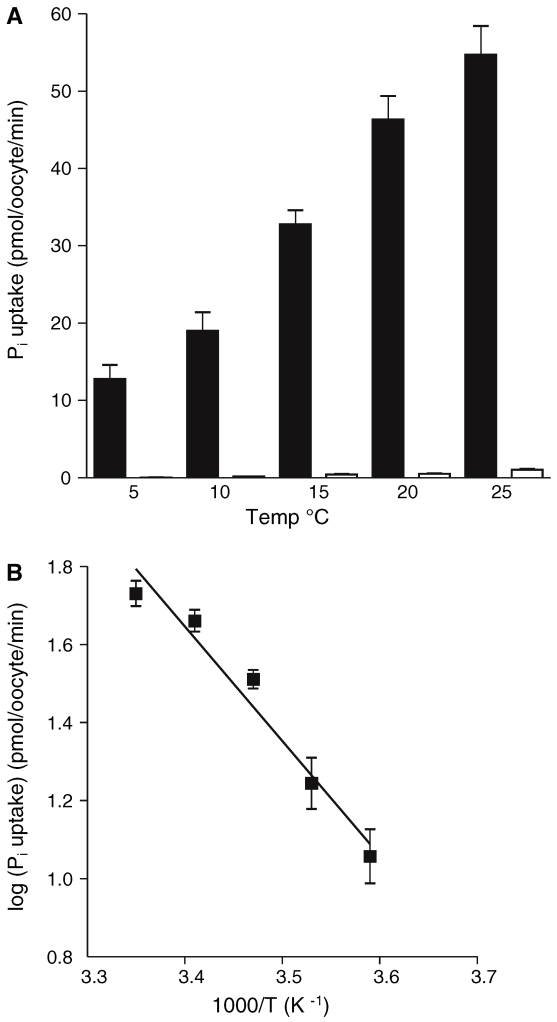

Fig. 1 Temperature dependence of $^{32}P_i$ uptake. (*A*) Uptake for NaPi-IIb-injected oocytes (*filled columns*) and noninjected oocytes (*empty columns*) from the same donor frog plotted as a function of incubation temperature. (*B*) Data for NaPi-IIb from *A* replotted as an Arrhenius plot (Eq. 3). The slope of the linear regression line was reported as –2,942 ± 335.3 K^{-1}, equivalent to E_a = 13.5 ± 1.5 kcal mol^{-1}

J Membrane Biol (2007) 215:81–92

showed a reasonably linear relationship. We fit these data using a linear regression algorithm (r^2 = 0.96), and from the fitted slope we obtained an estimate of the apparent activation energy for the transport process, E_a = 13.5 ± 1.5 kcal mol^{-1}, which corresponds to a 10°C temperature coefficient (Q_{10}) of 2.3 (Eq. 4). These values are typical for an enzyme-mediated process and exceed those expected for a simple diffusion-mediated process (Van Winkle 1995).

The transport cycle for electrogenic NaPi-II cotransporters is proposed to involved transitions between a number of states (Forster et al. 2002), and the contributions of the respective partial reactions between states to the overall temperature dependence can therefore best be studied using electrophysiology. Figure 2A shows representative current recordings from the same oocytes expressing flounder NaPi-IIb at 20°C and 10°C in response to voltage steps for 80 ms in the range –160 to +80 m*V* from a holding potential of –60 m*V*. At 20°C, in the absence of external P_i (with superfusion in ND100), we observed presteady-state relaxations superimposed on the oocyte capacitive charging transient, as we have previously reported for flounder NaPi-IIb (Forster et al. 1997, 2000; Virkki et al. 2006a, b). These relaxations were suppressed in the presence of 1 mM P_i. At 10°C, the relaxations were clearly slower, and therefore we doubled the pulse width to ensure that a steady-state current was reached. Like the data at 20°C, the relaxations at 10°C were suppressed with 1 mM P_i. The P_i-dependent current was obtained by subtracting the records in ND100 from the corresponding records in ND100+P_i (Fig. 2A, lower data set). The steady-state P_i-dependent current (I_{P_i}) was smaller at the lower temperature. Figure 2B shows pooled *I-V* data (n = 4) obtained from similar records as shown in Figure 2A, normalized to I_{P_i} at –100 m*V* at 20°C, for a larger range of temperatures and intermediate test voltages. For this steady-state analysis, we omitted the responses for $V \geq 0$ m*V* because the data were contaminated by endogenous activating currents.

We have previously reported that the type II Na^+/P_i cotransporters exhibit an uncoupled leak mode (Forster et al. 1998, 2000). This can be observed using the P_i transport blocker PFA, which specifically inhibits the leak current. To determine the temperature dependence of the leak-mode activity, we recorded the response to PFA (1 mM) (*not shown*) at different temperatures and normalized the data to I_{P_i} for each cell in response to 1 mM P_i at –100 m*V* and 20°C. The steady-state PFA-induced changes in holding current (I_{PFA}) for the flounder isoform were typically ≤10% of I_{P_i} (Forster et al. 2000) and, like I_{P_i}, strongly temperature-dependent as shown for the data sets pooled and normalized to the corresponding I_{P_i} for each cell in Figure 2C. Note that each data point is the difference between the holding current in ND100 + PFA and ND100,

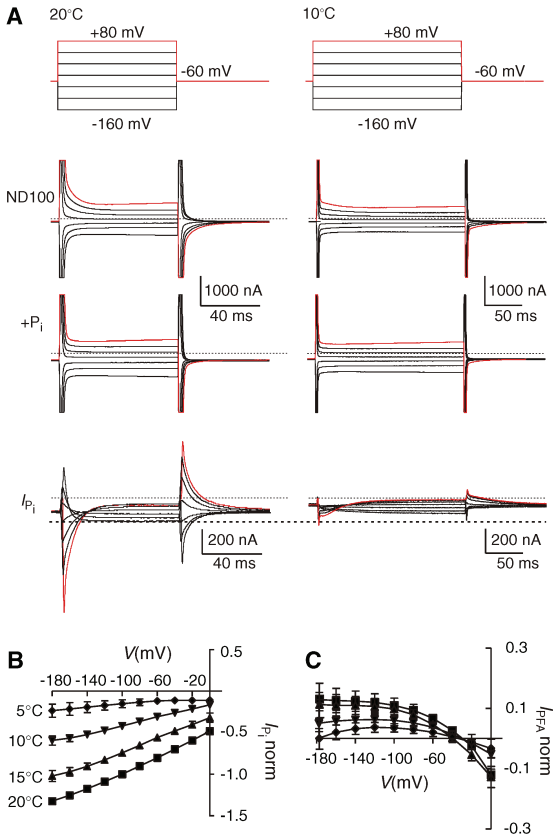

Fig. 2 Steady-state temperature dependence of substrate-induced currents. (*A*) Representative current recordings from an oocyte that expressed NaPi-IIb, made at 20°C (*left*) and 10°C (*right*). Currents were recorded in response to the voltage jump protocol from a holding potential of –60 m*V* to potentials in the range –160 to 80 m*V* at 40-m*V* intervals, in the absence (ND100) and presence of P_i (1 mM, total). *Dotted lines* indicate the steady-state zero current level. The P_i-dependent current (I_{P_i}) was obtained from the difference between corresponding traces in ND100+P_i and ND100. Note that a longer pulse was used at 10°C to ensure that a steady state was reached. For each data set, traces at +80 m*V* are shown in *red*. *Dashed line* indicates I_{P_i} at –160 m*V*, 20°C to aid comparison. (*B*) *I-V* plots of I_{P_i} at the indicated temperatures. Data are shown as means ± SEM (n = 4), normalized to I_{P_i} at 20°C and –100 m*V*. (*C*) *I-V* plots of the PFA-induced change in holding current current (I_{PFA}). Data were obtained using the same protocols as in *A* except that 1 mM PFA was substituted for 1 mM P_i. For each oocyte, the I_{PFA} data were first normalized to I_{P_i} for each cell at –100 m*V* before pooling. Same symbols as in *B*

and the NaPi-IIb PFA-inhibited leak current would be given by -I_{PFA}, under the assumption that PFA fully blocks the leak current. Unlike I_{P_i}, these currents showed a current reversal in the range –30 to –20 m*V* that appeared to be temperature-independent. Determination of exact reversal potential was not possible because of the relatively small magnitude of I_{PFA} (current magnitudes in the range 10–15

nA at –100 m*V*) and uncertainties regarding the contribution of endogenous PFA response at potential extremes (Forster et al. 2000).

We compared the temperature dependence of the currents corresponding to the cotransport and leak modes by replotting the normalized *I-V* data in the form of Arrhenius plots (Fig. 3). For I_{P_i}, the data were well described by the fit of a linear regression line over a range of potentials from –180 to 0 m*V* (Fig. 3A). For I_{PFA}, the data were less reliable, particularly near the reversal potential. From the slopes of the Arrhenius plots, we obtained estimates of the activation energy for I_{P_i} and I_{PFA}, as shown in Figure 3C (*see* Eq. 3b). The E_a for I_{P_i} showed little variation with membrane potential and was larger than the E_a for I_{PFA} for all potentials. The mean E_a for I_{P_i} of ~15 kcal mol^{-1} corresponds to Q_{10} ~2.5 (Eq. 4), which is typical for values reported in other studies on electrogenic cotransporter membrane proteins (Beckman and Quick 2001; Binda et al. 2002; Wadiche and Kavanaugh 1998); and for I_{PFA}, the E_a corresponded to a Q_{10} ~2.0.

Temperature Dependence of Presteady-State Relaxations

We next investigated the effect of temperature on the presteady-state relaxations to determine if specific transitions might dominate the temperature dependence of the cotransport function. Figure 4A shows representative presteady-state currents for the ON transition from the holding potential to the step potential, recorded from the same oocyte, superfused with ND100 at four temperatures. In each case, we applied baseline correction to remove the steady-state currents. As we reduced the temperature, the relaxations superimposed on the capacitive charging transient became slower and the initial amplitude decreased. There also appeared to be less charge movement for the same voltage change in the hyperpolarizing direction compared with depolarizing steps, which suggested an alteration in the voltage dependence of the charge distribution. The effect of temperature on the presteady-state relaxations was reversible. This was established for representative experiments (n = 3) in which temperature was reduced progressively from 20°C to 5°C and then the test protocol was repeated at 20°C, whereupon the time course and amount of charge were unchanged (*data not shown*).

We quantified these data by fitting the total relaxation with a double exponential function to yield two time constants, the slower of which (τ_s) is shown superimposed on the total current (Fig. 4A). The voltage dependence of the time constants is shown in Figure 4B for ND100 and in the absence of external Na^+ ions (ND0) and for three temperatures (20°C, 15°C and 10°C) (n = 6). Fits to the data at 5°C proved too unreliable because of noise contamination

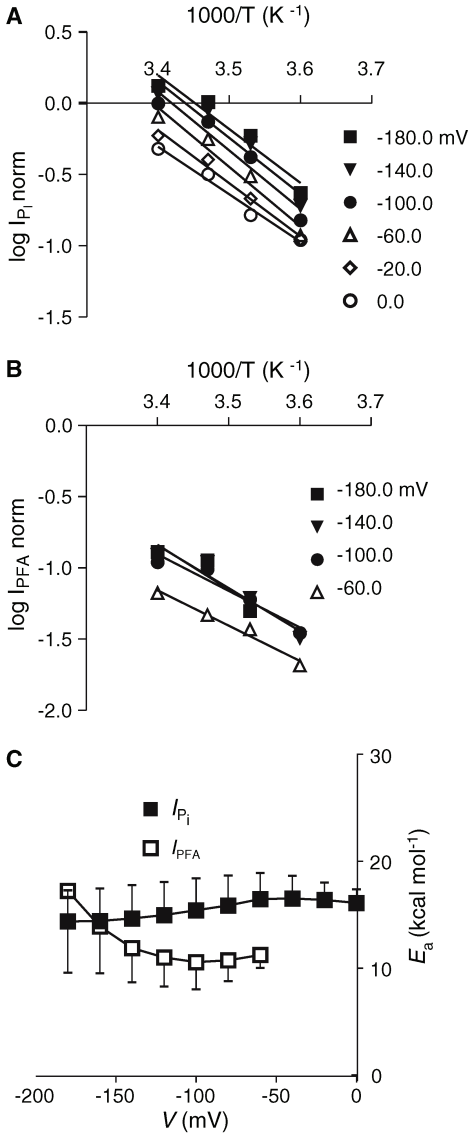

Fig. 3 Temperature dependence of I_{P_i} and I_{PFA}. (*A*) Arrhenius plots of the normalized magnitude of I_{P_i} replotted from the data in Figure 2B for the membrane potentials indicated. *Straight lines* represent linear regression fits to the data points to yield the apparent E_a given by Eq. 3. (*B*) Arrhenius plots for normalized I_{PFA} replotted from the data in Figure 2C for the membrane potentials indicated. *Straight lines* represent linear regression fits to the data points to yield E_a. (*C*) E_a plotted as a function of membrane potential for P_i- (I_{P_i}, *filled squares*) and PFA-induced change in holding current (I_{PFA}, *open squares*). Note that for I_{PFA} we were unable to determine E_a for potentials close to the I_{PFA} reversal potential because of data unreliability

of the signal at low amplitudes. The faster time constant (τ_f) (Fig. 4B, inset) became slower with decreasing temperature and showed little voltage dependence. As in

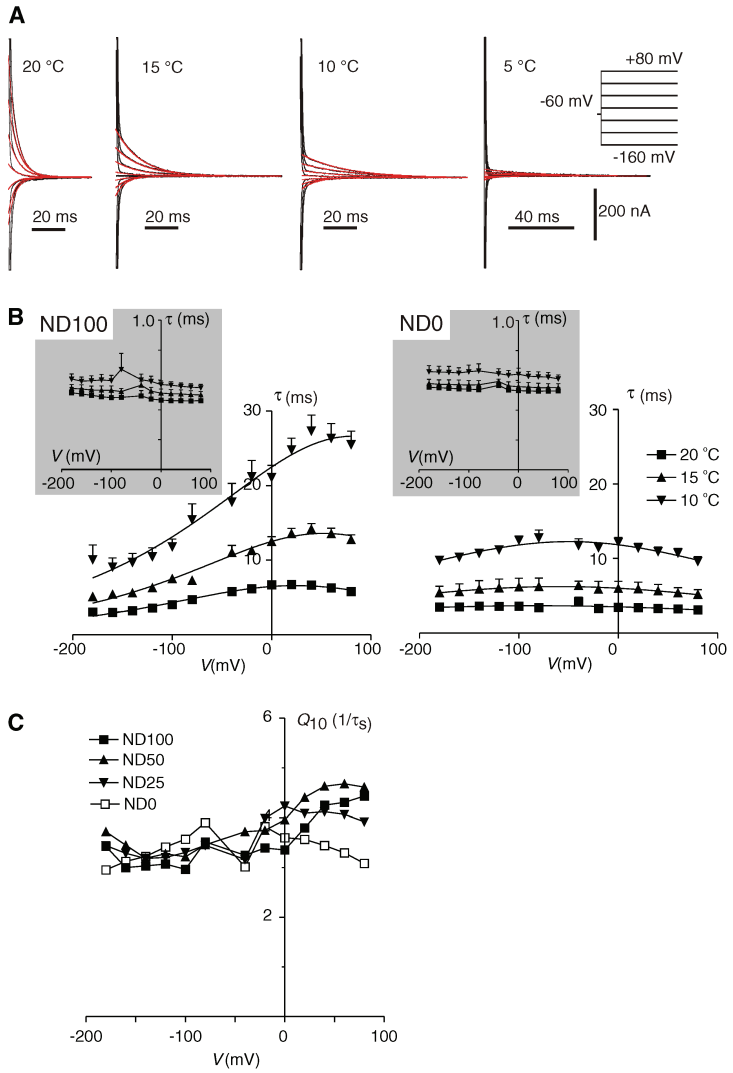

Fig. 4 Temperature effects on the kinetics of presteady-state currents. (*A*) Presteady-state relaxations recorded from the same oocyte in response to voltage steps from a holding potential of –60 m*V* to voltages in the range –180 to +80 m*V* at the four temperatures indicated. The steady-state holding currents were subtracted for each data set. *Red traces* indicate the slower fitted component derived from the two-exponential fit to the complete trace, commencing approximately 1 ms after the voltage step onset. (*B*) Voltage dependence of the main relaxation time constant (τ-*V*) reported by a two-exponential fit to the data in *A* for the three temperatures indicated, corresponding to the fitted curves in *A*. *Continuous lines* are fits with Eq. 2 to the data points. *Left*: Superfusion in ND100. *Right:* Superfusion in ND0. *Inset:* Temperature and voltage dependence of the fast component. Data at 5°C were too unreliable to determine the slow relaxation time constant. (*C*) Voltage dependence of Q_{10} of the reciprocal of the main relaxation time constant ($1/\tau_s$) for the external indicated Na^+ concentrations. Data points are joined by lines for visualization. Q_{10} was calculated from the ratio of $1/\tau_s$ at 20°C to $1/\tau_s$ at 10°C (n = 6)

previous studies, we assumed that this component represented the capacitive charging of the oocyte. Its temperature dependence may result from a temperature dependence of the membrane capacitance (White 1970) that would result in slower membrane charging. The small voltage dependence of this component most likely results from a systematic error in the fits because it was observed at all Na^+ concentrations and temperatures.

The slower time constant (τ_s) that we assumed to be associated with NaPi-IIb showed strong temperature and voltage dependence (Fig. 4B, C). For ND100 and ND0 superfusion, τ_s increased approximately threefold for a decrease in temperature from 20°C to 10°C. For ND100 superfusion, the voltage at which τ_s peaked shifted toward depolarizing potentials as the temperature decreased, whereas for ND0, a shift of the peak τ_s was less obvious. When expressed as Q_{10} (Fig. 4C), the temperature dependence of the relaxation rate constant ($1/\tau_s$) showed little dependence on Na^+ for $V < 0$. In contrast, for depolarizing potentials, Q_{10} increased for nonzero Na^+ concentrations. This behavior suggested that, in addition to the overall slowing of the relaxation rates with decreasing temperature, the voltage dependence of the Na^+ interaction with the NaPi-IIb protein was more temperature-dependent than that of the empty carrier alone.

To study the underlying mechanism in more detail, we determined the dependence of charge movement on external Na^+ ranging from 0 (ND0) to 125 (ND125) mM. Numerical integration of the slower relaxations yielded an estimate of the charge (Q_{ON}) moved for each voltage step from V_h to the

corresponding target potential as shown in Figure 5A at two temperatures. To facilitate comparison of data sets, the data were fit with Eq. 1, shifted by the predicted Q_{hyp} and normalized to Q_{max} for ND100 at 20°C. At 20°C (Fig. 5A, left), a decrease in external Na^+ resulted in a hyperpolarizing shift in the charge distribution similar to the shift reported in previous studies (Forster et al. 1997; Virkki et al. 2006a, b). At 10°C, a similar hyperpolarizing shift with decreasing Na^+ concentration was documented. For a given Na^+ concentration, there was also a relative hyperpolarizing shift of the charge distribution at the lower temperature. For superfusion in ND100, the *Q-V* behavior with respect to temperature corresponded qualitatively to that observed for the peak of the τ_s-*V* at ND100 (Fig. 4B, left).

The temperature dependence of the Boltzmann fit parameters with varying external Na^+ is summarized in

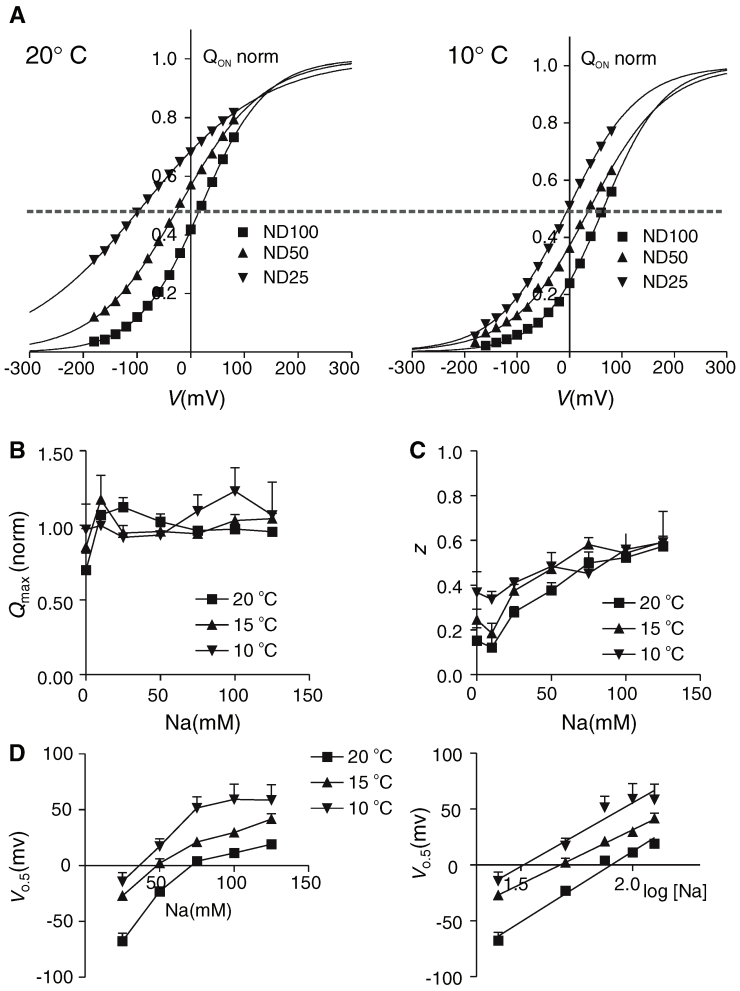

Fig. 5 Temperature dependence of fit parameters from *Q-V* data. (*A*) Voltage dependence of the charge (*Q-V*) associated with the slow relaxation component for the same cell as in Fig. 4A *A* at 20°C (*left*) and 10°C (*right*) at three external Na^+ concentrations (ND100, 100 mM; ND50, 50 mM; ND25, 25 mM). *Continuous lines* are fits with Eq. 1 to the data points. Data for each Na^+ concentration were normalized to the predicted Q_{max} from the curve fit and offset by Q_{hyp}. The fit parameters were as follows: at 20°C, $V_{0.5}$ = 20 ± 2 m*V* (ND100), –21 ± 4 m*V* (ND50), –90 ± 9 m*V* (ND25) and z = 0.42 ± 0.01 (ND100), 0.32 ± 0.02 (ND50), 0.22 ± 0.02 (ND25); at 10°C, $V_{0.5}$ = 65 ± 17 m*V* (ND100), 38 ± 19 m*V* (ND50), –2.8 ± 4.2 m*V* (ND25) and z = 0.44 ± 0.05 (ND100), 0.35 ± 0.05 (ND50), 0.37 ± 0.02 (ND25). The absolute Q_{max} values for individual cells at 20°C and 100 mM Na^+ ranged 11.5–29.6 nC. (*B*) Maximum available charge, Q_{max}, reported by Boltzmann fit plotted as a function of Na^+ pooled from six cells and normalized to the Q_{max} reported from fit to ND100 data at 20°C. (*C*) Apparent valence, z, reported by Boltzmann fit plotted as a function of Na^+ (n = 6). (*D*) Midpoint voltage ($V_{0.5}$) reported by Boltzmann fit plotted as a function of Na^+ (n = 6) and the same data replotted on a log[Na] scale and fitted with a linear regression line with slopes 126 ± 11 m*V* (20°C), 97 ± 3 m*V* (15°C) and 114 ± 15 m*V* (10°C)

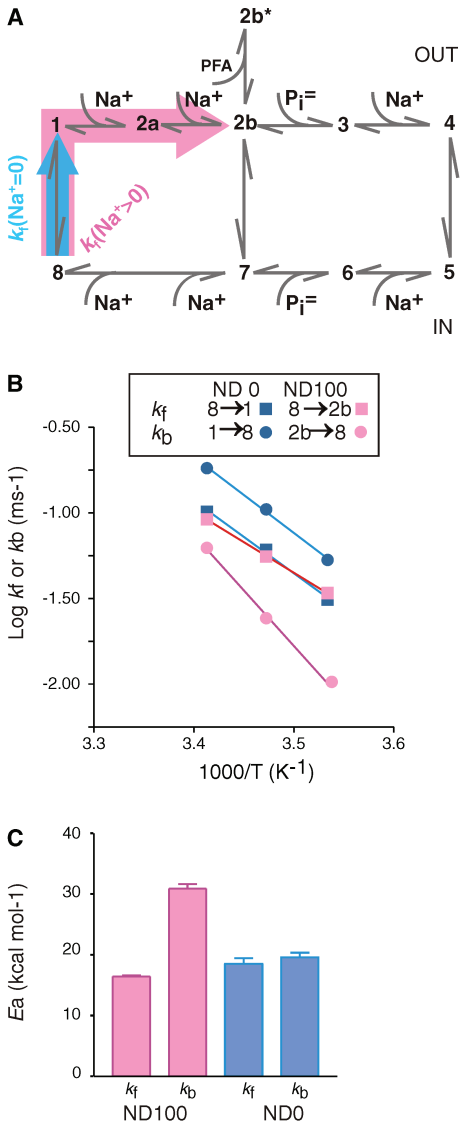

Fig. 6 Temperature dependence of partial reaction rates. (*A*) A kinetic scheme of electrogenic type II Na^+/P_i cotransport. Two Na^+ ions are proposed to bind before P_i binding can occur, and transition 2a⇒2b is voltage-dependent (Virkki et al. 2006b). The PFA-blockable leak current is, in part, due to the translocation of Na^+ ions between states 2a or 2b and 7. In the presence of PFA, the transporter occupies an inactive state (2b*). With saturating P_i, the transport cycle proceeds through states 3 and 4 to the fully loaded carrier. *Pink block arrow* indicates the partial reactions that contribute to presteady-state charge movement with Na^+ in the superfusion medium. *Blue block arrow* indicates the empty carrier partial reaction (ND0 superfusion). The direction of the forward reaction (k_f) is indicated for each. (*B*) Arrhenius plots of the zero-voltage rate constants (k_f, k_b) derived from fitting the time constants of the presteady-state relaxations (Fig. 4B) to Eq. 2. *Inset* identifies the rate constant with the lumped transitions according to the kinetic scheme in *A* for the two experimental superfusion conditions: ND100 (*pink symbols*) and ND0 (*blue symbols*). For ND100 superfusion, three partial reactions are lumped into one. Lines are linear regression fits to data points. (*C*) E_a for k_f and k_b derived from the slopes of the linear regression fits to the data in *B*. Error bars indicate error reported by fit

Figure 5B-D (n = 6). As expected, Q_{max}, the total mobile charge, normalized to that at ND100 and 20°C for each cell (to account for differences in expression level) was relatively insensitive to temperature (Fig. 5B). At 10°C, this parameter was subject to more uncertainty, where the signal-to-noise ratio was worse. Moreover, the normalized Q_{max} remained reasonably constant for nonzero Na^+. The apparent valence (z), derived from the maximum slope of the Boltzmann fits, decreased with decreasing Na^+; however, there was no statistical significance with respect to temperature (one-way analysis of variance, $P < 0.05$) (Fig. 5C). Finally, the voltage at which 50% of the charge was moved ($V_{0.5}$) decreased with diminishing Na^+ (Fig. 5D), and there was a clear temperature-dependent shift of this parameter. When the $V_{0.5}$ data were replotted on a log [Na^+] scale, the linear regression fits gave slopes for Na^+ varying from 125 to 25 mM of 126 ± 11 mV (20°C), 97 ± 3 mV (15°C) and 114 ± 15 mV (10°C). These slopes were not significantly different over the 10°C range of temperature ($P < 0.05$).

Discussion

This report describes the effect of temperature on the kinetics of a type II Na^+/P_i cotransporter expressed in *Xenopus* oocytes. Our estimates of the temperature dependence for the cotransport mode behavior obtained from uptake and electrophysiology assays, expressed as E_a, are in good agreement with one another. This is to be expected because we have shown that there is a tight correlation between charge translocation and P_i cotransport (Forster et al. 1999; Virkki et al. 2005b). Moreover, the corresponding Q_{10} of ~2.3–2.5 for the P_i-dependent current agrees with estimates reported for other cation-coupled electrogenic cotransporters, such as SGLT1 (Hazama et al. 1997; Parent and Wright 1993), rGAT1 (Binda et al. 2002) and GAT4 (Karakossian et al. 2005). For the cotransport mode of NaPi-IIb, the E_a of the P_i-dependent current (I_{Pi}) was essentially independent of membrane potential in the range where the transport rate is strongly voltage-dependent, i.e., for $V < 0$ mV. If we assume that 1 mM P_i is sufficient to ensure ''V_{max}'' conditions for all temperatures investigated, then our finding also accords with the behavior of SGLT1, for which the temperature dependence of the predicted maximum electrogenic sugar-induced

current was also reported to be independent of V (Parent and Wright 1993). A V_{max} effect on the electrogenic activity of the human NaPi-IIa isoform expressed in *Xenopus* oocytes was also documented, with a Q_{10} of ~3 (Wagner 1998), and this study also established that the apparent affinity of P_i was not significantly altered by temperature.

For the leak mode, quantified as I_{PFA}, E_a was smaller than that for the cotransport mode. The uncertainty in the fit, especially for hyperpolarizing potentials, did not allow us to make a definite statement about the voltage dependence of E_a for the leak mode. The difference in E_a for these two modes suggests distinct transport mechanisms. Certainly, compared to two other cotransport systems, the temperature dependence of the NaPi-IIb leak mode is too large for it to result only from a simple channel-like conductance. For the glutamate transporter EAAT1 (Beckman and Quick 2001; Wadiche and Kavanaugh 1998) and the GABA transporter GAT4 (Karakossian et al. 2005), Q_{10} values close to unity were found for their respective leak modes, consistent with an electrodiffusive mechanism. In contrast, for the sodium-coupled glucose transporter SGLT1, an E_a = 21 ± 3 kcal mol^{-1} was documented (Loo et al. 1999). Like NaPi-IIb in the present study, this finding suggests that the leak mode in SGLT1 also involves large conformational changes. On the other hand, from the steady-state data alone, we are unable to exclude the possibility that there is an additional ''channel'' component of the leak pathway, which may also be PFA-sensitive and conductive for other ions, including Cl^- (I. C. Forster, L. V. Virkki, A. Bacconi, unpublished observations). Caution should also be observed with respect to overinterpreting the apparent differences in E_a for the two modes, given the uncertainties reported by the fitting algorithm and the fact that for flounder NaPi-IIb I_{PFA} is typically ≤10% of I_{Pi} and therefore more prone to contamination from endogenous PFA-dependent currents (Forster et al. 2000). It should also be noted that E_a determined from the Arrhenius plot represents an effective estimate in which the transport process (leak or cotransport mode) is lumped into a single reaction that obeys first-order kinetics. This is an oversimplification because a number of partial reactions have already been identified as contributors to the overall cotransport cycle (Forster et al. 1998; Virkki et al. 2005b, 2006b), any of which might dominate the overall temperature dependence (Fig. 6A). From our data, we can conservatively conclude that the estimates of E_a for the leak mode strongly indicate that conformational changes take place that are inconsistent with an exclusively electrodiffusive transport process.

From the presteady-state data analysis, we found that the relaxations in the presence and absence of external Na^+ showed significant temperature dependence (Fig. 4). As expected, the predicted Q_{max} from the Boltzmann data was insensitive to temperature for Na^+ >25 mM. This result confirmed that we were able to detect all the charge over the temperature range used, except at low Na^+ concentrations, where the curve fitting and numerical integration were less reliable. It also confirmed that the number of active transporters in the membrane did not change with temperature. Moreover, we observed no significant temperature dependence of the apparent valence (z) for the Boltzmann fit.[1] In contrast, the midpoint voltage ($V_{0.5}$) of the Q-V distribution for a given Na^+ concentration was shifted toward depolarizing potentials as the temperature was lowered (Fig. 5C), whereas the slopes of the $V_{0.5}$ *vs.* log[Na^+] plots were not statistically altered by temperature. The linear dependence of $V_{0.5}$ on log[Na^+] is the behavior predicted, e.g., for a two-state ''ion-well'' model for voltage–dependent Na^+ interaction with a carrier (Mager, Cao and Lester 1998; Mager et al. 1996; Virkki et al. 2006b). The Q-V relation for this model is a modified version of Eq. 1 to take account of Na^+ dependence of the binding reaction:

$$Q = Q_{max}/[(1 + \{[Na^+]/K^{Na}\exp(-Ve\delta/kT)\}n_{Na}] + Q_{hyp} \quad (5)$$

where K^{Na} is a zero-voltage Na^+ binding constant that corresponds to [Na^+] when half the charge has moved and n_{Na} is the number of Na^+ ions that bind at a hypothetical site located a fraction δ through the membrane field.[2] For NaPi-IIb, we have shown that n_{Na} = 1 (Virkki et al. 2006b) and the slope of $V_{0.5}$ *vs.* log[Na^+] = 2.303 kT/(eδ), from which we can estimate δ. Our data (Fig. 5C) suggest that δ is not a function of temperature, which implies that Na^+ ions move through the same fraction of the transmembrane field, independent of temperature. The mean of the slopes at the three test temperatures gave δ = 0.51, which is consistent with our previous analyses of the NaPi-IIb presteady-state kinetics (Virkki et al. 2006a, b). On the other hand, the intercept with the log[Na^+] axis shifted to the left with decreasing temperature, which indicated that K^{Na} decreased with decreasing temperature. In terms of the simple two-state model for charge translocation (see Materials and Methods), K^{Na} can also be expressed as the ratio of the zero-voltage rates (k_f, k_b), and therefore the observed dependence of K^{Na} on temperature could result from a change in either rate constant or both.

[1] The dependence of z on [Na^+] is a consequence of fitting a single Boltzmann function to the Q-V data. The valence estimated from the single fit is a weighted value that depends on the relative contributions from the empty carrier and Na^+ binding partial reactions. Similar behavior was observed by fitting a single Boltzmann to presteady-state data generated by a three-state model that simulates the empty carrier and one voltage-dependent Na^+ binding step (I. C. Forster, unpublished data).

Table 1 Temperature dependence of fit parameters for τ-V data

Temp (°C)	ND100			ND0		
	k_f (ms^{-1})	k_b (ms^{-1})	z	k_f (ms^{-1})	k_b (ms^{-1})	z
20	0.092 ± 0.004	0.063 ± 0.003	0.40 ± 0.02	0.102 ± 0.009	0.183 ± 0.011	0.18 ± 0.05
15	0.056 ± 0.003	0.024 ± 0.003	0.40 ± 0.03	0.061 ± 0.001	0.105 ± 0.002	0.23 ± 0.01
10	0.034 ± 0.002	0.010 ± 0.002	0.37 ± 0.04	0.031 ± 0.001	0.053 ± 0.002	0.27 ± 0.02

Fit parameters are given by Eq. 3. Errors are standard errors reported by fit algorithm

To distinguish between these possibilities, we fitted the τ_s-V data (Fig. 4B) for superfusion in ND100 with Eq. 2 to obtain estimates for k_f and k_b, as summarized in Table 1. These data confirmed that both rates became slower with decreasing[2] temperature. To further quantify the temperature dependence of the fit-derived reaction rates, we plotted these data in the Arrhenius form (Fig. 6B). For ND100 superfusion, the data show that the temperature dependence of the effective backward rate (k_b) of the lumped Na^+ interaction (i.e., by considering the transitions 8⇔1⇔2a⇔2b as a single transition [Fig. 6A]) was greater than that of the effective forward reaction (k_f). In terms of a simple ion–well model, we interpret this as indicating that the apparent affinity for Na^+ ions increases with decreasing temperature. We also fitted the τ_s-V data for ND0 superfusion with Eq. 2, to investigate the temperature dependence of the empty carrier (transition 8⇔1, Fig. 6A). Here, the Arrhenius analysis showed that the temperature dependence for the effective k_b and k_f was similar and close to that of k_f with ND100 superfusion (Fig. 6B). Figure 6C summarizes these findings in terms of the activation energy for each rate constant.

Our finding that E_a determined under voltage clamp for the cotransport mode is essentially independent of membrane potential suggests that a major electroneutral conformational change occurs during the transport cycle. One likely candidate for the corresponding transition, according to the scheme of Figure 6A, is the translocation of the fully loaded carrier (transition 4⇔5), which we have previously proposed to be electroneutral (Forster et al. 1998) but without experimental evidence. In the present study, this proposal is supported by our finding that E_a for the empty carrier zero-voltage rate constants corresponds closely to the E_a estimated from the steady-state analysis for the cotransport mode. Thus, in the absence of membrane potential, the partial reactions that describe the reorientation of the empty and fully loaded carrier are energetically similar. On the other hand, given that we have no information about the voltage dependence of the partial reactions between intracellularly oriented states, we cannot exclude that conformational changes associated with other transitions between states 5 and 8 also contribute to the voltage-independent activation energy observed for cotransport.

[2] In applying this model to NaPi-IIb, we have lumped the empty carrier transition (1–8, Fig. 6A) and Na^+ binding transitions (1–2a, 2a–2b) into a single transition. A more accurate description of the presteady-state kinetics would require fitting the presteady-state relaxations to >2 exponentials and using at least a two Boltzmann fit to the data. We were unable to extract more than one component of nonendogenous presteady-state charge movement by exponential curve fitting with confidence. Moreover, attempts to fit a double Boltzmann function to our Q-V data (e.g., as undertaken by Krofchick, Huntley and Silverman [2004] for SGLT1) were equally unsuccessful because of fit uncertainties with the larger number of free parameters.

Acknowledgement This work was supported by grants to H. M. from the Swiss National Science Foundation and the Gebert Rüf Foundation (http://www.grstiftung.ch).

References

Accardi A, Miller C (2004) Secondary active transport mediated by a prokaryotic homologue of ClC Cl^- channels. Nature 427:803–807

Adams SV, DeFelice LJ (2002) Flux coupling in the human serotonin transporter. Biophys J 83:3268–3282

Beckman ML, Quick MW (2001) Substrates and temperature differentiate ion flux from serotonin flux in a serotonin transporter. Neuropharmacology 40:526–535

Binda F, Bossi E, Giovannardi S, Forlani G, Peres A (2002) Temperature effects on the presteady-state and transport-associated currents of GABA cotransporter rGAT1. FEBS Lett 512:303–307

Birnir B, Loo DD, Wright EM (1991) Voltage-clamp studies of the Na^+/glucose cotransporter cloned from rabbit small intestine. Pfluegers Arch 418:79–85

Chen XZ, Coady MJ, Jalal F, Wallendorff B, Lapointe JY (1997) Sodium leak pathway and substrate binding order in the Na^+-glucose cotransporter. Biophys J 73:2503–2510

DeFelice LJ (2004) Transporter structure and mechanism. Trends Neurosci 27:352–359

Eskandari S, Loo DD, Dai G, Levy O, Wright EM, Carrasco N (1997) Thyroid Na^+/I^- symporter. Mechanism, stoichiometry, and specificity. J Biol Chem 272:27230–27238

Forster I, Hernando N, Biber J, Murer H (1998) The voltage dependence of a cloned mammalian renal type II Na^+/P_i cotransporter (NaPi-2). J Gen Physiol 112:1–18

Forster IC, Biber J, Murer H (2000) Proton-sensitive transitions of renal type II Na^+-coupled phosphate cotransporter kinetics. Biophys J 79:215–230

Forster IC, Kohler K, Biber J, Murer H (2002) Forging the link between structure and function of electrogenic cotransporters:

The renal type IIa Na^+/P_i cotransporter as a case study. Prog Biophys Mol Biol 80:69–108

Forster IC, Loo DD, Eskandari S (1999) Stoichiometry and Na^+ binding cooperativity of rat and flounder renal type II Na^+-P_i cotransporters. Am J Physiol 276:F644-F649

Forster IC, Wagner CA, Busch AE, Lang F, Biber J, Hernando N, Murer H, Werner A (1997) Electrophysiological characterization of the flounder type II Na^+/P_i cotransporter (NaPi-5) expressed in *Xenopus laevis* oocytes. J Membr Biol 160:9–25

Hazama A, Loo DD, Wright EM (1997) Presteady-state currents of the rabbit Na^+/glucose cotransporter (SGLT1). J Membr Biol 155:175–186

Karakossian MH, Spencer SR, Gomez AQ, Padilla OR, Sacher A, Loo DD, Nelson N, Eskandari S (2005) Novel properties of a mouse gamma-aminobutyric acid transporter (GAT4). J Membr Biol 203:65–82

Kohler K, Forster IC, Stange G, Biber J, Murer H (2002a) Identification of functionally important sites in the first intracellular loop of the NaPi-IIa cotransporter. Am J Physiol 282:F687–F696

Kohler K, Forster IC, Stange G, Biber J, Murer H (2002b) Transport function of the renal type IIa Na^+/P_i cotransporter is codetermined by residues in two opposing linker regions. J Gen Physiol 120:693–703

Krofchick D, Huntley SA, Silverman M (2004) Transition states of the high-affinity rabbit Na^+/glucose cotransporter SGLT1 as determined from measurement and analysis of voltage-dependent charge movements. Am J Physiol 287:C46–C54

Loo DDF, Hirayama BA, Meinild A-K, Chandy G, Zeuthen T, Wright EM (1999) Passive water and ion transport by cotransporters. J Physiol 518:195–202

Mager S, Cao Y, Lester HA (1998) Measurement of transient currents from neurotransmitter transporters expressed in *Xenopus* oocytes. Methods Enzymol 296:551–566

Mager S, Kleinberger-Doron N, Keshet GI, Davidson N, Kanner BI, Lester HA (1996) Ion binding and permeation at the GABA transporter GAT1. J Neurosci 16:5405–5414

Otis TS, Jahr CE (1998) Anion currents and predicted glutamate flux through a neuronal glutamate transporter. J Neurosci 18:7099–7110

Parent L, Wright EM (1993) Electrophysiology of the Na^+/glucose cotransporter. Soc Gen Physiol Ser 48:263–281

Segel IH (1976) Biochemical Calculations. Wiley, New York

Sonders MS, Amara SG. (1996) Channels in transporters. Curr Opin Neurobiol 6:294–302

Van Winkle L (1995) Biomembrane Transport. Academic Press, San Diego

Virkki LV, Forster IC, Bacconi A, Biber J, Murer H (2005a) Functionally important residues in the predicted 3rd transmembrane domain of the type IIa sodium-phosphate co-transporter (NaPi-IIa). J Membr Biol 206:227–238

Virkki LV, Forster IC, Biber J, Murer H (2005b) Substrate interactions in the human type IIa sodium-phosphate cotransporter (NaPi-IIa). Am J Physiol 288:F969–F981

Virkki LV, Forster IC, Hernando N, Biber J, Murer H (2003) Functional characterization of two naturally occurring mutations in the human sodium-phosphate cotransporter type IIa. J Bone Miner Res 18:2135–2141

Virkki LV, Murer H, Forster IC (2006a) Mapping conformational changes of a type IIb Na^+/P_i cotransporter by voltage clamp fluorometry. J Biol Chem 281:28837–28849

Virkki LV, Murer H, Forster IC (2006b) Voltage clamp fluorometric measurements on a type II Na^+-coupled P_i cotransporter: Shedding light on substrate binding order. J Gen Physiol 127:539–555

Wadiche JI, Kavanaugh MP (1998) Macroscopic and microscopic properties of a cloned glutamate transporter/chloride channel. J Neurosci 18:7650–7661

Wagner CA (1998) Elektrophysiologische Untersuchungen an den renalen Natrium-Phosphat-Kotransportern NaPi-3 (Mensch) und NaPi-7 (Maus). Doctoral diss., University of Tübingen, Tübingen

White SH (1970) A study of lipid bilayer membrane stability using precise measurements of specific capacitance. Biophys J 10:1127–1148

Yao X, Pajor AM (2000) The transport properties of the human renal Na(+)-dicarboxylate cotransporter under voltage-clamp conditions. Am J Physiol 279:F54–F64

Part III

Discussion and Outlook

"While the functions and purposes of a protein are invariant in biology, the view adopted by biologists often evolves with time sculpted by prevailing database and interpretations" [135]. PiT1 and PiT2 (Na^+ -coupled phosphate transporters of the SLC20 family) have been assigned varying roles and given different aliases since their discovery. Because mammalian cells have not evolved mechanisms to welcome viral invaders on purpose, viruses exploit ubiquitous cell surface proteins to enter the cell and replicate. As viral targets, PiT1 and PiT2 were called "viral receptors" Glvr-1 and Ram-1, respectively. When these proteins were found to mediate Na^+ coupled P_i cotransport into cells, they were renamed like their prokaryotic paralogs (PiT). Due to their ubiquitous distribution (investigated at mRNA level, see fig. **??**) PiT1 and PiT2 were considered to be phosphate house-keeping transporters. One of the main findings of this thesis has been a redefinition of the role of PiT2 from that of housekeeping to physiologically regulated proximal tubule phosphate reabsorption. In this work a thorough characterization of the transport kinetics of one isoform (*Xl*PiT1) was performed and the renal localization and dietary regulation of a member of the SLC20 family was reported for the first time.

Transport mechanism. The novel electrogenic kinetics of the members of the PiT family present a contrasting view of Na^+-driven P_i cotransport with respect to that of the well-characterized members of the SLC34 family (NaPi-IIa/b), and these kinetic differences are underscored by the lack of sequence homology at the molecular level.

The solute transport families SLC20 and SLC34 both mediate Na^+/P_i cotransport through different molecular mechanisms and they show a preference for one of the two **P_i species** that are most abundant at physiological pH: PiT transporters prefer monovalent P_i ($H_2PO_4^-$) in contrast to all three SLC34 family proteins that prefer divalent P_i (HPO_4^{2-}) [69, 136, 137].

NaPi II and NaPi III also differ in their substrate **stoichiometry**. NaPi-IIa and NaPi-IIb transport three Na^+ ions per transport cycle (see fig. 3.3), with the translocation of one net positive charge, whereas NaPi-IIc only cotransports two Na^+ ions and is electroneutral. Like NaPi-IIc PiT also transports two Na^+ ions per cycle (see fig. 7.2) but with one net positive charge. These differences result in a large difference in P_i concentrating capacity (as shown in Table 7.1), and the ability of a transport protein to create a substrate gradient across the membrane.

The two families differ in their **optimum pH range**: PiT1, which prefers $H_2PO_4^-$ has a V_{max} that is relatively insensitive to a large pH variation (6.2-8), whereas for NaPi-IIa and b, which prefer HPO_4^{2-}, the V_{max} is significantly reduced for pH <8 [82, 132].

A significant finding in this work was the insensitivity of *Xl*PiT1 to **phosphonoformic acid (PFA)**. This contrasts with the behavior of NaPi-IIa, b, c, which all show significant

inhibition by PFA under the same conditions. Oocytes expressing *Xl*PiT1 show an invariant ^{32}P uptake even after incubation with 6 mM of PFA and 0.1 mM P_i (Ravera, Stange, Forster, unpublished: see fig. 7.1). When analyzed using two-electrode voltage clamp, oocytes expressing *Xl*PiT1 do not present any reduction of P_i induced current in presence of PFA (up to 6 mM). These data contrast to those of Villa-Bellosta et al. 2008 [138] who characterized the inhibition by PFA on PiT1 and PiT2 by ^{32}P uptake. Oocytes expressing rat PiT2 show a reduced ^{32}P uptake in presence of 6 mM of PFA and 0.1 mM P_i compared to those exposed only to 0.1 mM P_i. However for PFA concentration > 1 mM, an endogenous leak can be induced in oocytes. This would have the effect of reducing the membrane potential and the driving force for cotransport, which could result in an apparent inhibition by PFA.

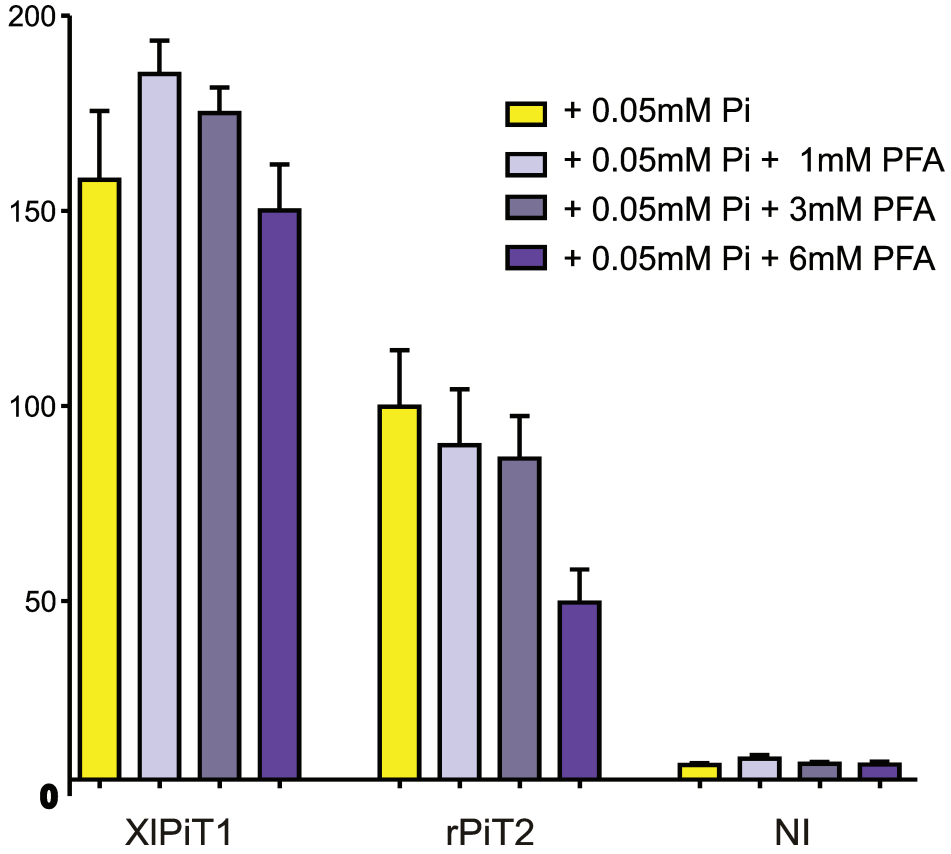

Figure 7.1: The effect of PFA on ^{32}P uptake in oocytes expressing *Xl*PiT1 and ratPiT2, NI = non injected.

The difference in preferred P_i species can also explain why PFA inhibits P_i transport by SLC34, but not by SLC20, because under physiological conditions PFA is a divalent anion.

It appears that in contrast to SLC34 proteins, Li^+ can substitute for Na^+ as the driving cation, although the P_i induced currents are only 10% of those recorded with Na^+. Moreover, arsenate can also substitute for P_i as the driven substrate. Like SLC34 proteins, PiT1 and 2

also may provide a pathway for arsenate to enter the cell and exert its toxic effects.

The **voltage dependence** of PiT requires that at least one partial reaction in the transport cycle is membrane voltage (V_m) dependent. This implies that mobile charges must sense the V_m, for example charged amino acid residues intrinsic to the protein or charged substrates (e.g., Na^+) moving within the transmembrane electric field. For example, the decrease of $K_{0.5}^{Na}$ with hyperpolarizing potentials (Fig. 4F in Ravera et al. 2007 [132]) suggests that Na^+ interaction with the transporter is voltage dependent, whereby a more negative V_m would increase the likelihood of Na^+ binding. The lack of detectable pre-steady-state currents in SLC20 prevents assigning voltage dependence to any particular step in the transport cycle, unlike for NaPi-IIa and -IIb [132].

Our substrate-dependence data strongly suggest for *Xl*PiT-1 an **ordered binding** for the substrates, as indicated by the dependence of $K_{0.5}^{P_i}$ on Na^+ concentration and $K_{0.5}^{Na}$ on P_i (Fig.3 in Ravera et al. 2007 [132]). We hypothesize that a Na^+ ion is the first to bind (see fig. 7.2). For P_i as the variable substrate, the dependence of $I_{P_i}^{max}$ on Na^+ is consistent with Na^+ also being the last substrate to bind. Consistent with the 2:1 Na^+:P_i stoichiometry, a possible binding order, based on analogy with the electrogenic SLC34 transporters, might therefore be Na^+:$H_2PO_4^-$:Na^+. The increase in apparent cooperativity for Na^+ interaction observed at pH 8.0 would also support this scheme, whereby the decreased availability of $H_2PO_4^-$ at pH 8.0 would increase the apparent dissociation constant associated with the proposed first Na^+-binding step, thus conferring a greater cooperativity to the overall Na^+ interaction. On the other hand, the V_{max} effect observed for P_i, with Na^+ as the variable substrate, would not be consistent with this scheme and suggests that a more complex binding/debinding mechanism exists that may involve both ordered and random partial reactions (see fig. 7.2) [82].

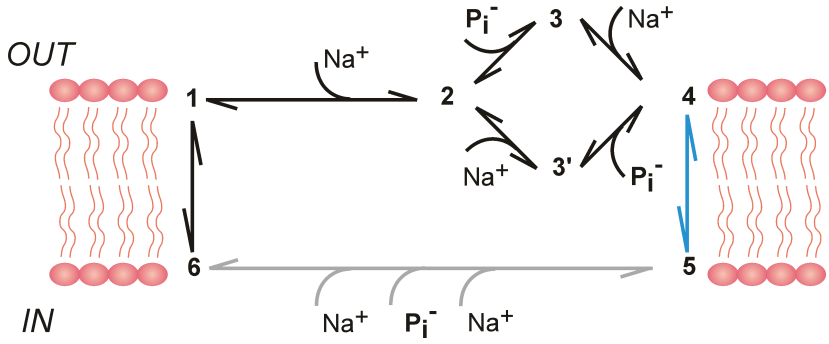

Figure 7.2: Proposed transport mechanism scheme for PiT1 from Virkki et al.2007 [82].

Because NaPi-IIc and PiT transport only 2 Na^+ ions, less Na^+ is loaded into the cell and less energy is required to maintain the cell's negative membrane potential, resulting in a reduced energetic cost of transporting P_i.

The following table summarizes some of the features of the SLC34 and SLC20 members.

	Substrates	Stoichiometry Na^+:P_i: Q	Electrogenic	Concentrating Capacity	PFA inhibition
NaPi-IIa	Na^+, HPO_4^{2-}, Arsenate	3:1:1	Yes	10,000	Yes
NaPi-IIb	Na^+, HPO_4^{2-}, Arsenate	3:1:1	Yes	10,000	Yes
NaPi-IIc	Na^+, HPO_4^{2-}, Arsenate	2:1:0	No	100	Yes
PiT-1	Na^+, $H_2PO_4^-$, Li^+, Arsenate	2:1:1	Yes	1,000	No
PiT-2	Na^+, $H_2PO_4^-$, Li^+, Arsenate	2:1:1	Yes	1,000	No

Table 7.1: Main differences between the SLC34 and SLC20 family members, adapted from Virkki et al. 2007 [82].

Kidney localization and physiological regulation. Three important findings have emerged from this study on expression levels and regulation of PiT2 in the kidney: *first*, the localization of PiT-2 to the apical brush border, in contrast with the proposal that PiTs are all basolaterally located. Tenenhouse and co-workers reported that NaPi-IIc protein is significantly upregulated in mice homozygous for the disrupted NaPi-IIa gene [79] and that NaPi-IIc protein is highly upregulated in $Npt2^{-}/^{-}$ mice and accounts for residual BBM Na^+/P_i cotransport in this mutant model. The hypothesis of a third phosphate transporter in the kidney BBM was made possible by the finding that PiT proteins are insensitive to PFA. *Second*, switching from a low to high dietary phosphate suppresses NaPi-IIa/c-mediated transport (PFA sensitive) by 32% and PiT2-mediated transport (PFA insensitive) by 73%, suggesting that Pit-2 is a highly regulated protein. *Third*, the three players of apical phosphate reuptake (NaPi-IIa/c and PiT-2) adapt to changes in dietary phosphate via protein re-distribution differently from PiT-2 wich shows an intermediate time course between NaPi-IIa and NaPi-IIc .

By performing ^{32}P uptake assays on brush border membrane vesicle preparation from rats that had been conditioned on high or low P_i diets, we could distinguish between a "PFA sensitive" and a "PFA-insensitive" component of P_i transport. One candidate for the "PFA-insensitive" component would be PiT2, which was shown by immunohistochemistry and western blot to be expressed and regulated by dietary Pi. Immunoblot analysis demonstrated a clear difference in the time course of down regulation of PiT2 protein compared with NaPi-IIa and NaPi-IIc.

That the time course of regulation of PiT2 in response to a switch between high and low P_i diet and vice versa is different from both NaPi-IIa and NaPi-IIc, suggests a different regulatory pathway. We can speculate that PiT2 might play a role in fine tuning overall P_i reabsorption under different dietary conditions. Another potential and unique role for PiT2 in the kidney come from a consideration of the kinetic properties of SLC20 proteins [132] and the related malaria *plasmodium Falciparum* PfPiT [121], expressed in *Xenopus* oocytes.

The transport of either P_i species across a membrane will affect the pH, as it shifts the equilibrium of the reaction $H_2PO_4^- \rightleftharpoons HPO_4^{2-} + H^+$. Since PiT proteins transport $H_2PO_4^-$, we would expect that this would cause a concomitant acid loading of the cell. In contrast, type II Na^+/P_i cotransporters, which mediate HPO_4^{2-} transport, would alkalinize the cell. Whether the transport rates of type II or type III Na^+/P_i cotransporters in their natural environments are high enough to affect cell pH is not known. Our own experience with expressing type II and type III Na^+/P_i cotransporters in *Xenopus* oocytes would suggest that the pH changes would be insignificant.

About 70% of filtered P_i is reabsorbed in the kidney proximal tubule. If we hypothesize that only the type II Na^+/P_i cotransporters are present, considering a glomerular filtration rate of 180 L/day, a serum P_i concentration of 1 mM and a pH of 7.4 in the lumen of the proximal tubule, since $H_2PO_4^-$ remains, we can estimate an effective secretion of 40 mmoles of H^+ per day in the proximal tubular lumen. That PiT2 is also in the proximal tubular brush border membrane, may constitute one more means to effect the regulation of the acid loading in the proximal tubule [139].

The existence of multiple transporters for the same substrate in the proximal apical membrane s not unusual. Apical H^+ extrusion utilizes the multi-subunit H^+-ATPase and two Na^+ /H^+ exchanger isoforms and glucose uptake involves at least two isoforms. The diverse characteristic of the transporters serves to ensure flexible substrate specificity as well as multiple mechanisms and kinetics of transport regulation, which would be difficult to achieve by a single transporter. Axial changes in luminal potential difference and Na^+ concentration are minimal but changes in luminal pH and total phosphate concentrations are large: early to late proximal tubule: pH 7.4 - 6.8, $[P_i]$ 1.4 - 0.4 mM.

Micropuncture studies have shown that the pH in the proximal tubule can fall by up to 0.78 pH units relative to arterial blood in rats previously loaded with NH_4Cl [140]. At pH 7.4, the ratio $[HPO_4^{2-}]/[H_2PO_4^-] = 4$, which decreases to 1.6 at pH 6.6, at which the NaPi-IIa/c transport rate will be reduced by 50% [59, 82]. Because we expect PiT2 transport activity to be unaffected by changes in luminal pH, to have a different regulation pathway compared to the type II of NaPi, and a preference for different phosphate species, the presence of both types of transporter may be necessary to ensure the complete P_i reabsorption from the primary urine.

Structure-function studies. Knowing the structure of a transporter is essential to understand its mechanisms and possible interactions with accessory proteins, and physiological regulation. Unfortunately, no crystal structure of Pit1 & 2 or their bacterial homologs is available, and information about the structure-function relationships is insufficient to build

a structural model.

From the analysis of the sequence of the SLC34 members it appears that there is an inverted repeated motif, common to the Na^+-coupled cotransporters. Also *Xl*PiT1 shows an internal repeated motif in the sequence as shown by Salaün et al.2001 [126] (blue region in fig.3.8). This repeated motif is important because it could be involved in the coordination of the substrates during their translocation across the membrane. The crystal structure of the leucine transporter (LeuT) [33] shows a repeated motif which is involved in the substrate-binding, and this has been observed also for the glucose transporter vSGLT1 [141] and for the serotonine transporter SERT [47].

We proposed a topology model based on in silico investigations: hydrophathy analysis, secondary structure prediction analysis, motif scans and we adopted these predictions using data found in the literature. We started to validate our model by investigating the surface accessibility. We began with the first predicted extracellular loop that we hypothesize to be, first accessible from the external solution, second involved in the substrates coordination. We based our assumption on experimental data about the same region in PiT2 expressed in cell culture. This region is highly conserved among species and two charged residues Glu-87 and Asp-95 correspond to residues in PiT2 that if mutated show a 8-16 times reduced ^{32}P uptake [131]. SCAM allowed us to evaluate each residues in this region by comparing the mutants behavior with the wild type one as shown for example by Lambert et al. for NaPi-IIa [37]. We screened the mutants by ^{32}P uptake and two-electrode voltage clamp. Our data are preliminary, but so far we can confirm that part of this region is accessible from the external solution. Some of the mutants show a reduction in the P_i-induced current and ^{32}P uptake after incubation with MTSET ([2-(trimethylammonium)ethyl]methanethio-sulfonate) suggesting that the residues in that area are important in the binding of the substrates, the labelling could reduce access to the substrate binding site or impede transitions between conformational changes during the transport cycle. Some of the mutants show an increase in the ^{32}P uptake in presence of MTSET suggesting that area can be close to binding site and can allow a larger volume due to the presence of the thiol reagent. The rates of the reaction between the MTS reagent and the cysteines introduced in different positions are different and this indicates a variations accessibility. Some of the mutants show a different apparent P_i affinity compared with the wild type, such as mutant S86C, or a different voltage dependence like the R90C or I93C or V96C, suggesting the importance of these sites in determining the voltage dependent kinetics.

Outlook

There are many open questions that will need consideration in future studies:

- TRANSPORT MECHANISM - It will be important to define the precise binding order for substrate and co-substrate. To have more information about the transport mechanism of PiT will be useful to find PiT-specific inhibitors; one possible strategy would be to investigate monovalent P_i derivatives.

- LOCALIZATION AND PHYSIOLOGICAL REGULATION - Adaptation of renal P_i handling in response to changing dietary P_i is well-documented, yet the systemic and local signaling pathways remain to be elucidated. From the systemic viewpoint, one might hypothesize that a P_i sensor is involved, which would require identification. Other factor influences the phosphate reabsorption regulation in the kidney acting on NaPi type II like PTH, vitamin D, FGF23 etc. All these factors are potential effectors of the PiT level regulation.

- STRUCTURE-FUNCTION - Screening of substrate apparent affinity and of voltage dependence needs to be completed to better understand the importance of the first predicted extracellular loop in the interaction with the substrates, the identification of a putative voltage sensor, and to elucidate the secondary structure of this region predicted from MTS accessibility. Based on our topology model, *Xl*PiT1 presents, charged residues in the transmembrane field, these residues are potential candidates for the interaction with the substrates and the study of mutations at these sites could provide important information about the transport mechanism and the structure of the transporter.

Bibliography

[1] B. Alberts, D. Bray, J.Lewis, M.Raff, K. Roberts, and J.D. Watson. *Molecular Biology of The cell-Third Edition*. Garland Publishing, 1994.

[2] H. Sui, B.G. Han, J.K. Lee, P. Walian, and B.K. Jap. Structural basis of water-specific transport through the AQP1 water channel. *Nature*, 414(6866):872–878, 2001.

[3] F. Khalili-Araghi, J. Gumbart, P.-C. Wen, M. Sotomayor, E. Tajkhorshid, and K. Schulten. Molecular dynamics simulations of membrane channels and transporters. *Curr Opin Struct Biol*, 19(2):128–137, Apr 2009.

[4] A.L. Gonzales, W. Lee, S.R. Spencer, R.A. Oropeza, J.V. Chapman, J.Y. Ku, and S. Eskandari. Turnover rate of the gamma-aminobutyric acid transporter GAT1. *J Membr Biol*, 220(1-3):33–51, Dec 2007.

[5] P.L. Jorgensen. Isolation and characterization of the components of the sodium pump. *Q Rev Biophys*, 7(2):239–274, May 1974.

[6] J. Brahm. Temperature-dependent changes of chloride transport kinetics in human red cells. *J Gen Physiol*, 70(3):283–306, Sep 1977.

[7] W. F. Boron and E. L. Boulpaep. *Medical Physiology*. Elsevier, 2005.

[8] H. Lodish, Arnold Berk, L. S. Zipursky, P. Matsudaira, D. Baltimore, and J. Darnell. *Molecular Cell Biology*. 2000.

[9] D.A. Doyle, J. Morais Cabral, R.A. Pfuetzner, A. Kuo, J.M. Gulbis, S.L. Cohen, B.T. Chait, and R. MacKinnon. The structure of the potassium channel: molecular basis of K^+ conduction and selectivity. *Science*, 280(5360):69–77, Apr 1998.

[10] J. Abramson, I. Smirnova, V. Kasho, G. Verner, H. R. Kaback, and S. Iwata. Structure and mechanism of the lactose permease of Escherichia coli. *Science*, 301(5633):610–615, Aug 2003.

[11] B. Hille. *Ion Channels of Excitable Membranes, Third Edition*. 2001.

[12] W.F. Widdas. Inability of diffusion to account for placental glucose transfer in the sheep and consideration of the kinetics of a possible carrier transfer. *J Physiol*, 118(1):23–39, Sep 1952.

[13] O. Jardetzky. Simple allosteric model for membrane pumps. *Nature*, 211(5052):969–970, Aug 1966.

[14] M.S. Sonders and S.G. Amara. Channels in transporters. *Curr Opin Neurobiol*, 6(3):294–302, Jun 1996.

[15] A. Accardi, L. Kolmakova-Partensky, C. Williams, and C. Miller. Ionic currents mediated by a prokaryotic homologue of CLC Cl- channels. *J Gen Physiol*, 123(2):109–119, Feb 2004.

[16] L.J. DeFelice and T. Goswami. Transporters as channels. *Annu Rev Physiol*, 69:87–112, 2007.

[17] R. Dutzler, E.B. Campbell, and R. MacKinnon. Gating the selectivity filter in ClC chloride channels. *Science*, 300(5616):108–112, Apr 2003.

[18] R. Dutzler. A structural perspective on ClC channel and transporter function. *FEBS Lett*, 581(15):2839–2844, Jun 2007.

[19] P. Luger. A channel mechanism for electrogenic ion pumps. *Biochim Biophys Acta*, 552(1):143–161, Mar 1979.

[20] A. Su, S. Mager, S.L. Mayo, and H.A. Lester. A multi-substrate single-file model for ion-coupled transporters. *Biophys J*, 70(2):762–777, Feb 1996.

[21] J.N. Cammack, S. V. Rakhilin, and E.A. Schwartz. A GABA transporter operates asymmetrically and with variable stoichiometry. *Neuron*, 13(4):949–960, Oct 1994.

[22] S. Risso, L.J. DeFelice, and R.D. Blakely. Sodium-dependent GABA-induced currents in GAT1-transfected HeLa cells. *J Physiol*, 490 (Pt 3):691–702, Feb 1996.

[23] L.J. DeFelice and A. Galli. Fluctuation analysis of norepinephrine and serotonin transporter currents. *Methods Enzymol*, 296:578–593, 1998.

[24] G.R. Dubyak. Ion homeostasis, channels, and transporters: an update on cellular mechanisms. *Adv Physiol Educ*, 28(1-4):143–154, Dec 2004.

[25] L.J. DeFelice, S.V. Adams, and D.L. Ypey. Single-file diffusion and neurotransmitter transporters: Hodgkin and Keynes model revisited. *Biosystems*, 62(1-3):57–66, 2001.

[26] D.W. Hilgemann and C.C. Lu. GAT1 (GABA:Na^+:Cl^-) cotransport function. database reconstruction with an alternating access model. *J Gen Physiol*, 114(3):459–475, Sep 1999.

[27] I.C Forster, K. Köhler, J. Biber, and H. Murer. Forging the link between structure and function of electrogenic cotransporters: the renal type IIa Na^+-P_i cotransporter as a case study. *Prog. Biophys. Mol. Biol.*, 80:69–108, 2002.

[28] Y. Jiang, A. Lee, J. Chen, V. Ruta, M. Cadene, B.T. Chait, and R. MacKinnon. X-ray structure of a voltage-dependent K^+ channel. *Nature*, 423(6935):33–41, May 2003.

[29] Q.X. Jiang, D.N. Wang, and R. MacKinnon. Electron microscopic analysis of KvAP voltage-dependent K^+ channels in an open conformation. *Nature*, 430(7001):806–810, Aug 2004.

[30] R. Dutzler, E.B. Campbell, M. Cadene, B.T. Chait, and R. MacKinnon. X-ray structure of a ClC chloride channel at 3.0 å reveals the molecular basis of anion selectivity. *Nature*, 415(6869):287–294, Jan 2002.

[31] C. Hunte, E. Screpanti, M. Venturi, A. Rimon, E. Padan, and H. Michel. Structure of a Na^+/H^+ antiporter and insights into mechanism of action and regulation by pH. *Nature*, 435(7046):1197–1202, Jun 2005.

[32] D. Yernool, O. Boudker, Y. Jin, and E. Gouaux. Structure of a glutamate transporter homologue from *Pyrococcus horikoshii*. *Nature*, 431(7010):811–818, Oct 2004.

[33] A. Yamashita, S. K Singh, T. Kawate, Y. Jin, and E. Gouaux. Crystal structure of a bacterial homologue of Na^+/Cl^--dependent neurotransmitter transporters. *Nature*, 437(7056):215–223, Sep 2005.

[34] M. H. Akabas, D. A. Stauffer, M. Xu, and A. Karlin. Acetylcholine receptor channel structure probed in cysteine-substitution mutants. *Science*, 258(5080):307–310, Oct 1992.

[35] H.R. Kaback, M. Sahin-Tth, and A.B. Weinglass. The kamikaze approach to membrane transport. *Nat Rev Mol Cell Biol*, 2(8):610–620, Aug 2001.

[36] X.B. Tang, J. Fujinaga, R. Kopito, and J.R. Casey. Topology of the region surrounding Glu681 of human AE1 protein, the erythrocyte anion exchanger. *J Biol Chem*, 273(35):22545–22553, Aug 1998.

[37] G. Lambert, I.C. Forster, J. Biber, and H. Murer. Cysteine residues and the structure of the rat renal proximal tubular type II sodium phosphate cotransporter (rat NaPi IIa). *J. Membr. Biol.*, 176:133–141, 2000.

[38] A. Karlin and M.H. Akabas. Substituted-cysteine accessibility method. *Methods Enzymol*, 293:123–145, 1998.

[39] Q. Zhu and J.R. Casey. Topology of transmembrane proteins by scanning cysteine accessibility mutagenesis methodology. *Methods*, 41(4):439–450, Apr 2007.

[40] D.A. Stauffer and A. Karlin. Electrostatic potential of the acetylcholine binding sites in the nicotinic receptor probed by reactions of binding-site cysteines with charged methanethiosulfonates. *Biochemistry*, 33(22):6840–6849, Jun 1994.

[41] J. Wu, D. Hardy, and H.R. Kaback. Tertiary Contacts of Helix V in the Lactose Permease Determined by Site-Directed Chemical Cross-Linking in Situ. *Biochemistry*, 38 (8):pp 23202325, 1999.

[42] I.N. Smirnova, V. Kasho, and H.R. Kaback. Protonation and sugar binding to LacY. *Proc Natl Acad Sci U S A*, 105(26):8896–8901, Jul 2008.

[43] W.L. Hubbell, H.S. Mchaourab, C. Altenbach, and M.A. Lietzow. Watching proteins move using site-directed spin labeling. *Structure*, 4(7):779–783, Jul 1996.

[44] E.J. Hustedt and A.H. Beth. Nitroxide spin-spin interactions: applications to protein structure and dynamics. *Annu Rev Biophys Biomol Struct*, 28:129–153, 1999.

[45] W.L. Hubbell, D.S. Cafiso, and C. Altenbach. Identifying conformational changes with site-directed spin labeling. *Nat Struct Biol*, 7(9):735–739, Sep 2000.

[46] A. Salas-Burgos, P. Iserovich, F. Zuniga, J.C. Vera, and J. Fischbarg. Predicting the three-dimensional structure of the human facilitative glucose transporter GLUT1 by a novel evolutionary homology strategy: insights on the molecular mechanism of substrate migration, and binding sites for glucose and inhibitory molecules. *Biophys J*, 87(5):2990–2999, Nov 2004.

[47] L.R. Forrest, Y.-W. Zhang, M.T. Jacobs, J. Gesmonde, L. Xie, B.H. Honig, and G. Rudnick. Mechanism for alternating access in neurotransmitter transporters. *Proc Natl Acad Sci U S A*, 105(30):10338–10343, Jul 2008.

[48] C. Nourry, S.G.N. Grant, and J.P. Borg. PDZ domain proteins: plug and play! *Sci STKE*, 2003(179):RE7, Apr 2003.

[49] S. Shenolikar and E.J. Weinman. NHERF: targeting and trafficking membrane proteins. *Am J Physiol Renal Physiol*, 280(3):F389–F395, Mar 2001.

[50] M.J. Mahon and G.V. Segre. Stimulation by parathyroid hormone of a NHERF-1-assembled complex consisting of the parathyroid hormone I receptor, phospholipase Cbeta, and actin increases intracellular calcium in opossum kidney cells. *J Biol Chem*, 279(22):23550–23558, May 2004.

[51] D.W. Hilgemann, S. Feng, and C. Nasuhoglu. The complex and intriguing lives of PIP2 with ion channels and transporters. *Sci STKE*, 2001(111), Dec 2001.

[52] G. Palmer, J.P. Bonjour, and J. Caverzasio. Expression of a newly identified phosphate transporter/retrovirus receptor in human SaOS-2 osteoblast-like cells and its regulation by insulin-like growth factor I. *Endocrinology*, 138(12):5202–5209, Dec 1997.

[53] K.A. Hruska, S. Mathew, R. Lund, P. Qiu, and R. Pratt. Hyperphosphatemia of chronic kidney disease. *Kidney Int*, 74(2):148–157, Jul 2008.

[54] T. Berndt and R. Kumar. Novel mechanisms in the regulation of phosphorus homeostasis. *Physiology*, 24:17–25, Feb 2009.

[55] T.J. Berndt and F.G. Knox. *The Kidney*, chapter Renal regulation of phosphate excretion., pages 2511–2532.

[56] I.C. Forster, L.V. Virkki, E. Bossi, H. Murer, and J. Biber. Electrogenic kinetics of a mammalian intestinal type IIb Na^+/P_i cotransporter. *J Membr Biol*, 212(3):177–190, 2006.

[57] I.C. Forster, N. Hernando, J. Biber, and H. Murer. Proximal tubular handling of phosphate: A molecular perspective. *Kidney Int*, 70(9):1548–1559, Nov 2006.

[58] C. Bergwitz, N.M. Roslin, M. Tieder, J.C. Loredo-Osti, M. Bastepe, H. Abu-Zahra, D. Frappier, K. Burkett, T.O. Carpenter, D. Anderson, M. Garabedian, I. Sermet, T.M. Fujiwara, K. Morgan, H.S. Tenenhouse, and H. Juppner. SLC34A3 mutations in patients with hereditary hypophosphatemic rickets with hypercalciuria predict a key role for the sodium-phosphate cotransporter NaPi-IIc in maintaining phosphate homeostasis. *Am J Hum Genet*, 78(2):179–192, Feb 2006.

[59] H. Murer, N. Hernando, I.C. Forster, and J. Biber. Proximal tubular phosphate reabsorption: molecular mechanisms. *Physiol Rev*, 80(4):1373–1409, Oct 2000.

[60] P.Q. Barret. and P.S. Aroson. Glucose and alanine inhibition of phosphate transport in renal microvillus membrane vesicles. *Am J Physiol Renal Fluid Electrolyte Physiol*, 242:126–131, 1982.

[61] J. Dunlop and T. Phung. Phosphate and slow vacuolar channels in Beta *vulgaris*. *Australian J Plant Physiol*, 25:709–718, 1998.

[62] D.R. Laver, G.K.E. Lenz, and A.F. Dulhunty. Phosphate ion channels in sarcoplasmic reticulum of rabbit skeletal muscle. *J Physiol*, 535.3:pp.715728, 2001.

[63] J. Biber, N. Hernando, I. Forster, and H. Murer. Regulation of phosphate transport in proximal tubules. *Pflugers Arch*, Aug 2008.

[64] M. Custer, F. Meier, E. Schlatter, R. Greger, A. Garcia-Perez, J. Biber, and H. Murer. Localization of NaPi-1, a Na-Pi cotransporter, in rabbit kidney proximal tubules. I. mrna localization by reverse transcription/polymerase chain reaction. *Pflugers Arch*, 424(3-4):203–209, Aug 1993.

[65] A.E. Busch, A. Schuster, S. Waldegger, C.A. Wagner, G. Zempel, S. Broer, J. Biber, H. Murer, and F. Lang. Expression of a renal type I sodium/phosphate transporter (NaPi-1) induces a conductance in xenopus oocytes permeable for organic and inorganic anions. *Proc Natl Acad Sci U S A*, 93(11):5347–5351, May 1996.

[66] H. Murer, I.C. Forster, and J. Biber. The sodium phosphate cotransporter family SLC34. *Pflugers Arch.*, 447(5):763–767, Feb 2004.

[67] M. Custer, M. Ltscher, J. Biber, H. Murer, and B. Kaissling. Expression of Na-Pi cotransport in rat kidney: localization by RT-PCR and immunohistochemistry. *Am J Physiol*, 266:F767–F774, 1994.

[68] L. Beck, A.C. Karaplis, N. Amizuka, A.S. Hewson, H. Ozawa, and H.S. Tenenhouse. Targeted inactivation of Npt2 in mice leads to severe renal phosphate wasting, hypercalciuria, and skeletal abnormalities. *Proc. Natl. Acad. Sci. USA*, 95:5372–5377, 1998.

[69] I.C. Forster, D.D. Loo, and S. Eskandari. Stoichiometry and Na^+ binding cooperativity of rat and flounder renal type II Na^+-P_i cotransporters. *Am. J. Physiol.*, 276:F644–F649, 1999.

[70] L.V. Virkki, H. Murer, and I.C. Forster. Voltage clamp fluorometric measurements on a type II Na^+-coupled Pi cotransporter: shedding light on substrate binding order. *J Gen Physiol*, 127(5):539–555, May 2006.

[71] O. Andrini, C. Ghezzi, H. Murer, and I. Forster. The leak mode of type II Na^+-P_i cotransporters. *Channels (Austin)*, 2(5), Sep 2008.

[72] A.E. Busch, C.A. Wagner, A. Schuster, S. Waldegger, J. Biber, H. Murer, and F. Lang. Properties of electrogenic Pi transport by a human renal brush border Na^+/Pi transporter. *J Am Soc Nephrol*, 6(6):1547–1551, Dec 1995.

[73] H. Hilfiker, O. Hattenhauer, M. Traebert, I. Forster, H. Murer, and J. Biber. Characterization of a murine type II sodium-phosphate cotransporter expressed in mammalian small intestine. *Proc Natl Acad Sci U S A*, 95(24):14564–14569, Nov 1998.

[74] H. Xu, J.F. Collins, L. Bai, P.R. Kiela, and F.K. Ghishan. Regulation of the human sodium-phosphate cotransporter NaP(i)-IIb gene promoter by epidermal growth factor. *Am J Physiol Cell Physiol*, 280(3):C628–C636, Mar 2001.

[75] K. Arima, E.R. Hines, P.R. Kiela, J.B. Drees, J.F. Collins, and F.K. Ghishan. Glucocorticoid regulation and glycosylation of mouse intestinal type IIb Na-P(i) cotransporter during ontogeny. *Am J Physiol Gastrointest Liver Physiol*, 283(2):G426–G434, Aug 2002.

[76] O. Hattenhauer, M. Traebert, H. Murer, and J. Biber. Regulation of small intestinal Na-P(i) type IIb cotransporter by dietary phosphate intake. *Am J Physiol*, 277(4 Pt 1):G756–G762, Oct 1999.

[77] H. Xu, L. Bai, J.F. Collins, and F.K. Ghishan. Age-dependent regulation of rat intestinal type IIb sodium-phosphate cotransporter by 1,25-(OH)(2) vitamin D(3). *Am J Physiol Cell Physiol*, 282(3):C487–C493, Mar 2002.

[78] H. Segawa, I. Kaneko, A. Takahashi, M. Kuwahata, M. Ito, I. Ohkido, S. Tatsumi, and K. Miyamoto. Growth-related renal type II Na/Pi cotransporter. *J Biol Chem*, 277(22):19665–19672, May 2002.

[79] H.S. Tenenhouse, J. Martel, C. Gauthier, H. Segawa, and K. Miyamoto. Differential effects of Npt2a gene ablation and X-linked Hyp mutation on renal expression of Npt2c. *Am J Physiol Renal Physiol*, 285(6):F1271–F1278, Dec 2003.

[80] C. Madjdpour, D. Bacic, B. Kaissling, H. Murer, and J. Biber. Segment-specific expression of sodium-phosphate cotransporters NaPi-IIa and -IIc and interacting proteins in mouse renal proximal tubules. *Pflugers Arch*, 448(4):402–410, Jul 2004.

[81] Hiroko Segawa, Setsuko Yamanaka, Mikiko Ito, Masashi Kuwahata, Masayuki Shono, Tadashi Yamamoto, and Ken ichi Miyamoto. Internalization of renal type IIc Na-Pi cotransporter in response to a high-phosphate diet. *Am J Physiol Renal Physiol*, 288(3):F587–F596, Mar 2005.

[82] L.V. Virkki, J. Biber, H. Murer, and I.C. Forster. Phosphate transporters: a tale of two solute carrier families. *Am J Physiol Renal Physiol*, 293(3):F643–F654, Sep 2007.

[83] R.A. Weiss and C.S. Tailor. Retrovirus receptors. *Cell*, 82(4):531–533, Aug 1995.

[84] B. O'Hara, S.V. Johann, H.P. Klinger, D.G. Blair, H. Rubinson, K.J. Dunn, P. Sass, S.M. Vitek, and T. Robins. Characterization of a human gene conferring sensitivity to infection by gibbon ape leukemia virus. *Cell Growth Differ*, 1(3):119–127, Mar 1990.

[85] D.G. Miller, R.H. Edwards, and A.D. Miller. Cloning of the cellular receptor for amphotropic murine retroviruses reveals homology to that for gibbon ape leukemia virus. *Proc Natl Acad Sci U S A*, 91(1):78–82, Jan 1994.

[86] M. van Zeijl, S.V. Johann, E. Closs, J. Cunningham, R. Eddy, T.B. Shows, and B. O'Hara. A human amphotropic retrovirus receptor is a second member of the gibbon ape leukemia virus receptor family. *Proc Natl Acad Sci U S A*, 91(3):1168–1172, Feb 1994.

[87] B.J. Mann, B.J. Bowman, J. Grotelueschen, and R.L. Metzenberg. Nucleotide sequence of pho-4+, encoding a phosphate-repressible phosphate permease of N*eurospora crassa*. *Gene*, 83(2):281–289, Nov 1989.

[88] S.V. Johann, J.J. Gibbons, and B. O'Hara. GLVR1, a receptor for gibbon ape leukemia virus, is homologous to a phosphate permease of N*eurospora crassa* and is expressed at high levels in the brain and thymus. *J Virol*, 66(3):1635–1640, Mar 1992.

[89] M.P. Kavanaugh, D.G. Miller, W. Zhang, W. Law, S.L. Kozak, D. Kabat, and A.D. Miller. Cell-surface receptors for gibbon ape leukemia virus and amphotropic murine retrovirus are inducible sodium-dependent phosphate symporters. *Proc Natl Acad Sci U S A*, 91:7071–7075, 1994.

[90] Z. Olah, C. Lehel, W.B. Anderson, M.V. Eiden, and C.A. Wilson. The cellular receptor for gibbon ape leukemia virus is a novel high affinity sodium-dependent phosphate transporter. *J Biol Chem*, 269(41):25426–25431, Oct 1994.

[91] P. Daram, S. Brunner, C. Rausch, C. Steiner, N. Amrhein, and M. Bucher. Pht2;1 encodes a low-affinity phosphate transporter from Arabidopsis. *Plant Cell*, 11(11):2153–2166, Nov 1999.

[92] R.M. Harris, D.C. Webb, S.M. Howitt, and G.B. Cox. Characterization of PitA and PitB from E*scherichia coli*. *J Bacteriol*, 183(17):5008–5014, Sep 2001.

[93] H.W. van Veen. Phosphate transport in prokaryotes: molecules, mediators and mechanisms. *Antonie Van Leeuwenhoek*, 72(4):299–315, Nov 1997.

[94] J.F. Collins, L. Bai, and F.K. Ghishan. The SLC20 family of proteins: dual functions as sodium-phosphate cotransporters and viral receptors. *Pflugers Arch*, 447(5):647–652, Feb 2004.

[95] P. Martinez and B.L. Persson. Identification, cloning and characterization of a derepressible Na^+-coupled phosphate transporter in S*accharomyces cerevisiae*. *Mol Gen Genet*, 258(6):628–638, Jun 1998.

[96] W.K. Versaw and R.L. Metzenberg. Repressible cation-phosphate symporters in N*eurospora crassa*. *Proc Natl Acad Sci U S A*, 92:3884–3887, 1995.

[97] M.C. Mansilla and D. de Mendoza. The B*acillus subtilis* cysP gene encodes a novel sulphate permease related to the inorganic phosphate transporter (Pit) family. *Microbiology*, 146 (Pt 4):815–821, Apr 2000.

[98] W. Uckert, G. Willimsky, F.S. Pedersen, T. Blankenstein, and L. Pedersen. RNA levels of human retrovirus receptors Pit1 and Pit2 do not correlate with infectibility by three retroviral vector pseudotypes. *Hum Gene Ther*, 9(17):2619–2627, Nov 1998.

[99] S. Tatsumi, H. Segawa, K. Morita, H. Haga, T. Kouda, H. Yamamoto, Y. Inoue, T. Nii, K. Katai, Y. Taketani, K.I. Miyamoto, and E. Takeda. Molecular cloning and hormonal regulation of PiT-1, a sodium-dependent phosphate cotransporter from rat parathyroid glands. *Endocrinology*, 139(4):1692–1699, Apr 1998.

[100] L. Bai, J.F. Collins, and F.K. Ghishan. Cloning and characterization of a type III Na-dependent phosphate cotransporter from mouse intestine. *Am J Physiol Cell Physiol*, 279(4):C1135–C1143, Oct 2000.

[101] E. Zoidis, C. Ghirlanda-Keller, M. Gosteli-Peter, J. Zapf, and C. Schmid. Regulation of phosphate (Pi) transport and NaPi-III transporter (Pit-1) mRNA in rat osteoblasts. *J Endocrinol*, 181(3):531–540, Jun 2004.

[102] L.B. Nielsen, F.S. Pedersen, and L. Pedersen. Expression of type III sodium-dependent phosphate transporters/retroviral receptors mRNAs during osteoblast differentiation. *Bone*, 28(2):160–166, Feb 2001.

[103] P. Frei, B. Gao, B. Hagenbuch, A. Mate, J. Biber, H. Murer, P.J. Meier, and B. Stieger. Identification and localization of sodium-phosphate cotransporters in hepatocytes and cholangiocytes of rat liver. *Am J Physiol Gastrointest Liver Physiol*, 288(4):G771–G778, Apr 2005.

[104] J.C. Leung, M. Barac-Nieto, K. Hering-Smith, and D.M. Silverstein. Expression of the rat renal PiT-2 phosphate transporter. *Horm Metab Res*, 37(5):265–269, May 2005.

[105] C.J. Boyer, A.D. Baines, E. Beaulieu, and R. Bliveau. Immunodetection of a type III sodium-dependent phosphate cotransporter in tissues and OK cells. *Biochim Biophys Acta*, 1368(1):73–83, Jan 1998.

[106] M. Nishimura and S. Naito. Tissue-specific mRNA expression profiles of human solute carrier transporter superfamilies. *Drug Metab Pharmacokinet*, 23(1):22–44, 2008.

[107] J. Caverzasio and J.P. Bonjour. Characteristics and regulation of Pi transport in osteogenic cells for bone metabolism. *Kidney Int*, 49(4):975–980, Apr 1996.

[108] J. Guicheux, G. Palmer, C. Shukunami, Y. Hiraki, J.P. Bonjour, and J. Caverzasio. A novel in vitro culture system for analysis of functional role of phosphate transport in endochondral ossification. *Bone*, 27(1):69–74, Jul 2000.

[109] G. Palmer, J. Zhao, J. Bonjour, W. Hofstetter, and J. Caverzasio. In vivo expression of transcripts encoding the Glvr-1 phosphate transporter/retrovirus receptor during bone development. *Bone*, 24(1):1–7, Jan 1999.

[110] A. Suzuki, C. Ghayor, J. Guicheux, D. Magne, S. Quillard, A. Kakita, Y. Ono, Y. Miura, Y. Oiso, M. Itoh, and J. Caverzasio. Enhanced expression of the inorganic phosphate transporter Pit-1 is involved in BMP-2-induced matrix mineralization in osteoblast-like cells. *J Bone Miner Res*, 21(5):674–683, May 2006.

[111] Y. Yoshiko, G.A. Candeliere, N. Maeda, and J.E. Aubin. Osteoblast autonomous Pi regulation via Pit1 plays a role in bone mineralization. *Mol Cell Biol*, 27(12):4465–4474, Jun 2007.

[112] M.L. Chien, J.L. Foster, J.L. Douglas, and J.V. Garcia. The amphotropic murine leukemia virus receptor gene encodes a 71-kilodalton protein that is induced by phosphate depletion. *J Virol*, 71(6):4564–4570, Jun 1997.

[113] A. Suzuki, G. Palmer, J.P. Bonjour, and J. Caverzasio. Stimulation of sodium-dependent inorganic phosphate transport by activation of Gi/o-protein-coupled receptors by epinephrine in MC3T3-E1 osteoblast-like cells. *Bone*, 28(6):589–594, Jun 2001.

[114] A. Suzuki, G. Palmer, J.P. Bonjour, and J. Caverzasio. Stimulation of sodium-dependent phosphate transport and signaling mechanisms induced by basic fibroblast growth factor in MC3T3-E1 osteoblast-like cells. *J Bone Miner Res*, 15(1):95–102, Jan 2000.

[115] S. Jono, M.D. McKee, C.E. Murry, A. Shioi, Y. Nishizawa, K. Mori, H. Morii, and C.M. Giachelli. Phosphate regulation of vascular smooth muscle cell calcification. *Circ Res*, 87(7):E10–E17, Sep 2000.

[116] X. Li, H.-Y. Yang, and C.M Giachelli. Role of the sodium-dependent phosphate cotransporter, Pit-1, in vascular smooth muscle cell calcification. *Circ Res*, 98(7):905–912, Apr 2006.

[117] I. Fernandes, R. Bliveau, G. Friedlander, and C. Silve. NaPO(4) cotransport type III (PiT1) expression in human embryonic kidney cells and regulation by PTH. *Am J Physiol*, 277(4 Pt 2):F543–F551, Oct 1999.

[118] M.A. Khadeer, Z. Tang, H.S. Tenenhouse, M.V. Eiden, H. Murer, N. Hernando, E. J. Weinman, M.A. Chellaiah, and A. Gupta. Na^+-dependent phosphate transporters in the murine osteoclast: cellular distribution and protein interactions. *Am J Physiol Cell Physiol*, 284(6):C1633–C1644, Jun 2003.

[119] H.S. Tenenhouse, C. Gauthier, J. Martel, F.A. Gesek, B.A. Coutermarsh, and P.A. Friedman. Na+ -phosphate cotransport in mouse distal convoluted tubule cells: evidence for Glvr-1 and Ram-1 gene expression. *J Bone Miner Res*, 13(4):590–597, Apr 1998.

[120] G. Wang, G. Williams, H. Xia, M. Hickey, J. Shao, B. L. Davidson, and P.B. McCray. Apical barriers to airway epithelial cell gene transfer with amphotropic retroviral vectors. *Gene Ther*, 9(14):922–931, Jul 2002.

[121] K.J. Saliba, R.E. Martin, A. Brer, R.I. Henry, C.S. McCarthy, M.J. Downie, R.J. W. Allen, K.A. Mullin, G.I. McFadden, S. Brer, and K. Kirk. Sodium-dependent uptake of inorganic phosphate by the intracellular malaria parasite. *Nature*, 443(7111):582–585, Oct 2006.

[122] P. Bøttger, S.E. Hede, M. Grunnet, B. Høyer, D.A. Klaerke, and L. Pedersen. Characterization of transport mechanisms and determinants critical for Na^+-dependent Pi symport of the PiT family paralogs human PiT1 and PiT2. *Am J Physiol Cell Physiol*, 291(6):C1377–C1387, Dec 2006.

[123] R. Villa-Bellosta, Y.E. Bogaert, M. Levi, and V. Sorribas. Characterization of phosphate transport in rat vascular smooth muscle cells: implications for vascular calcification. *Arterioscler Thromb Vasc Biol*, 27(5):1030–1036, May 2007.

[124] F. Corpet, J. Gouzy, and D. Kahn. The ProDom database of protein domain families. *Nucleic Acids Res*, 26(1):323–326, Jan 1998.

[125] M.H. Saier, B.H. Eng, S. Fard, J. Garg, D.A. Haggerty, W.J. Hutchinson, D.L. Jack, E.C. Lai, H.J. Liu, D.P. Nusinew, A.M. Omar, S.S. Pao, I.T. Paulsen, J.A. Quan, M. Sliwinski, T.T. Tseng, S. Wachi, and G.B. Young. Phylogenetic characterization of novel transport protein families revealed by genome analyses. *Biochim Biophys Acta*, 1422(1):1–56, Feb 1999.

[126] C. Salaün, P. Rodrigues, and J.M. Heard. Transmembrane topology of PiT-2, a phosphate transporter-retrovirus receptor. *J Virol*, 75(12):5584–5592, Jun 2001.

[127] P. Bøttger and L. Pedersen. The central half of Pit2 is not required for its function as a retroviral receptor. *J Virol*, 78(17):9564–9567, Sep 2004.

[128] K. Dreyer, F.S. Pedersen, and L. Pedersen. A 13-amino-acid Pit1-specific loop 4 sequence confers feline leukemia virus subgroup B receptor function upon Pit2. *J Virol*, 74(6):2926–2929, Mar 2000.

[129] S.V. Johann, M. van Zeijl, J. Cekleniak, and B. O'Hara. Definition of a domain of GLVR1 which is necessary for infection by gibbon ape leukemia virus and which is highly polymorphic between species. *J Virol*, 67(11):6733–6736, Nov 1993.

[130] L. Pedersen, M. van Zeijl, S.V. Johann, and B. O'Hara. Fungal phosphate transporter serves as a receptor backbone for gibbon ape leukemia virus. *J Virol*, 71(10):7619–7622, Oct 1997.

[131] P. Bøttger and L. Pedersen. Evolutionary and experimental analyses of inorganic phosphate transporter PiT family reveals two related signature sequences harboring highly conserved aspartic acids critical for sodium-dependent phosphate transport function of human PiT2. *FEBS J*, 272(12):3060–3074, Jun 2005.

[132] S. Ravera, L.V. Virkki, H. Murer, and I.C. Forster. Deciphering PiT transport kinetics and substrate specificity using electrophysiology and flux measurements. *Am J Physiol Cell Physiol*, 293(2):C606–C620, Aug 2007.

[133] A. Werner, J. Biber, J. Forgo, M. Palacin, and H. Murer. Expression of renal transport systems for inorganic phosphate and sulfate in x*enopus laevis* oocytes. *J Biol Chem*, 265(21):12331–12336, Jul 1990.

[134] K. Hofmann and W. Stoffel. TM*base* - A *database of membrane spanning proteins segments*. Biol. Chem. Hoppe, 1993.

[135] O.W. Moe. PiT-2 coming out of the pits. *Am J Physiol Renal Physiol*, 2009.

[136] A. Bacconi, L.V. Virkki, J. Biber, H. Murer, and I.C. Forster. Renouncing electroneutrality is not free of charge: switching on electrogenicity in a Na^+-coupled phosphate cotransporter. *Proc Natl Acad Sci U S A*, 102(35):12606–12611, Aug 2005.

[137] L.V. Virkki, I.C. Forster, J. Biber, and H. Murer. Substrate interactions in the human type IIa sodium-phosphate cotransporter (NaPi-IIa). *Am J Physiol Renal Physiol*, 288(5):F969–F981, May 2005.

[138] S. Ravera, R. Villa-Bellosta, V. Sorribas, G. Stange, M. Levi, H. Murer, J. Biber, and I.C. Cameron Forster. The na^+/p_i cotransporter pit-2 (SLC20A220A2 is expressed in the apical membrane of rat renal proximal tubules and regulated by dietary p_i. *Am J Physiol Renal Physiol*, 2008.

[139] Marta Nowik, M. Rita Lecca, Ana Velic, Hubert Rehrauer, Andr W Brndli, and Carsten A Wagner. Genome-wide gene expression profiling reveals renal genes regulated during metabolic acidosis. *Physiol Genomics*, 32(3):322–334, Feb 2008.

[140] C.W. Gottschlk, W.E. Lassiter, and M. Mylle. Localization of urine acidification in the mammalian kidney. *Am J Physiol*, 198:581–585, Mar 1960.

[141] S. Faham, A. Watanabe, G.M. Besserer, D. Cascio, A. Specht, B.A. Hirayama, E.M. Wright, and J. Abramson. The crystal structure of a sodium galactose transporter reveals mechanistic insights into Na^+/sugar symport. *Science*, 321(5890):810–814, Aug 2008.

List of Figures

Silvia Ravera

Curriculum Vitae

Date of birth: 5.10.1977
Place of birth: Alessandria, Italy
Nationality: Italian
Private adress: Schaffhauserstrasse 355, CH-8050, Zurich
Tel: 0041-786973169 , 0039-3496875494
Work adress: University of Zurich, Institute of Physiology,
Winterthurerstrasse 190, CH-8056, Zurich
Tel: 0041 - 0446355054
E-mail: raveras@physiol.unizh.ch
Residence permit: B (end 2012)

Education

- 2005 (October) University of Zurich, Faculty of MNF, Institute of Physiology, PhD (in course). ZIHP - Center for Integrative Human Physiology - PhD program
- 2004 (November) University of Turin, Faculty of Pharmacy, Master degree with honours in Pharmaceutical Chemistry and Technology. Thesis: "Calorimetric study of antitumor drugs"
- 1996 High School, Liceo scientifico "G. Galilei", Alessandria, Italy

Additional courses

- 2008 (May 11^{th} - May 19^{th}) International School of Biophysics A. Borsellino "Channels and Transporters"
- 2008 (February - June) Migros Schule, Zurich, A2 German Course
- 2007 (February - June) University of Zurich, Protein Biophysics Course
- 2006 (September) University of Zurich, "Scientific Writing Course"
- 2006 (September) LTK Module 1E "Introductory Course in Laboratory Animal Science"
- 2006-7 (October - February) ETH, Sprache Zentrum, Zurich, Upper-Intermediate English Course
- 2004-2005 (November - June) Shenker Institute of English language, Turin, Italy: Intermediate level course
- 1994 (July) cole des Roches, Verneuil-sur-Avre, France: Advanced course of French language

Work Experience

- 2005 Training in a Pharmacy, "Farmacia Nizza, dott. Sacco", Turin, Italy
- 2001-2002 Stage at the Advanced Biotechnology Centre, Genoa, Italy on "Synthesis of molecules active as antitumor drugs"
- International Conference "Horizons in Hydrogen Bond Research", Turin September 3-7, 2001. Local Organization Committee

Computer Skills

- Operating systems: Windows
- Software: Micrisoft Office, LaTeX, Hyperchem, PyMol, GraphPad Prism, pClamp, CorelDRAW, Adobe Photoshop
- Internet Databanks

Languages

- Italian, mother tongue
- English, fluent (spoken, written)
- French, fluent (spoken, written)
- German, scholastic

Publications

- Bacconi A, Ravera S, Virkki LV, Murer H, Forster IC. "Temperature dependence of steady-state and presteady-state kinetics of a type IIb Na^+/P_i cotransporter" J Membr Biol. 2007 215(2-3):81-92
- Ravera S, Virkki LV, Murer H, Forster IC. "Deciphering PiT transport kinetics and substrate specificity using electrophysiology and flux measurements" Am J Physiol Cell Physiol. 2007 293(2):C606-20
- Kovermann P, Meyer S, Hrtensteiner S, Picco C, Scholz-Starke J, Ravera S, Lee Y, Martinoia E. "The Arabidopsis vacuolar malate channel is a member of the ALMT family" Plant J. 2007 52(6):1169-80.
- Ravera S, Villa-Bellosta R, Sorribas V, Stange G, Levi M, Murer H, Biber J, Forster IC. "The Na^+/P_i cotransporter PiT-2 (SLC20A2) is expressed in the apical membrane of rat renal proximal tubules and regulated by dietary P_i" Am J. Physiol Renal Physiol. 2008

Conferences

- American Society of nefrology, Renal Week 2008, November 4 - 9, 2008. Talk: "Expression and dietary regulation of PiT-1/2 in rat kidney"
- Swiss Physiological Society Annual Meeting, September 11, 2008. Talk: "Structure-function studies on the PiT1 expressed in *Xenopus* oocytes"
- Goettingen Transporter November, 2007. Talk: " Structure-function studies on *Xenopus* PiT1"
- The 86th Annual Meeting of The German Physiological Society, March 25-28, 2007. Talk: "Novel transport kinetics of the type III Na^+-coupled P_i-cotransporter family"
- Goettingen Transporter November, 2006. Talk: "Characterization of PiT-1/2 Na^+/P_i-cotransporters"
- XXXIII Natl. Conference of Physical Chemistry, June 20-25, 2004. Poster: "Calorimetric monitorig of the effect of antitumor drugs"
- 2005 Mediterranean Conference on Calorimetry and Thermal Analysis (MEDICTA2005), July 2-6, 2005. Poster "Study of cytotoxicity of antitumor drugs by isothermal microcalorimetry"

Acknowledgments

First I would like to thank Heini Murer, the big boss and the sponsor of my PhD, for all the ideas and suggestions. Many thanks for always being critical and supportive and for letting me “just to think about...”

I would like to thanks the members of my thesis committee, François Verrey and Laurent Schild for the ideas and the discussions during ours meetings.

I would like to thank Leila Virkki, former post doc in our group, for following me in my first steps in the lab life, for the suggestions and the shared time, at work and not only there.

Many many thanks to Nati always present and competent and “passionate” and to Jürg, for his advice and his helpful suggestions.

A great thanks is for Vicky, for all the conversations, for all the coffee shared, starting point of some really interesting ideas.

Many thanks are for Chiara and Olga for sharing with me my PhD, scientifically and personally.

A special thanks is for the “Caflisch group” for all the lunches, discussions, support, home-feelings...

A special thanks is for all the J-floor people, a great environment, scientifically speaking, but overall as human dimension.

And last but not least THANKS to my boss, Ian, for giving me this opportunity almost unseen, for teaching me, for supporting me always, for having make of me a better scientist.